MSc thesis

Bed level changes in the shoaling zone and surf zone under the influence of cross-shore effects at a time scale of minutes

Chris Zeeuw van der Laan
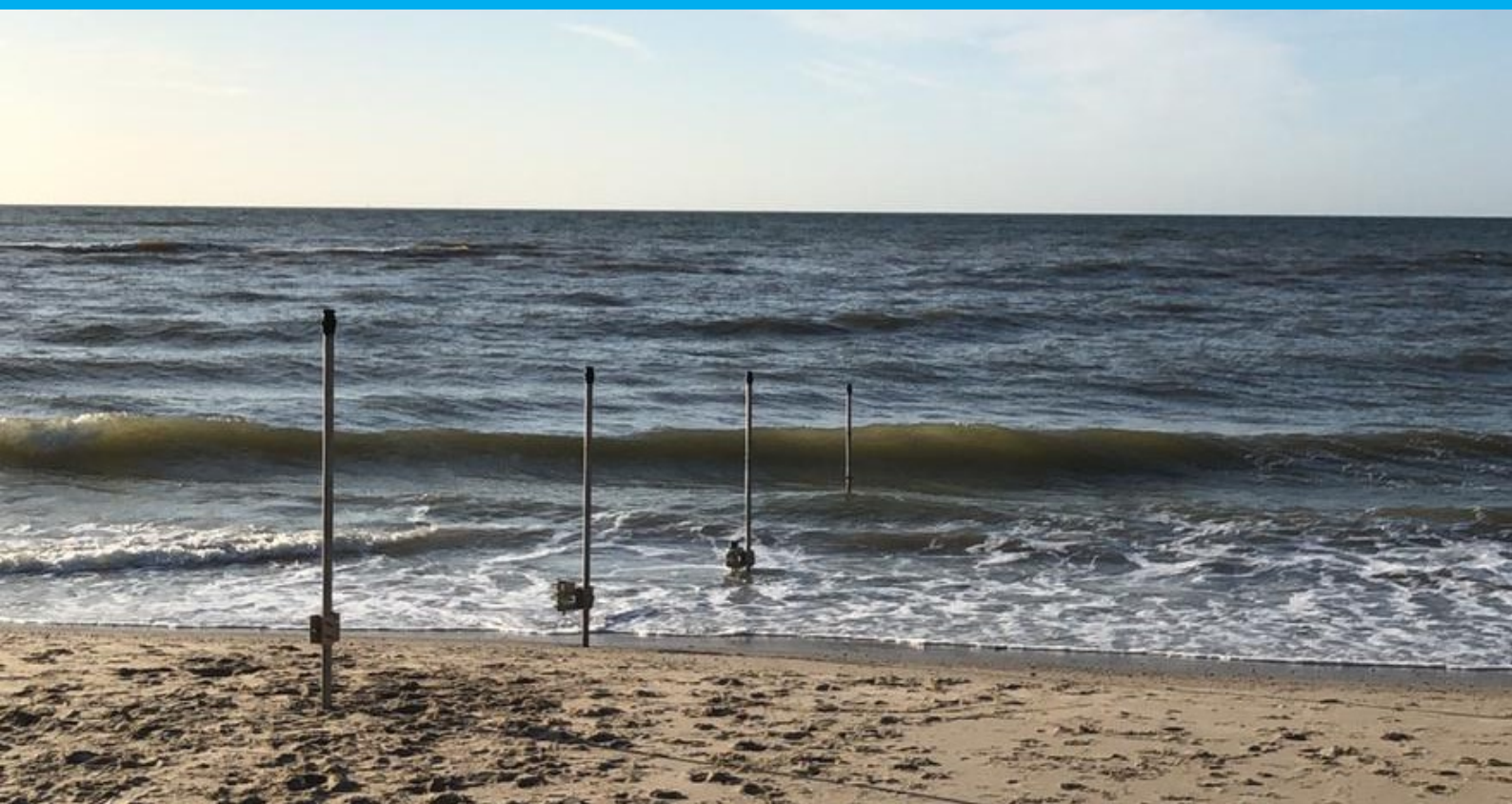
TUDelft

MSc thesis

Bed level changes in the shoaling zone and surf zone under the influence of cross-shore effects at a time scale of minutes

by

Chris Zeeuw van der Laan

to obtain the degree of Master of Science
at the Delft University of Technology,

An electronic version of this thesis is available at `http://repository.tudelft.nl/`.

TUDelft

Abstract

Cities are built close to the sea, and are protected against water by defence systems. These defence systems can be man-made, such as dikes and flood defence systems, or can be natural, such as beaches or cliffs. It is important to keep a close watch on these natural defences, to ensure that the risk of flooding remains low. In order to manage the natural defences, understanding of its system and behavior is crucial. Different models have been used to replicate these systems and to estimate their resilience to different storms. These models use different timescales, ranging from a single storm to multiple years. However, due to its complexity, these natural defence systems are not fully understood. As a result, errors occur in these models (Roelvink and Brøker, 1993). Most models are calibrated using observations with a time span of hours or more, but Nielsen and Shimamoto (2015) observed that a sandbar was able to react to a changing water level within minutes under regular waves and wondered if this is also the case in a field study. This report seeks to answer how the bed level of a beach behaves in a timescale of minutes.

The beach is studied with high-resolution observations of the bed level using two echo sounders. The bed level is observed at an interval of 10 minutes. Next to that, the waves at the beach are observed using pressure sensors with a frequency of 8 Hz. Several results were found. First, the bed level changed with a maximum of 20 centimeters during a single tide and there is no tidal signal visible in the bed level. Secondly, the significant wave during the week of observations was between 0.4 meters and 1.2 meters high and increased throughout the week. Lastly, the observations of the bed level had a significant degree of uncertainty.

The bed level changes observed are linked to short waves, and flow velocity under these waves. The relative wave height is used to link these bed level changes to the short wave processes. These changes are most evident in the breaking zone. The flow velocity and the bed level changes are studied using the parametric cross-shore model (Mariño-Tapia et al., 2007a). This model was unable to predict the bed level changes with direct correlation to the observed changes. But the waves in the model differed from the waves observed. When the difference between the waves was reduced, the model was able to predict the bed level behavior with a correlation of 0.61. However, this was not the case for the observations made closer to shore. Both results indicate that bed level behavior in deeper water is better understood rather than closer to shore. Therefore, more research should be done in the inner surf zone.

In order to study small scale effects accuracy is important. feather research should be done when devices are able to accurately observe the bed level changes in the breaker zone and inner surf zone.

Contents

List of symbols

Symbol	Description	Unit
a	wave amplitude	[m]
a_{crest}	crest amplitude of the wave	[m]
c	wave celerity	[m]
c_f	drag coefficient	[-]
c_g	speed of the wave group	[m/s]
C_1	drag constant sediment particles	[-]
C_2	friction constant sediment particles	[-]
d	local water depth	[m]
d_{50}	the median grain diameter	[m]
d_b	the depth at where waves start breaking	[m]
E	energy	$[kg\ m^2/s^2]$
F	energy flux	$[kg\ m^3/s^3]$
g	gravitational acceleration ($g \approx 9.81$)	$[m/s^2]$
h	bed-level	[m]
H	wave height	[m]
H_{br}	wave height due to depth limited breaking	[m]
H_{sr}	wave height due to shoaling and refraction	[m]
k	wave number	[rad/m]
K_{ref}	refraction coefficient	[-]
K_{sh}	shoaling coefficient	[-]
L	wave length	[m]
M	number of units in formula	[-]
n	bed-level porosity	[-]
N	number of units in formula	[-]
P	pressure	$[kg/m\ s^2]$
P_{water}	pressure due to water	$[kg/m\ s^2]$
$P_{atmospheric}$	pressure due to air	$[kg/m\ s^2]$
Q	sediment transport	$[m^3/s]$
R	submerged specific gravity	$[kg/m^3]$
Sk	wave skewness	[-]
S_b	bed-level sediment transport	$[m^3/s]$
S_s	suspended sediment transport	$[m^3/s]$
t	time	[s]
T	wave period	[s]
u_l	long wave flow velocity	[m/s]
u_s	short wave flow velocity	[m/s]
u_t	total flow velocity	[m/s]
$\bar{u}$	mean currents	[m/s]
v	viscosity	$[kg/m\ s]$
w	the fall velocity of sediment in water	[m/s]
Y	Hankel matrix	[-]
z	bed-level	[m]
γ	wave breaker parameter	[-]
ϵ_b	efficiency parameter bed-level sediment transport	[-]
ϵ_s	efficiency parameter suspended sediment transport	[-]
θ	angle of waves	[°]
ρ_{sea}	density of the sea water	$[kg/m^3]$

(To be continued)

Symbol	Description	Unit
$\rho_{sediment}$	density of the sediment	$[kg/m^3]$
ω	wave frequency	[rad/s]
$tan(\phi)$	response angle of the beach	[°]

Sign	description	meaning
$\bar{x}$	over line	average over time
$\tilde{x}$	tilde	wave related component
x_0	lower 0	deep water sign
$\langle \, \rangle$	brackets	wave averaged
x'	qoute mark	transpose
$\lvert \, \rvert$	vertical bar	absolute

1

Introduction

1.1. Background information

Beaches and dunes are the natural defence line from the seas. Many people are living close to these coastal regions. Therefore, it is crucial to know what storms the beach can withstand and if the beach should be strengthened to be more resilient to the sea. However, it is not easy to determine how much sand there is at a beach, and how resilant a beach is for a storm. For instance, when a storm hits a coast, sediment moves from the shore to the sea. But when there are mild waves, the sediment is transported from the sea to the land, recovering the beach (Bascom, 1953; Shepard, 1950). How fast this process takes place depends not only on the hydrodynamics but also on the state of the beach and the sandbars (Coco et al., 2014). Wang et al. (2006) observed that a beach slope was able to recover after a hurricane, the upper part of the beach was able to recover in 90 days in Florida. Birkemeier (1979) observed that half of the eroded sediment during a storm was restored in a single day in New Jersey. Furthermore, Thom and Hall (1991) concluded that a beach at the south coast of Australia needed at least a couple of years to completely recover from a storm. How fast the beach is eroding during a storm and how long it takes for the beach to recover during calmer periods are crucial factors to predict how safe coastal regions are to inhabit.

Over the years, coastal engineers have developed different models to predict the sediment transport and shape of the beach. These different models serve different purposes(Amoudry and Souza, 2011). There are models that predicts an average beach profile over many years, for example the model of Bruun (1953) and Dean (1977). This model predicts a cross-shore bed level profile based on empirically equations. The empirically based equations provide an approximation for the bed level at certain depths. Still, they lack the more complicated bed level features.

Another example is the model that predicts how the complete beach behaves during different storms. Roelvink et al. (2009) used X-beach to predict the bed level erosion and aggregation in a wave flume over hours and for waves of 0.8 meters and was able to predict the bed level with a R^2 higher than 0.9. Spaans (2019) uses also a x-beach model to simulate onshore sediment transportation during calm conditions over the duration of a tide at the Dutch coast. The model was not able to accurately predict the bed level changes over days. The x-beach model underestimates the onshore transport of sediment (Spaans, 2019).

Lastly, there are models that focus on onshore sandbar migration over a timescale of hours during calm days (Fernández-Mora et al., 2015; Hoefel and Elgar, 2003; Hsu et al., 2006). These models predicted sandbar behavior over 3 hours intervals, based on different short wave processes. The models were able to predict bed level changes with reasonable accuracy at different locations. Fernández-Mora et al. (2015) showed that the model of Hoefel and Elgar (2003), that uses the acceleration differences below waves, was better at predicting the bed level changes closer to shore, but the Hsu et al. (2006), that uses the velocity below waves, model was able to better predict the bed level further offshore.

All of the above described models predict bed level changes with intervals over hours or more which, in this research, are considered as models with a large timescale. However, there have been observations that bed level is changing within minutes. Van Den Ende (2017), for example, used PIV measuring devices in a wave flume to show that sediment transport under a single wave event is dominated by flow velocities of the water. Puleo et al. (2014) observed

bed level at Perran Beach in Perranporth in the United Kingdom. Puleo et al. (2014) observed the swash zone and inner surf zone with a precision of 1mm on a timescale of a single wave and found that bed level changes are dominated by the differences of the flow velocity. This indicates that on a small time scale, bed level changes are dominated by velocity moments. Puleo et al. (2014) observed that bed level changes in the order of centimeters over minutes.

Nielsen and Shimamoto (2015) provide another example of a short timescale. They observed that a sandbar is able to respond to changing water levels within minutes in a flume experiment with a regular waves of 1.34 meters with a period of 7.9 seconds. The study of Nielsen and Shimamoto (2015) uses the data of a flume experiment, described by C. Kraus and Larson (1988). In that experiment, researchers changed the water level over time to simulate the tide. The sandbar that was between the surf zone and the shoaling zone was able to respond quickly and move to a new equilibrium within 15 minutes. This showed that bed level can respond in minutes to changes in the water level. (Nielsen and Shimamoto, 2015, p 3), in their conclusion, called "for more laboratory and field experiments with sufficient time resolution [...]". To see if the observations are visible in other situations.

Most of the above mentioned studies were based on a cross-shore profile. This is a simplified way of studying the beach. The problem of predicting beach behavior due to changing conditions has been challenging researchers for years Roelvink and Brøker (1993). This is because a beach system is complex in- and of itself, with short-waves, long-waves and water flow currents involved. Researchers try to simplify these processes in different ways to be able to study them.CERC (1984), for example, estimates long-shore sediment transport based on the power of waves and the angle at which these waves move towards the beach. By only including a single effect, the process of sediment transport is simplified.

Another simplification, which is used in different studies, is to separate the beach into two directions. These are the alongshore direction and the cross-shore direction. The alongshore direction is the direction parallel to the beach. The cross-shore is perpendicular to the beach. This simplification is granted if the beach acts along shore uniform. In this research the cross-shore effects are studied, therefore only the cross-shore profile is used.

1.2. Research question

The models described above are able to fairly accurately predict the bed level. However, these models are calibrated using data with large intervals between their measurements. This means that these models glance over changes that happen on a smaller timescale, i.e. minutes or seconds. Furthermore, Nielsen and Shimamoto (2015) argued that bed level was able to respond to changing water levels within minutes, meaning that the bed levels does change within minutes. Therefore, the question arises:

- How does the bed level behave on a time scale of minutes in the surf zone and the shoaling zone?

The models described in section 1.1 above use short wave induced sediment transport to predict the bed level changes (Fernández-Mora et al., 2015; Hoefel and Elgar, 2003; Hsu et al., 2006). Can short wave processes be linked to bed level changes? The models use two different methods of predicting the bed level, one model included the accelerations of the water flow (Hoefel and Elgar, 2003) and one that only included the water flow (Hsu et al., 2006). Both models were able to predict the sandbar migration (Fernández-Mora et al., 2015). Van Den Ende (2017) showed that on a small scale only velocity is important, therefore it is tested if a velocity based model is able to predict the observed changes.

- How well suited are short wave processes to predict bed level changes?

- How accurate is a velocity based model in predicting the bed level changes in the shoaling and surf zone?

1.3. Literature

1.3.1. Cross-shore zones

Cross-shore beaches are classified into different zones, based on the hydraulic processes and morphological processes. The cross-shore zones are classified based on the different waves. When waves move from deep water to the shore, they first move in to the shoaling zone, the reduced depth causes the waves to slow down and steepen. Waves break when they become too steep, and this happens in the breaker zone. The waves continue as white rolling waves (bores) towards the shore. This zone is called the surf zone. The swash zone is where these bores collapse. This research focuses from the shoaling zone to the surf zone, similar as Nielsen and Shimamoto (2015) observed the sandbar changes.
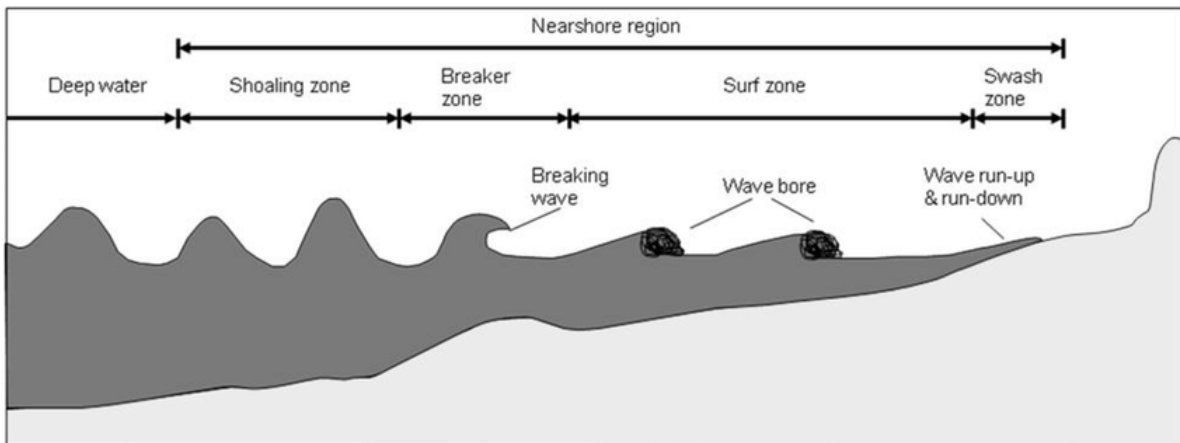
Figure 1.1: Shows a cross-shore beach with different zones, based on wave processes, (van Rooijen, 2011).

1.3.2. Hydrodynamics

In deep water the water surface consist of different waves. Munk (1951) classified the different waves based on energy and frequency. The classification is shown in figure 1.2. This research focuses on wind generated waves (short waves) and infra gravity waves (long waves), as these influence bed level changes on a small time scale (Van Den Ende, 2017). The waves in this paper are described by the linear wave theory.
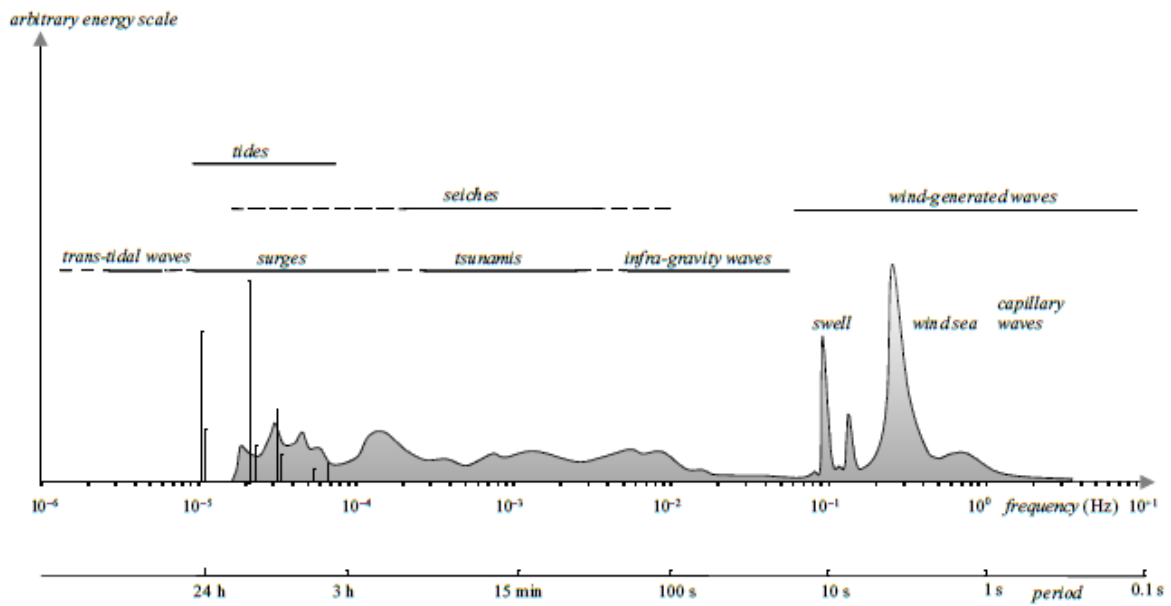
Figure 1.2: Wave energy is categorised into different frequencies. It shows the full energy spectrum that can be observed in a wavefield, Holthuijsen (2009) after Munk (1951).

The linear wave theory, which describes the deep waves and roughly the evolution of waves in the nearshore, is based on two equations: the mass balance equation and the momentum equation. The theory assumes that water is an ideal fluid, is incompressible, has a constant density, and has no viscosity. One of the results of the linear wave theory is a harmonic wave that describes water level elevation, water speed, and water acceleration. Figure 1.3 shows the water flow below a wave. The water flow effects decrease over depth.
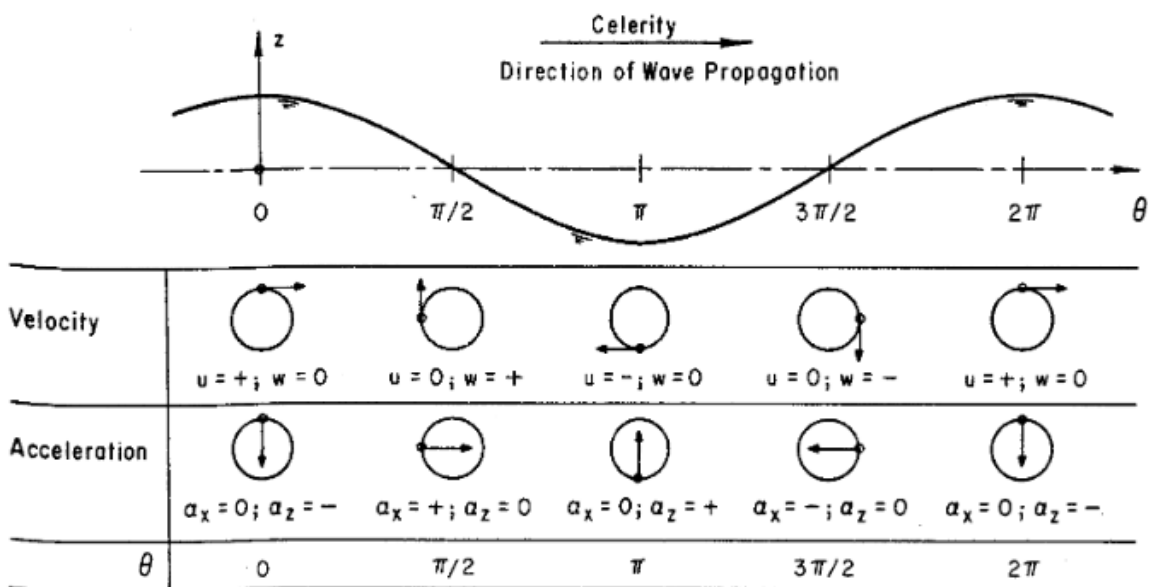
Figure 1.3: Describes harmonic wave elevations and the velocity below the wave and the acceleration below the wave, (CERC, 1984).

The hydrodynamics that drive bed level changes consist of three different water flows: short wave related flow velocity, long wave related flow velocity, and mean current (Mariño-

Tapia et al., 2007b; Van Den Ende, 2017), resulting in equation 1.1. In this section first the short waves related flow velocity will be discussed, secondly the long-waves related flow velocity is explained, and lastly the mean currents are elaborated.

$$u_t = \bar{u} + u_s + u_l \qquad (1.1)$$

When waves move from deeper water into shallower water, the orbital motion of the waves is effected by the limited depth. The shape and the height of the waves change as the waves move closer to shore; the waves become non-linear (Brinkkemper, 2013). Wave non-linearity is described by two different shape changes: the wave skewness and the wave asymmetry. In figure 1.4, the differences are shown. The skewed wave is characterised by a higher crest of the wave and a flatter, less deep, trough. The asymmetrical wave has a different distance between the crest and the trough.
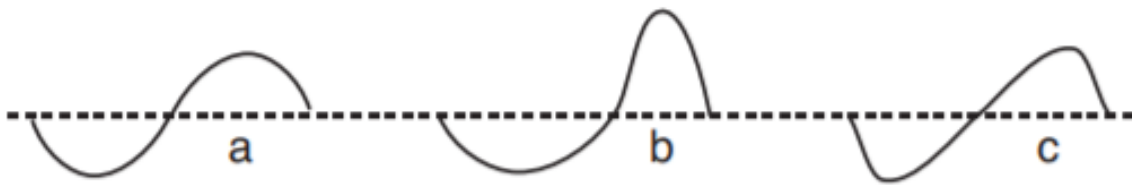
Figure 1.4: The dotted line is the average water level over distance; a is showing a harmonic linear deep water wave, b is a skewed wave, and c is an asymmetrical wave (Brinkkemper, 2013) .

When the shape of a wave changes, the velocity and acceleration change under this wave. When a wave is skewed, there is a difference between the velocity amplitude at the trough and the crest. The flow velocity is higher at the onshore directed flow during the crest. Wave asymmetry changes the acceleration, which becomes faster at the trough than the crest. The faster acceleration causes pressure differences, which in turn causes more sediment transport onshore (Drake and Calantoni, 2001)

The non-linear effect increases until a wave reaches a maximum height. Depending on the steepness, bottom slope, and the water level, a wave breaks (Battjes and Janssen, 1978). When it collapses, the skewness decreases and the asymmetry continues to increase towards the beach, the wave gets a sawtooth shape (Svendsen, 2006).

According to Short (1999) there are three different kinds of long waves in the nearshore: the edge waves, the bound long waves and the leaky waves. The edge wave is a long wave that is trapped in the nearshore and will cause alongshore differences (Short, 1999). These are ignored, as the aim of this research is the cross-shore effects. The bound long waves are generated by the incident short waves. The long bound waves have a set-down under groups of high waves and a set-up between the low wave groups (Mansard and Barthel, 1985). This means that during high waves there is an offshore directed flow of the long bound wave due to the trough, and during smaller waves there is an onshore directed flow of the long bound wave due to the crest. The leaky waves are long waves that are depended on the short waves, these wave can be reflected back from the beach (Short, 1999). Long-waves have smaller amplitudes than short waves therefore the flow velocity due to long-waves is smaller than short wave.
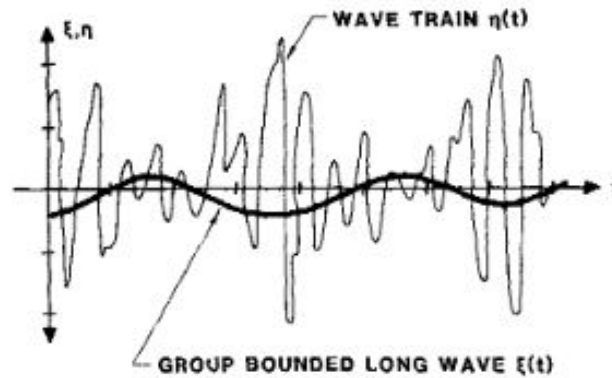
Figure 1.5: Representation of long bound waves, with short waves. The crest of the long wave is associated with the lower short waves and the trough is associated with the higher waves (Barthel and Funke, 1985).

In the nearshore waves generate different currents. The currents are flows in a single direction over time, referred to as mean currents. The mean current in the nearshore consisted of different flows: alongshore currents, the undertow, and stokes drift. Long shore currents are continues flows along the beach that occur due to non-perpendicular waves. The undertow is an offshore directed water flow near the bed. Stokes drift is caused by the depth difference between the crest and through of a wave. In this research only cross-shore effects are accounted for, and therefore undertow and stokes drift are explained in more detail.

When waves break, large amounts of water are transported towards the shore in the upper region of the water column (Svendsen, 1984), The broken waves can be described as hydraulic jumps moving towards the beach, called bores (Svendsen, 2006). To compensate for the water transported in the upper regions of the water column towards the shore, an offshore directed current is formed in the lower regions (Svendsen, 1984). The offshore directed current is called the undertow. The undertow is proportional to the energy dissipation of the waves when they break (Svendsen, 2006), and is the dominant process in the surf zone when waves are energetic (Russell and Huntley, 1999). Henderson and Allen (2004) observed that a sandbar was able to migrate closer to shore under breaking waves of 0.77 meters, and argued that closer to shore asymmetry can become dominant over undertow. Stokes drift is the result of water particles in the crest travelling with higher velocity onshore than the water particles in the trough travel offshore (Rijn, 2003). The result is that there is an onshore flow of water in the upper regions of the water. To compensate for this onshore flow, an offshore flow is formed in the lower part of the water column.
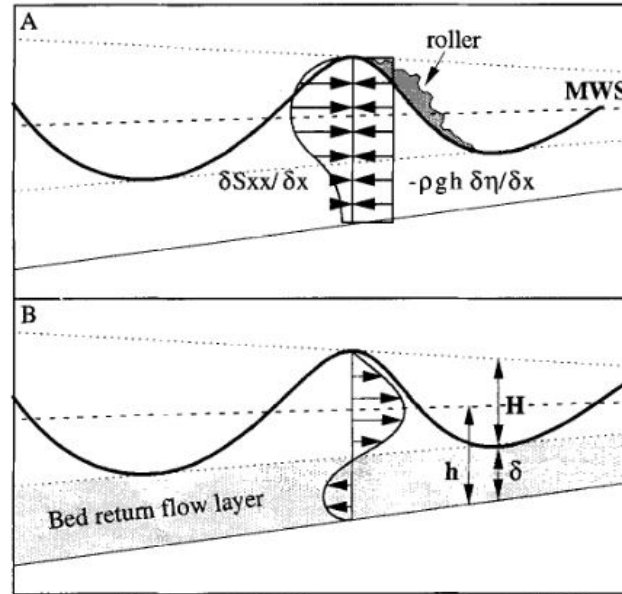
Figure 1.6: A) the effect of undertow, resulting in a near bed return current. B) the effect of Stokes drift (Masselink and Black, 1995)

1.3.3. Sediment transport

There are different methods to calculate sediment transport. Schoonees and Theron (1995) describe 10 different methods and compare them on their performance on two time scales; daily beach behavior and seasonal changes. In their results, the best group consist of: Bailard, Watanabe, Kriebel and Dean, and Larson and Kraus. The Bailard formula has been used in multiple studies to predict the bed level behavior of the surf zone with success (Fernández-Mora et al., 2015; Hoefel and Elgar, 2003; Hsu et al., 2006). Therefore the formula developed by Bailard and Inman (1981) is an suitable sediment transport formula.

Bagnold (1963) developed an energy-based model for sediment transport, based on the idea that sediment transport is proportional to the bed level friction. The bed level friction depends exponentially on the near bed flow velocity ((Jonsson, 1967) as seen in (Amoudry and Souza, 2011)). The model was developed initially for sediment transport in a downstream situation, for example in a river. Bowen (1981) rewrote Bagnold's work in order for it to predict wave-induced sediment transport. A year later, Bailard and Inman (1981) revised the model and added an efficiency factor. The model differentiates between suspended sediment transport and bedload transport. Suspended sediment transport are particles that travel in the water column, while bedload transport are particles that travel over the bed. Guza and B. Thornton (1985) showed that bedload transport depends on the third-order velocity moment and that the suspended sediment transport depends on the fourth-order velocity moment. There is a distinction between the two because sediment travels with different efficiencies. This means that:

$$\langle S_b \rangle \propto \langle u_t |u_t|^2 \rangle \tag{1.2}$$

$$\langle S_s \rangle \propto \langle u_t |u_t|^3 \rangle \tag{1.3}$$

A limitation of this method from Bailard and Inman (1981) is that it only includes velocity to predict bed level changes. However, as the waves changes shape the acceleration of the water changes. Drake and Calantoni (2001) showed that there can be sediment transport due to asymmetry. Hoefel and Elgar (2003) showed that onshore sediment transport depends on this acceleration. Fernández-Mora et al. (2015) showed that closer to shore the acceleration becomes more important. Still, Van Den Ende (2017) used high resolution experiment in a flume and showed that in the surf zone, sediment transport depends on the near bed velocity.

She showed that sediment transport is for 50 % depended on the short waves velocity, for 30 % on the mean currents and for 20 % on the long wave velocity, and found no influence by accelerations. Therefore velocity gives good results for sediment transport. The bed of the beach consists of sediment. The bed level changes when there is a difference of sediment moving in to and from a location. Therefore, bed level is directly influenced by the differences of sediment transport at a cross-shore profile.

1.3.4. Cross-shore velocity moments over a profile

Different studies (Mariño-Tapia et al., 2007b; Russell and Huntley, 1999; Tinker et al., 2007) have monitored flow velocities near the bed level on different beaches. Russell and Huntley (1999) collected their data on three beaches that where alongshore uniform and had no bars. the gradient of the beaches varied between 1° and 5.4° degrees. The tide at these beaches was semi diurnal, with a water level difference of more than 4 meters. The waves varied at the beaches between 1 and 3 meters, the largest alongshore current measured at the different beaches was 0.5 m/s, and the sensors were installed 0.1 meter from the bed level. The observations were done using intervals of 17 minutes to determine the first shape function. Russell and Huntley (1999) normalised the flow velocity with the method suggested by Bailard (1982) and Doering and Bowen (1987). They used the stirring of the waves and currents to make the flow velocity independent of the wave energy. The normalised flow velocity made it possible to see if there is a constant pattern for flow velocities at different cross-shore beaches. Russell and Huntley (1999) found there was a consistent pattern between flow velocity and the relative depth based on the breaking depth. Mariño-Tapia et al. (2007b) expended the data set using five different beaches. The average beaches slopes varied between 6° and 4.5° degrees, two of the beaches contained sandbars. Waves varied between 0.16 meters and 2.5 meters, and there was one location that had alongshore currents larger than 1 m/s. Mariño-Tapia et al. (2007b) expended the shape function to the complete cross-shore profile. Tinker et al. (2007) tested the shape function on beaches in France and England. During the experiment in France, the measurements were taken at the top of a sandbar. The results are in line with the shape function of Mariño-Tapia et al. (2007b).The results of Mariño-Tapia et al. (2007b) are shown in figure 1.7 and 1.8. This shows that the shape function is a method that can solve the complex hydrodynamics at a cross-shore beach profile.
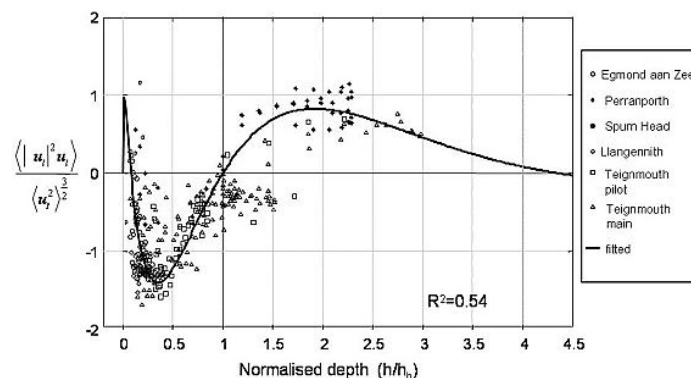
Figure 1.7: The third-order velocity moment for bedload transport, normalised and plotted against normalised depth. The x-axis shows the normalised depth over the cross-shore profile, and the y-axis is the third-order velocity moment for bedload transport normalised. Positive values of the y-axis make for onshore directed flow, while negative values make for offshore directed flow. The points in the plot are the different values found at different beaches (Mariño-Tapia et al., 2007b).
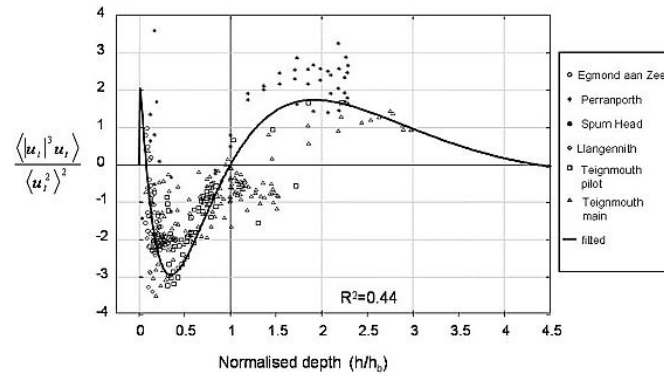
Figure 1.8: The fourth-order velocity moment for bedload transport normalised and plotted against normalised depth. The x-axis shows the normalised depth over the cross-shore profile, and the y-axis is the fourth-order velocity moment for bedload transport normalised. Positive values of the y-axis make for onshore directed flow, while negative values make for offshore directed flow.The points in the plot are the different values found at different beaches (Mariño-Tapia et al., 2007b).

Because sediment transport depends directly on flow velocity moments, the shape functions gives a similar shape for sediment transport. The pattern of the shape function is similar to the pattern seen in figure 1.10. Mariño-Tapia et al. (2007b) used the shape function to describe on a planar beach, to describe sandbar migration patterns 1.9. In figure (a) the creation of a sandbar is shown, as there is onshore sediment transport before the breaking point due to wave non-linear effects and offshore sediment transport due to undertow. In figure (b) and (c) the responses of the beach profile are sketched if the wave point changes. Mariño-Tapia et al. (2007a) used the shape function to predict sandbar migrations during the Duck 1994 experiment. The shape function was able to predict the sandbar migration between days over a period of 77 days with a correlation of 0.84.
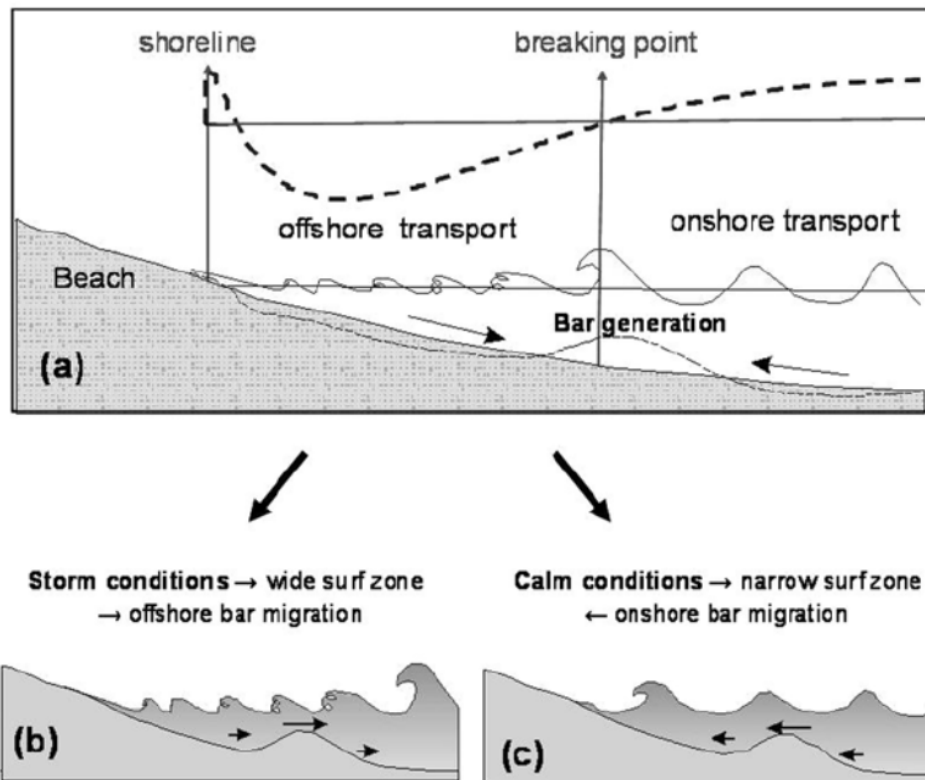
Figure 1.9: Figure a shows the sediment transport and bed level response at a cross-shore beach by the shape function. Figure b shows the offshore migration when waves break further offshore. Figure c shows the onshore migration when waves break closer to shore (Mariño-Tapia et al., 2007b).

The research of Mariño-Tapia et al. (2007b) showed that the shape function matches different conditions. Mariño-Tapia et al. (2007a) stated that the shape function can be used to predict bed level changes over time. The shape function is depended only on the breaker depth. However, there are three reasons why this method should be applied with care. Firstly, Masselink and Russell (2006) showed that velocity moments are not suited to predict bed level changes in the swash zone, as errors from the swash zone will grow and disturb the rest of the profile over time. Secondly, Mariño-Tapia et al. (2007a) explained that the method does not predict sediment transport correctly in the trough of a sandbar. Thirdly, when there are strong three dimensional effects, the model is also incapable of predicting the bed level accurately, as these three dimensional effects become dominant over the shape function (Mariño-Tapia et al., 2007a).

1.3.5. Short wave processes and bed level behavior
In section 1.3.3, the Bailard and Inman (1981) formula was explained. This formula depends on the near bed flow velocity moments to predict sediment transport. In section 2.2, the near bed flow velocities are explained and it is shown that the total velocity depends on different complex processes. This makes it difficult to compute sediment transport. However, Masselink et al. (2006) explained, based on different field studies, that there is a general pattern in sediment transport based on wave processes. Masselink et al. (2006) described how wave processes are depended on relative wave height, and that there is a generally observed sediment flow associated with these processes, as seen in figure 1.10.
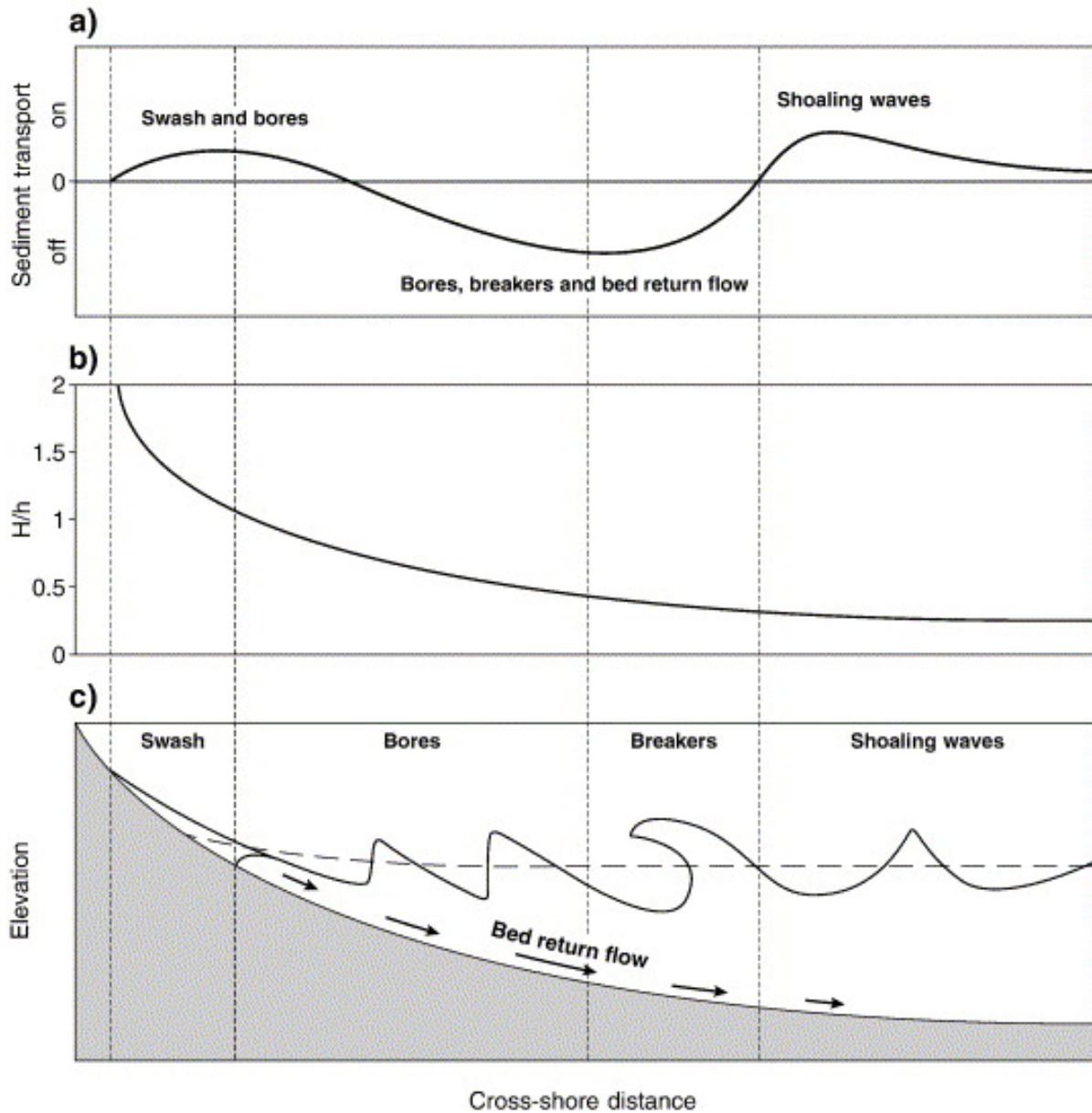
Figure 1.10: figure a), shows the sediment transport direction and possible magnitude of sediment transport on the y-axis. The x-axis shows the cross-shore distance. Figure b) shows relative wave height development over a profile with increasing values closer to shore. Figure c) shows the beach and different waves. This is a sketch of sediment transport under various processes and is only conceptual (Masselink et al., 2006).

Wave processes	Relative significant wave height
Shoaling waves	> 0.3
Breaking waves	0.3 - 0.5
Bores	0.5-1
Swash	< 1

Table 1.1: Classification of wave processes based on the significant relative wave height, based on Masselink et al. (2006),

1.4. Hypotheses

Based on the literature and background information there is an expected result . This is presented here as the hypothesis, per question stated in section 1.2 and explained why, and the hypothesis will be tested to see if it holds.

How does the bed level behave on a time scale of minutes in the surf zone and the shoaling zone?

Nielsen and Shimamoto (2015) showed that under a single wave climate a sandbar is able to keep up with the changing water level. Nielsen and Shimamoto (2015) observed that the bed level at the sandbar was able to change 0.5 meter during a single tide. However in the field study there is a wider wave field, this will decrease the response time of the bed level (Nielsen and Shimamoto, 2015). During the fieldwork the bed level will be observed and particularly at a sandbar, this will cause that the changes can be smaller than the changes in observed near at the sandbars. Nielsen and Shimamoto (2015) observed bed level moves with significant amounts in minutes, and it responses to changes in water level. Therefore in a field study a tidal signal will be observed in the bed level.

It is expected that the bed level moves with the tide, and there is a erosion and aggregation pattern visible of at least 10 centimeters when the tide passes over.

How well suited are short wave processes to predict bed level changes?

Masselink et al. (2006) linked sediment transport for a planar beach directly to short wave processes. If that is the case, then bed level changes in line with the sediment transport will be observed under the different wave processes. Since Masselink et al. (2006) used different relative wave height to identify different wave processes, there should be a pattern between bed level changes and relative wave height. Figure 1.11 is an alteration of the figure 1.10 to link sediment transport to relative wave height and link the sediment transport differences to bed level changes. The bed level should behave similar to this pattern. Here, large sedimentation rates are expected between the shoaling waves and breaking waves, and slow erosion rates for the rest of the wave process excluding the swash zone.
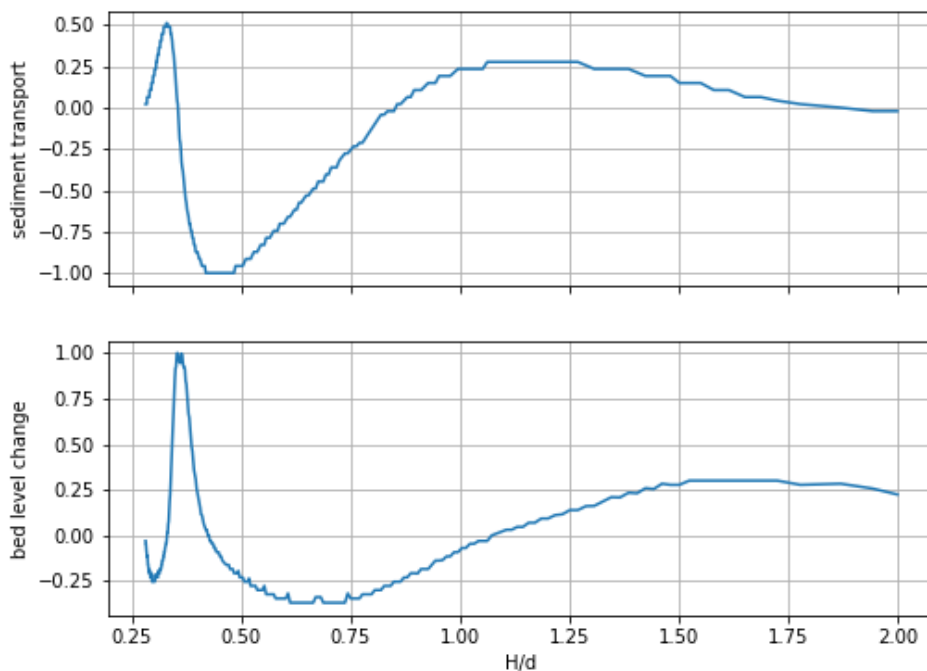
Figure 1.11: The top panel gives the relative sediment transport based on the relative wave height, the figure below gives the relative bed level change. The x-axis is the relative wave height, based on (Masselink et al., 2006).

There is a clear distinction between erosion and aggregation visible for different relative wave heights, and the average bed level change is within 5 % to the bed level change predicted by figure 1.11.

How accurate is a cross-shore velocity model able to predict the small scale bed level changes in minutes?

Wave breaking is depended on the water depth (Battjes, 1974). Therefore, if the tide

changes, the location where waves break also changes. Mariño-Tapia et al. (2007b) showed that the velocity moments at a cross-shore profile depend on the depth where waves break. Therefore, the velocity moments keep changing due to the tide. Guza and B. Thornton (1985) showed that sediment transport is directly proportional to the velocity moments. bed level changes are depended on the sediment transport. Nielsen and Shimamoto (2015); Puleo et al. (2014) observed that bed level changes on a time scale of minutes. Mariño-Tapia et al. (2007b) made a situation sketch for a planar beach, figure 1.9 (a) showing erosion in the shoaling zone, aggregation where the waves break, and erosion closer to shore. When the tide is passing over a location and the waves stay reasonable stable, the bed level should have a pattern of erosion and aggregation based on the short waves above.

Since Van Den Ende (2017) observed that in the surf zone sediment transport depends on velocity. Furthermore, the shape function can be used to provide near bed velocity moments during different conditions. A cross-shore model that uses the shape function should be able to predict the small bed level changes with a linear relation to the observations.

To test the relation between the observations and the predictions, correlation is used. Correlation measures the linear relationship between two signals. The Pearson correlation is used in this research. The correlation coefficient shows the strength of the relation between the signals. The rule of thumb with correlations according to Hinkle et al. (2003) correlations are: if a correlation between 1 and 0.9 is found, the signals are very highly correlated; if a correlation between 0.9-0.7 is found the signals are highly correlated; if a value between 0.7 and 0.5 is found the signal is moderately correlated; between 0.5 till 0.3 is low correlation and 0.3 till 0 little to no correlation. Negative values mean a negative relation.

The cross-shore model that only uses flow velocity is able to predict the bed level changes with a correlation of at least 0.3.

1.5. Research approach

To answer the central question. The research is divided into several chapters. In chapter 2, the setup of the model is described in greater detail. This model includes four different modules which are; the input module, the hydrodynamic module, the sediment transport module, and the morphology module. The data, collected from the fieldwork, is explained and analysed in chapter 3. In order to see if the model is able to predict bed level changes with accuracy, input conditions of the fieldwork conditions are needed. How this input is gathered will be explained in chapter 4. The results will be presented and compared in chapter 5. All of the information and results will be discussed in chapter 6, followed by a conclusion and recommendation for future research. The framework of the research is presented in figure 1.12.
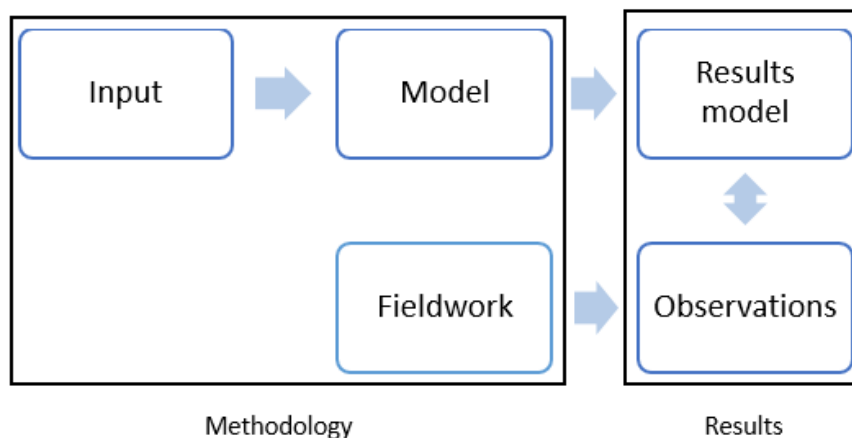
Figure 1.12: The overview of the research.

<div style="text-align: right">

2
Model

</div>
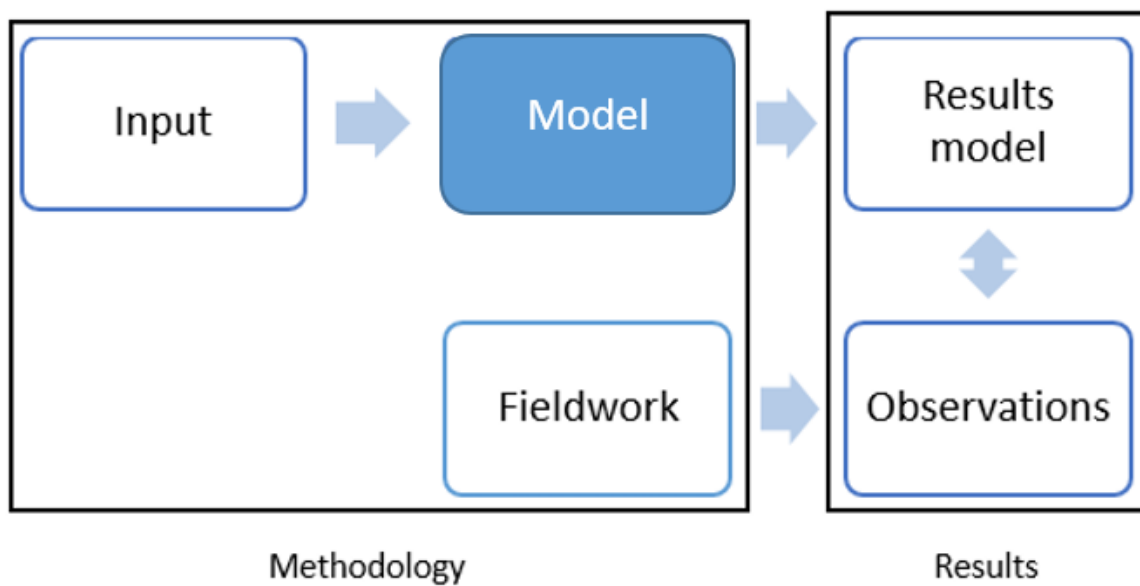
Figure 2.1: The chapter will cover the model.

Before the hypothesis can be tested, as suitable model needs to be developed. The model used in this research will theoretically describe how the bed level should respond to hydro-dynamic conditions on a small timescale. The model is a basic 1-D cross-shore model that only includes cross-shore wave processes.
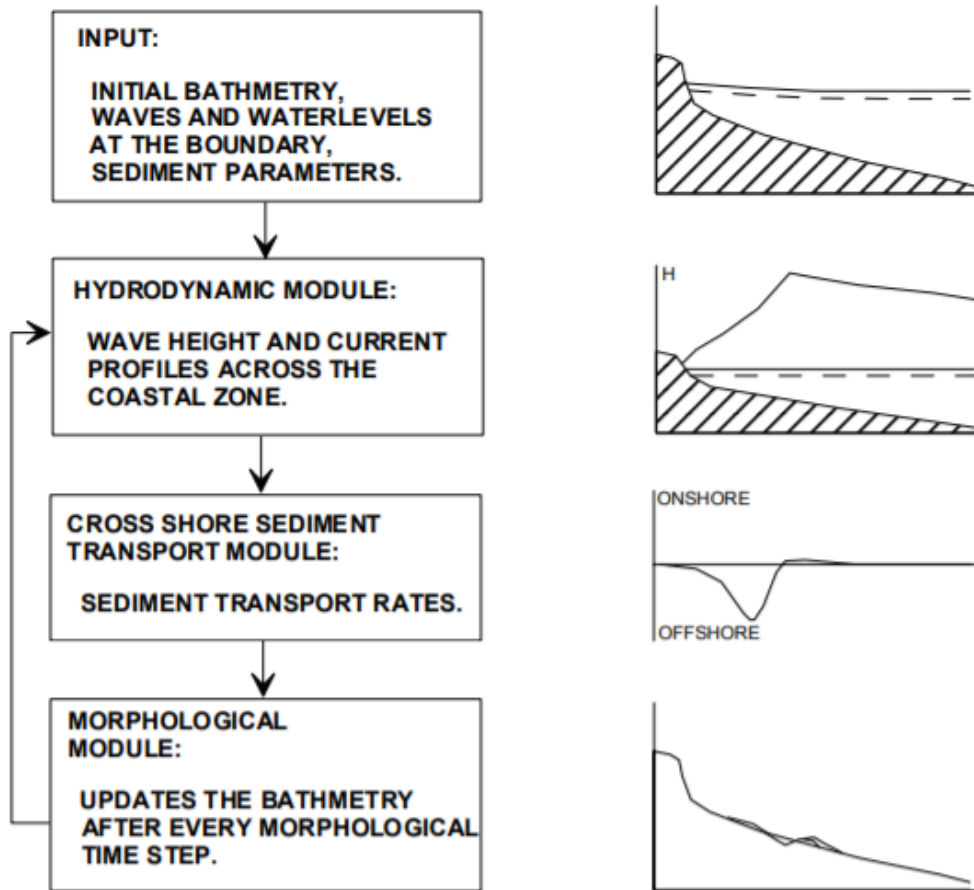
Figure 2.2: The diagram of the cross-shore model. The different boxes show the different modules that need to be resolved before the next module can be resolved. Arrows show how the model moves from module to module. Figures next to the boxes show the result after every module (Grasmeijer, 2002).

Figure 2.2 shows the principles of the cross-shore model. The boxes represent different steps in the model. The model starts with the input conditions and boundary conditions. The initial conditions, together with the boundary conditions, will be used to determine the hydrodynamics in this model. The sediment transport will be determined on the outcome of the hydrodynamics. The differences in sediment transport over the cross-shore model will induce morphological changes that will change the bed level. The bed level is updated to these changes, and the model will run again. In this chapter, every step of the model is described in detail.

2.1. Input module

The first step of the model is to define the input conditions. The input conditions are unique conditions to a particular case. The input conditions for this model consist of the initial bathymetry, the waves during the run of the model and the parameters.

2.1.1. Bed level profile

The initial bed level profile is the bed level at the beginning of the simulation. The bed level profile consists of different depth readings over a cross-shore distance. The cross-shore bed profile will be explained with bathymetry measurements of the Sand Engine made by De Zeeuw et al. (2017) (figure 2.3).
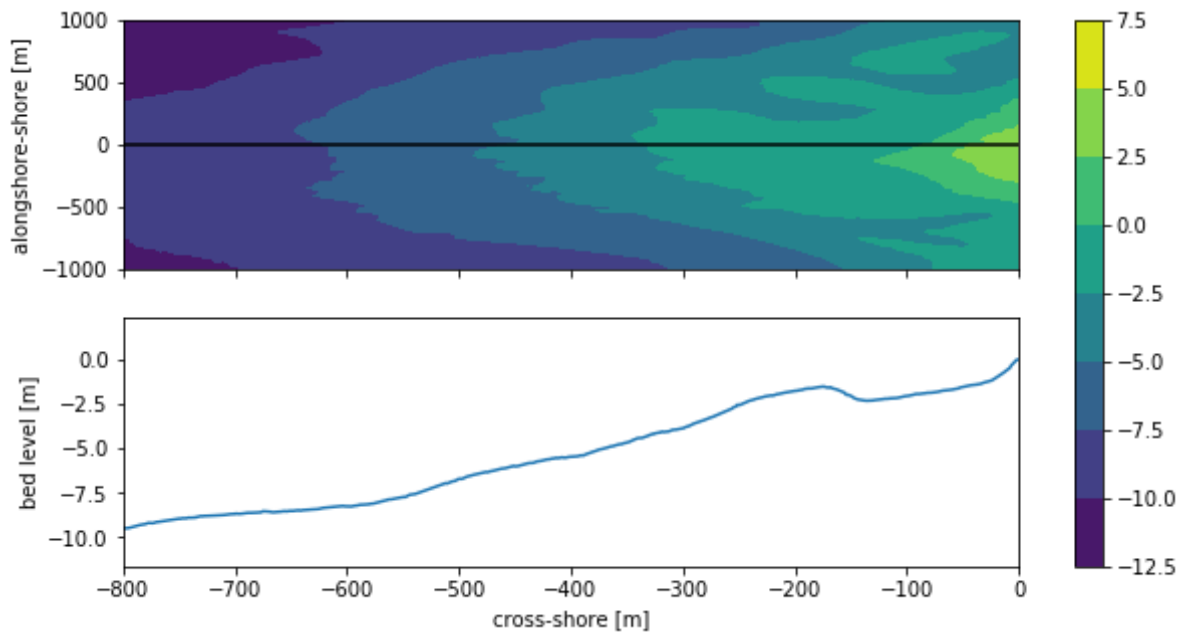
Figure 2.3: The figure above is the observation of a beach in alongshore direction and cross-shore direction. In the top panel the y-axis is the alongshore distance in meters, while the x-axis is the cross-shore distance in meters. The elevation of the bed level is shown in different colours. The associated depth in meters of each colour is presented in the bar on the right side. The panel below is the black line that shows the bed level profile in the cross-shore direction, in which the y-axis displays the bed level depth in meters.

2.1.2. Boundary conditions
The model is used too simulate what is happening in its domain with the bed level, however the model is influenced by what is happening at the edges. These edges are the boundary conditions. The 1D cross-shore model has two different boundaries, which are the water level elevation boundary and bed level boundary. The water level elevation boundary consists of the tide influencing the water level, and the waves that change over time which drive the processes in the model. The offshore bed level boundary is assumed to be stable during the simulation. The other bed level boundary is at the beach where it is assumed that there is no sediment transport above water. The boundary conditions, which are needed to simulate the bed level, consist of a tidal signal over time and significant waves characteristics over time.

2.1.3. Parameters
Parameters are values that are estimates and can vary at different beaches and conditions. In this model, there are multiple parameters. Most of the parameters will be derived from literature, and others will come from fieldwork (table 2.1).

Parameter	Symbol	Value
Hydrodynamics		
Wave breaker	γ	0.5 - 0.9 (Holthuijsen, 2009)
Sediment transport		
Drag coefficient	C_f	0.003 (Gallagher et al., 1998)
bed level transport efficiency	ϵ_b	0.15 (Gallagher et al., 1998)
Suspended transport efficiency	ϵ_s	0.01 (Gallagher et al., 1998)
Response angle of the beach	$tan(\phi)$	0.53 (Gallagher et al., 1998)
Drag constant	C_1	20 (Ferguson and Church, 2004)
Friction constant	C_2	1.1 (Ferguson and Church, 2004)
Morphology		
Porosity	n	0.4 (Luijendijk et al., 2017)

Table 2.1: Parameters used in the model

2.2. Hydrodynamics

After the input conditions are known, different processes are used to predict the changes over time. The first step is to determine the hydrodynamics. The hydrodynamics consists of two parts. The first part describes how the waves are propagating over the profile. The second part describes the transformation of waves to velocity estimates. The velocity estimates are needed for the next step to estimate sediment transport.

2.2.1. Waves

When simulating waves over a cross-shore profile, it is crucial to know which processes are important. In this research, the model is designed for nearshore coastal water based on significant wave height. The significant wave height is the average wave height of the highest one third of the all the waves. The most dominant processes in the nearshore are refraction/shoaling and depth induced breaking (Holthuijsen, 2009). These are the only processes that will be included in the cross-shore model.

Process	Oceanic waters	Shelf seas	Nearshore	Harbour
Wind generation	•••	•••	•	○
Quadruplet wave–wave interactions	•••	•••	•	○
White-capping	•••	•••	•	○
Bottom friction	○	••	••	○
Current refraction / energy bunching	○/•	•	••	○
Bottom refraction / shoaling	○	••	•••	••
Breaking (depth-induced; surf)	○	•	•••	○
Triad wave–wave interactions	○	○	••	•
Reflection	○	○	•/••	•••
Diffraction	○	○	•	•••

••• = dominant, •• = significant but not dominant, • = of minor importance, ○ = negligible.

Figure 2.4: Table of the processes involved in waves computations at different locations, and their influence (Holthuijsen, 2009).

The wave height over a cross-shore profile depends on shoaling and refraction and depth induced breaking. The wave height due to shoaling and refraction is determined with the

linear wave theory. This theory gives errors when estimating waves in transitional water depth and shallower waters as waves do not behave linear. However, it often predicts the wave characteristics with good accuracy (Masselink and Black, 1995; Plant et al., 2001). The wave height due to wave breaking is determined with the expression of Battjes (1974). The overall wave height is determined as a minimum value of the wave height due to shoaling and refraction and depth induced breaking.

$$H_{sr} = K_{sh} K_{ref} H_0 \tag{2.1}$$

$$H_{br} = \gamma d \tag{2.2}$$

$$H = min(H_{sr} H_{br}) \tag{2.3}$$

H_{sr} is the wave height depending on the shoaling and refraction processes, K_{sh} is the shoaling coefficient, K_{ref} is the refraction coefficient and H_0 is the wave height where the small zero indicates the deepwater value. γ is the breaker parameter, d is the local water depth and H_{br} is the maximum wave height before depth induced breaking. H is the local wave height

Shoaling happens when waves enter shallower water. The decreased depth causes the wave to reduce speed. Wave shoaling occurs when waves are in transitional depths. Waves are in transitional depth when the water depth divided by wavelength is less than 0.5 and more than 0.05. When waves shoal, their energy fluxes remains the same if energy loss is smaller than the speed reduction. The energy flux and energy of a wave is described by equation 2.4 and 2.5. Showing that when the speed decreases the wave height must increase so that the energy flux can remain constant, this effect is called shoaling.

$$F = E c_g \tag{2.4}$$

$$E = \frac{1}{8} \rho_{sea} g H^2 \tag{2.5}$$

F is the energy flux of the waves per meter. E is the energy of the wave. c_g is the group velocity of the wave. $\rho_s ea$ is the water density, g is the gravitational constant.

When waves are shoaling, the wave speed in transitional water depth should be determined. Wave speed can also be estimated with the linear wave theory (Airy, 1845). This theory estimates wave speed in transitional water depth based on a relation between wave frequency and wavelength, called the dispersion relation. The dispersion relation is an iterative process as wavelength depends on wavelength. Therefore the iteration is performed until a stable wavelength is found, meaning that the length of waves changes less than a millimetre per iteration.

$$L = \frac{gT^2}{2\pi} tanh(\frac{2\pi d}{L}) \tag{2.6}$$

Where L is the wavelength, T is the wave period.

The dispersion relationship gives the characteristics of the waves at transitional depths. The characteristics are used to estimate the wave celerity and the group wave celerity. The group wave celerity is used to determine the wave height increase due to shoaling.

$$k = \frac{2\pi}{L} \tag{2.7}$$

$$c = \sqrt{\frac{g}{k} tanh(kd)} \tag{2.8}$$

$$c_g = \frac{1}{2}(1 + \frac{2kd}{sinh(2kd)}) \qquad (2.9)$$

$$K_{sh} = \sqrt{\frac{c_{g0}}{c_g}} \qquad (2.10)$$

Where k is the wavenumber, c is the wave celerity.

Wave refraction happens as waves are moving slower in shallower water. When waves travel at an angle to the beach, the wave is at different depth over the length of the waves. The different depth causes the waves to turn to a more incident angle. This turning causes the waves to decrease in height over the profile.
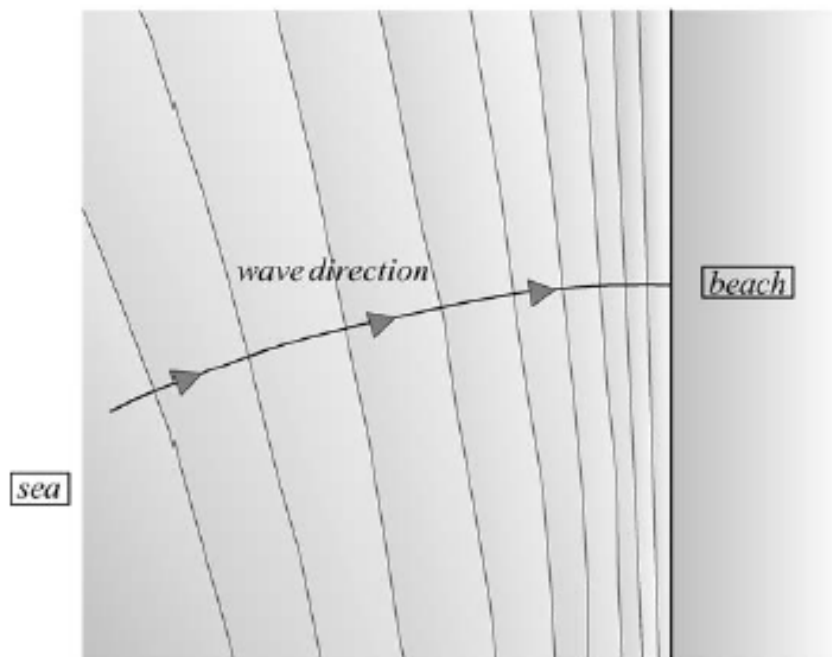
Figure 2.5: The angle turning of the waves when moving into shallower water (Holthuijsen, 2009).

$$sin(\theta) = \frac{c}{c_0} sin(\theta_0) \qquad (2.11)$$

$$K_{ref} = \sqrt{\frac{cos(\theta_0)}{\theta}} \qquad (2.12)$$

Where θ is the angel of the wave

Waves break when the they become too steep. Battjes (1974) found that maximum wave height depends on a ratio between the wave height and the depth. When a wave exceeds the ratio, the wave breaks. Battjes (1974) used a parameter to express this ratio γ, the breaker parameter. There have been different studies that show that the breaker index varies over different beaches. For instance, Battjes (1974) stated that the best result is gained with $\gamma = 0.8$, while Masselink et al. (2006) stated that significant waves break between $0.3 < \frac{H}{d} < 0.5$. Different values for gamma are found when using different waves for instance significant

wave gives a different value than the root mean square wave. The distribution of waves also effects the breaker parameter. The wave breaker parameter will be determined based on fieldwork based on the significant wave height, as this will provide the most accurate value. This is needed as the model depends significantly on the breaker depth.

There are limitations when estimating the waves over a profile using linear wave theory and depth induced wave breaking. When, only depth induced breaking is included to reduce wave height. However, there are more processes involved in waves in coastal waters. According to Holthuijsen (2009), bottom friction, current refraction, triad wave interactions and reflection are significant as well for wave height. However, to keep the model simple, we exclude these from the wave module. Due to the ignoring the energy losses, this can lead to deeper wave breaking depths. The use of linear wave theory, while waves are non-linear, is known to cause errors. However, it often predicts the wave characteristics with good accuracy (Masselink and Black, 1995; Plant et al., 2001).

2.2.2. Shape function

As was explained in section 1.3, the shape function will be used to determine sediment transport. The full shape function is derived from the observations made by Mariño-Tapia et al. (2007b) and is presented in equation 2.13 and 2.14. Mariño-Tapia et al. (2007b) also derived the velocity moments for the gravitational terms. However, when (Mariño-Tapia et al., 2007a) used the shape function to predict sand bar migration, they ignored the gravitational terms and explained that this would not have large effects on the bed level predictions and thus can be ignored. Therefore in this research, they are also ignored.

$$\langle|u_t^2|u_t\rangle = (sin(2\pi(\frac{d}{d_b})^{0.275})1.9(\frac{d}{d_b})^{0.14}e^{-0.45\frac{d}{d_b}})\langle u_t^2\rangle^{3/2} \tag{2.13}$$

$$\langle|u_t^3|u_t\rangle = (sin(2\pi(\frac{d}{d_b})^{0.275})4(\frac{d}{d_b})^{0.14}e^{-0.45\frac{d}{d_b}})\langle u_t^2\rangle^2 \tag{2.14}$$

The $\langle|u^2|u\rangle$ the equation for the third-order velocity moment. $\langle|u^3|u\rangle$ is the fourth-order velocity moment. Here d is the local water depth, d_b is the breaker depth and u_t is the total near bed velocity. The total near-bed velocity is used to unnormalize the shape function.

The flow velocities were normalised by dividing them by the stirring term, $\langle u_t^2\rangle^n$, following the method of Bailard and Inman (1981) and Doering and Bowen (1987). The depth was normalised by dividing the local depth by the breaker depth. To use the shape function to determine velocity moments, depending on the depth, the shape function needs to be unnormalized.

The shape function can be unnormalized with the total flow near the bed and the breaker depth. The breaker depth was derived in section 2.2.1 This is the deepest part where breaking waves are lower than shoaling waves. The total water velocity near the bed consists of three different components, as was explained in section 1.3 Mariño-Tapia et al. (2007a) used the mean currents and short wave oscillations to unnormalize the shape function. This will be done in similar fashion.

$$u_t = \bar{u} + u_s + u_l \tag{2.15}$$

When the total flow velocity is filled into the stirring term, the equation 2.15 becomes squared and averaged over wave groups. However, when first-order oscillatory components are wave averaged, they become zero. The term $\langle u_s u_l\rangle$ is negligible according to (Mariño-Tapia et al., 2007a; Russell and Huntley, 1999). This results in equation 2.16, which is used to normalise the shape functions flow velocity.

$$\langle u_t^2\rangle^n = (\bar{u}^2 + \langle\tilde{u_s}^2\rangle + \langle\tilde{u_l}^2\rangle)^n \tag{2.16}$$

now expressions are needed for the mean current, the short wave flow velocity and the long wave flow velocity.

The mean current of the total near-bed flow are the bed return currents, as was explained in section 1.3. Masselink and Black (1995) developed a method to estimate the near-bed flow velocity of bed return currents depending on the breaker parameter and depth and deep water wave height. The expression was able to predict bed return currents flow velocities with an accuracy of 10-20 percent of the observations in the surf zone (Masselink and Black, 1995).

$$\bar{u} = \frac{\frac{1}{8}\sqrt{\frac{g}{d}}\gamma^2 d}{1 - \frac{\gamma}{2}}(\exp-(\gamma\frac{d}{H_0})^2) \tag{2.17}$$

The short-wave oscillations are estimated based on linear wave theory, similar to Mariño-Tapia et al. (2007a). However, in shallow water waves behave non-linearly, and linear wave theory is considered unsuitable for predicting wave characteristics. However, Plant et al. (2001), showed that near-bed velocities in the surf zone are determined with correlations of R = 0.99 using linear wave theory.

$$\tilde{u_s} = \sqrt{(\frac{H}{2}\sqrt{\frac{g}{d}})2} \tag{2.18}$$

The oscillatory part of long-waves is not included. Grasmeijer (2002) stated that there is a need for further research before long-waves flows can be estimated successfully. However, the shape function includes all flow effects in the magnitude and direction of flow, because of that the effect of long waves can still be present in the flow momentum expression (Mariño-Tapia et al., 2007b) . Still, the velocities will be underpredicted because of the lack of long-waves. Van Den Ende (2017) showed that 80 per cent of the sediment transport is related to the short wave processes and the mean currents.

There are limitations to this shape function. Firstly, Hoefel and Elgar (2003) modelled sandbar migration based on wave asymmetry induced sediment transport due to flow acceleration skewness. The shape function is based only on flow velocity due to wave skewness, thereby ignoring the flow acceleration. However, it is still debatable as Hsu et al. (2006) also successfully predicted sandbar migration based on the velocity of flow. Fernández-Mora et al. (2015) tested both methods and showed that the Hoefel and Elgar (2003) system was a better method for the shallower regions of the profile. Wave asymmetry keeps increasing towards the shore as wave skewness is decreasing after wave breaking; this increases the effect of wave asymmetry induced sediment transport closer to shore. Secondly, when beach profiles contain more bars, there can be multiple breakpoints as waves break on the crest of the bar and in the trough, when the depth increases the waves re-shoal. The shape function can predict offshore transport in the through due to less depth than the breaker depth while studies have shown that in the trough of a sand bar there is onshore sediment transport (Thornton et al., 1996)). However, Tinker et al. (2007) tested the shape function on a bar of a beach and found velocity moments that were in line with the shape function. Thirdly, the shape function is only valid when undertow is the dominant mean flow. When there is a 3-D cell circulation, different processes are dominant to the shape function Mariño-Tapia et al. (2007b).

2.3. The sediment transport module
In this step, the velocity moments derived in the previous step are used to determine the sediment transport over the cross-shore profile.

2.3.1. The Bailard function
The complete function of Bailard includes a gravitational term and as was explained in section 2.2.2. Here, the gravitational term is ignored, which leads to the simplified formula for the Bailard function, as is shown in equation 2.19.

$$Q = \frac{\rho_{sea}C_f}{(\rho_{sediment}-\rho_{sea})g}(\frac{\epsilon_b}{tan(\phi)}\langle|u_t^2|u_t\rangle + \frac{\epsilon_s}{w}\langle|u_t^3|u_t\rangle) \tag{2.19}$$

Where Q is the sediment transport. $\rho_{sediment}$ is the density of sediment. C_f is the drag coefficient. ϵ_b is the parameter of the bed transport. ϕ is the sediment angle of response. ϵ_s is the parameter of the suspended transport. w is the fall velocity of sediment.

During the fieldwork, there were no samples taken of the sediment. However, the Sand Engine is a frequently studied place. From a recent paper, the sediment characteristics are used. The median sand diameter found at the intertidal part of the beach at the tip of the Sand Engine is 378 µm (Pit et al., 2020). The median sand diameter is needed to determine the fall velocity of the sediment in the water. Sediment fall velocity can be determined for a spherical object through the water with Stokes' law. However, when particles are more coarse, the settling speed can change due to the turbulent drag and friction that slows the particle. Ferguson and Church (2004) combined both these equations to a simple universal formula that can be used for sediment fall velocity equation 2.20.

$$w = \frac{Rgd_{50}}{C_1 v + \sqrt{0.75C_2Rgd_{50}}} \tag{2.20}$$

R is the submerged specific gravity, d_{50} is the median sand diameter. v is the kinematic viscosity of the seawater, the viscosity of the water at 17 Celsius is 1.0804 kg/ms. C_1 and C_2 are constants. When using a median grain diameter, it is recommended to use C_1 and C_2 as 20 and 1.1 (Furgeson and Church (2004), Raudkivi (1990)).

The Bailard functions have different parameters. The parameters are set to similar values of the ones found by Gallagher et al. (1998) to describe the duck 1994 experiment. The sediment diameter during the duck 1994 experiment varied between 250 and 120 µm, which differs from that of the Sand Engine. However, these are believed to give realistic sediment transport values. Changing the the parameters will only lead to larger or smaller bed level changes, and not the pattern.

2.4. Morphological module

The last step is the morphological change. The sediment transport differences are used to determine if there is a loss or gain of sediment at different locations of the profile. The loss or gain is used to update the profile. After the updated profile is checked for unrealistic slopes, and if a slope exceeds a realistic value, avalanching occurs. The bed level update due to differences in sediment transport is described in section 2.4.1. The avalanching is described in section 2.4.2 2.4.2.

2.4.1. Exner function

The morphological change can be expressed as a conservation of mass formula, which is determined with the Exner function (Amoudry and Souza, 2011). There should be a balance between sediment moving in and out of the profile and in bed level change. Expression equation 2.21 is a simple mass conservation formula. There are limitations with this expression as there cannot be any sediment in suspension in the water column so all transport is instantaneous and there is no sediment stored in the water. The bed level does not only consist of sand. Because of the porosity of sand, there is also water between the sand-grains. To account for this, the bed level is considered to be partly sediment and partly water. The porosity is important as the change of bed level is increased.

$$\frac{\delta z}{\delta t} = \frac{\delta Q}{\delta x}(\frac{1}{1-n}) \tag{2.21}$$

$\frac{\delta z}{\delta t}$ is the bed level change over time. $\frac{\delta Q}{\delta x}$ the difference of cross-shore sediment transport moving in and from a location over space. n is the porosity of the bed level. Luijendijk et al. (2017) used a porosity of 0.4 for a sediment model at the Sand Engine; therefore, the same value will be used in this model.

2.4.2. Avalanching function

The avalanching term is included to prevent unrealistic slopes in the bed level profile. Larson and Kraus (1989) found that the bed level can reach a maximum slope steepness of 28 degrees. Similar to their model S-Beach, this model will include an avalanching term. When the slope of the beach exceeds the maximum angle of 28 degrees, the model will avalanche - causing the sediment to move downslope - restoring the beach slope angle to 18 degrees.
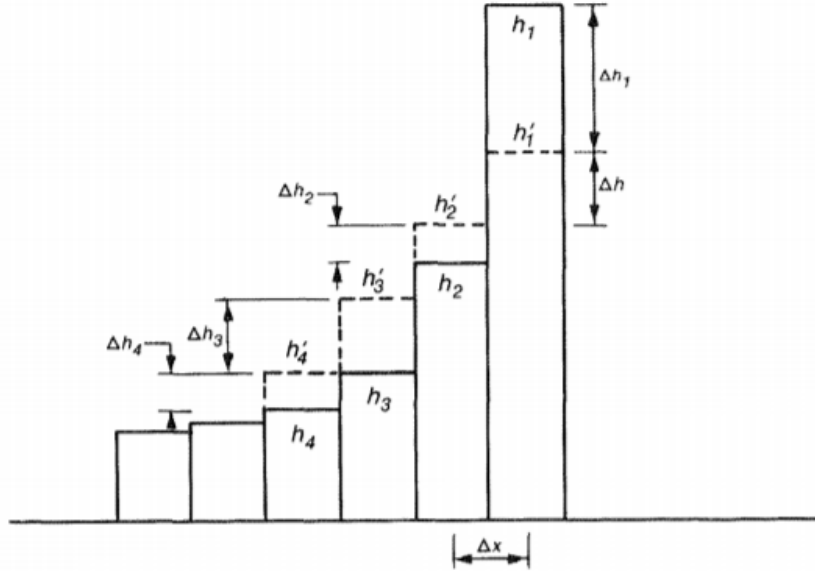
Figure 2.6: A definition sketch of avalanching. Where the angle between and is exceeding the maximum angle. The exceeding sediment is distributed over the nearby cells in the direction that the slope was exceeded until the slope is stable (Larson and Kraus, 1989).

The Δh_1 is determined in the same way as the S-Beach model by Larson and Kraus (1989). The formula determines how much of the original bed level height is lost and distributed over the neighbouring cells. the number of cells the avalanching term is spread ever is unknown, and iteration with equation 2.22 and 2.23 is performed until a stable slope is reached that matches the restore slope.

$$\Delta h_1 = -\frac{N-1}{N}h_1 + \frac{1}{N}\sum_{i=2}^{N} h_i + \frac{1}{2}(N-1)\Delta h \tag{2.22}$$

$$\Delta h_i = h_1 + \Delta h_1 - h_i - (i-1)\Delta h \tag{2.23}$$

Where is the first cell where the angel exceeds the maximum angle, N is the number of cells where the sediment is redistributed to, i is an indicator of the which cell, is the height of the cell. is the stable difference between two cells based on the restore angle.
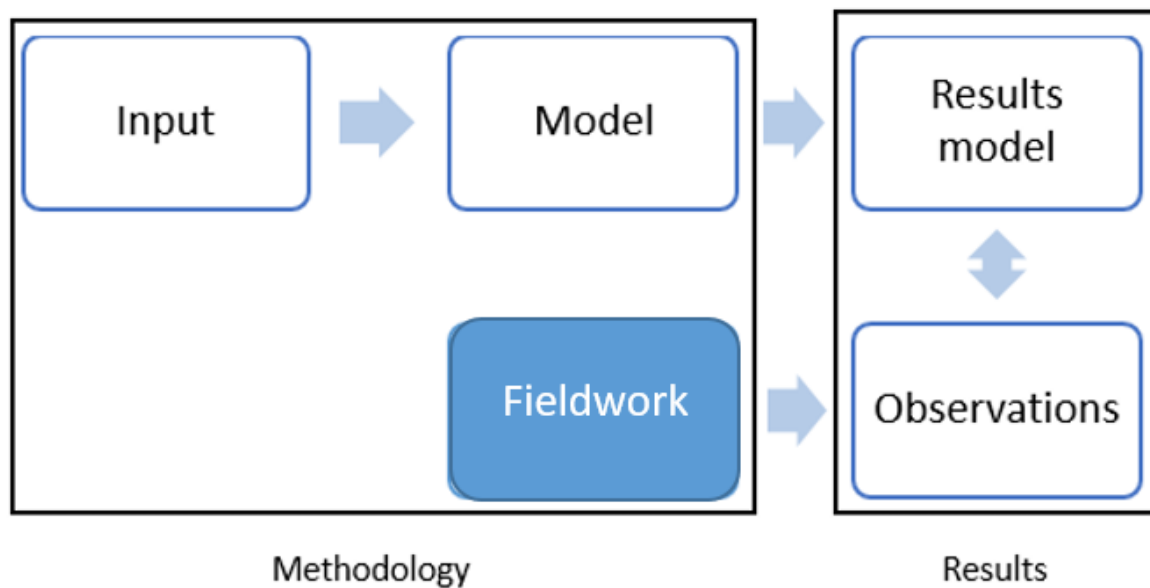
Figure 3.1: The chapter will cover the observations.

In this chapter it will be explained how the observations are made and local data of the beach is gathered an what devices and methods are used. Between the 21th and the 27th of September 2019, the fieldwork trip of the TU-delft was conducted at the Sand Engine. The data collected during the fieldwork is used in this report to show how the bed level is responding at a small time scale. Data was obtained using several devices, which will be elaborated on in 3.1. The setup up of the field work is explained in section 3.2, and the processing of the data collected is described in section 3.3.

3.1. Devices

3.1.1. Acoustic bed level sensors

The bed level is measured with an acoustic sensor of the type EA400 Echosounder. This device measures the bed level with a frequency of 0.1 Hz. The acoustic sensor sends out a sound wave. When the sound wave hits an object the wave is reflected back. The reflected sound wave is recorded by the acoustic sensor. To estimate the distance between the acoustic sensor and the object, the time between the wave being sent and the wave coming back must be measured. The acoustic sensor uses a conical sound wave of 5 degrees. The sensor measures the amount of the sound waves that are reflected back as intensity; small objects only give a small intensity, and large objects such as the bed level will provide a high intensity. The intensity gives a complete signal in the water column, from the bed level up to the sensor

(with an accuracy of 1 millimetre). During the week of fieldwork, the settings of the acoustic sensors where changed. The acoustic sensors were removed at the afternoon low tide on the 25th of September. The gain of the devices was switched from -6 decibel to -10 decibel and reinstalled on September 26 in the morning. The change of -6 decibel to -10 decibel did not have any effect on the final results.

3.1.2. High-frequency pressure sensor
The water pressure is measured with a sensor of the type RBRsolo3D. This device continuously measures the pressure above the sensor. Using the pressure, the water elevation can be calculated. The transformation from the pressure to water elevation is further explained in section 3.3. The sampling frequency of the pressure sensor was set at a frequency of 8 Hz. A more complete wave field can be gathered as the frequency of the pressure sensor increases.

3.1.3. CastAwayTM-CTD
The CastAwayTM-CTD diver is a device that provides crucial information about the water. The device is used to estimate the water density and temperature of the water. Water density is needed to convert the pressure to water level, and for sediment transport calculations in the model. The CTD device can compute the sea density with an accuracy of 0.02 kg/m3. It is convenient to know the temperature of the water, to be able to estimate the viscosity of the water – that is used to determine the fall velocity of sediment in the water – more accurate.

3.1.4. GPS
Real-time kinematic global positioning system (RTK-GPS) measurements are taken at low tide, to obtain the intertidal zone bathymetry. The grid measured 35 meters from the sensor in each direction alongshore (for a total of 70 meters). The accuracy of the GPS during the measurements lays between $\pm$ 0.02 m and $\pm$ 0.04 m, however human handling of the devices will increase the error.

3.2. Set-up fieldwork
The acoustic sensors and pressure sensors are installed on a beach profile. The sensors are installed as a pair, with one pressure sensor and one acoustic sensor on a scaffold pole. The sensors were installed 5 meters from each other, lined up in cross-shore direction. The sensors are installed at two places: the first one on 0.5 meters below the low tide, the second 5 meters closer to shore as can be seen in figure 3.2.
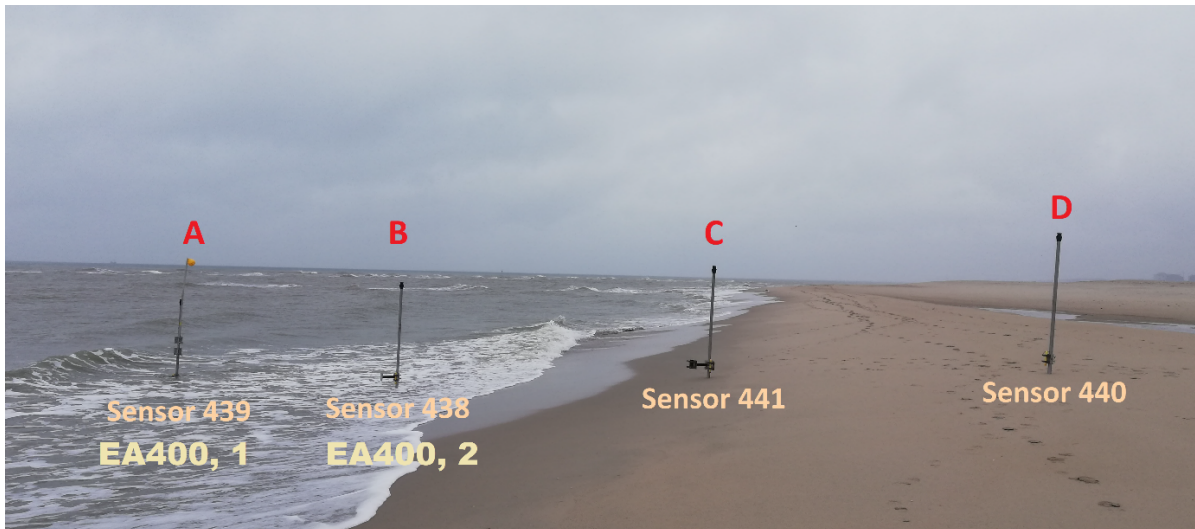
Figure 3.2: The setup of the fieldwork. Four poles on the beach, with pole A as the offshore pole and pole B as the onshore pole containing both a pressure sensor and an acoustic sensor. Pole D had a pressure sensor installed that is used to estimate the atmospheric pressure (the devices on pole C did not function and are thus ignored).

3.2.1. Raw data sensors

The sensors give raw data observations. Figure 3.3 contain raw acoustic data and figure 3.4 contain the pressure signal over time. These data sets need to be transferred to a single value over time to compare to the model output.
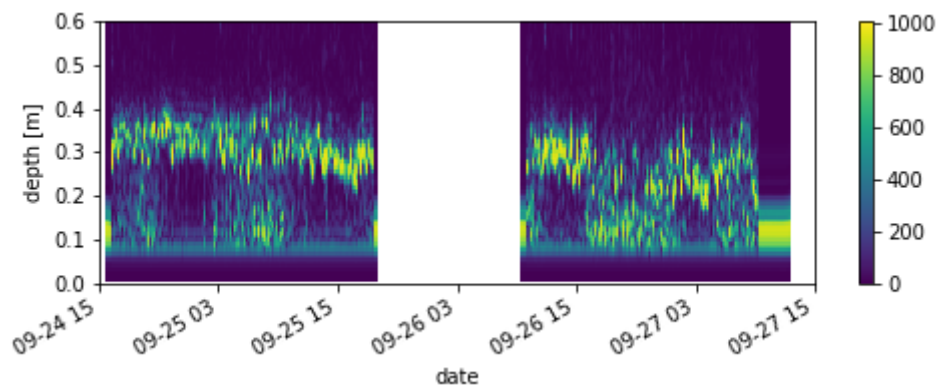
Figure 3.3: The acoustic data from the offshore sensor. The x-axis is the time the y-axis is the distance between the acoustic sensor and the received signal. The colours indicate the strength of the signal received where yellow indicates the strongest signal received at a certain depth.
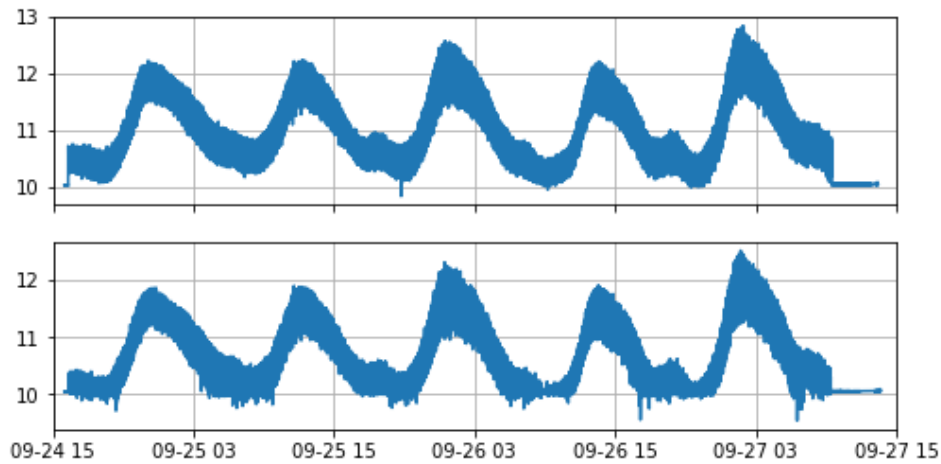
Figure 3.4: The pressure measured over time. The x-axis represents the time, the y-axis represents the pressure measured in N/cm^2. The top panel is the pressure signal of the offshore sensor. The panel below is the onshore sensor.

3.3. Data processing

3.3.1. Conversion from pressure fluctuations to water elevations fluctuations

The pressure measured with the sensors needs to be converted to water elevation. The pressure signal consists of two contributors: the atmospheric pressure, and the water pressure. The atmospheric pressure is the weight of the air and is measured with the pressure sensor that is installed at pole D in figure 3.2. If the pressure sensor of pole D is underwater, interpolation is used to estimate the atmospheric pressure for these time intervals. The water pressure consists of the hydrostatic pressure and the dynamic pressure. The hydrostatic water pressure depends on the mean water level. The dynamic pressure depends on the waves passing over and the phase of the waves, as shown in figure 3.5. The hydrostatic water pressure can be determined from the mean pressure minus the atmospheric pressure. The dynamic pressure is determined with the linear wave theory. The theory will induce errors as waves near the coast behave non-linear. However, as was mentioned in section 2.2, the theory has acceptable errors in the nearshore.
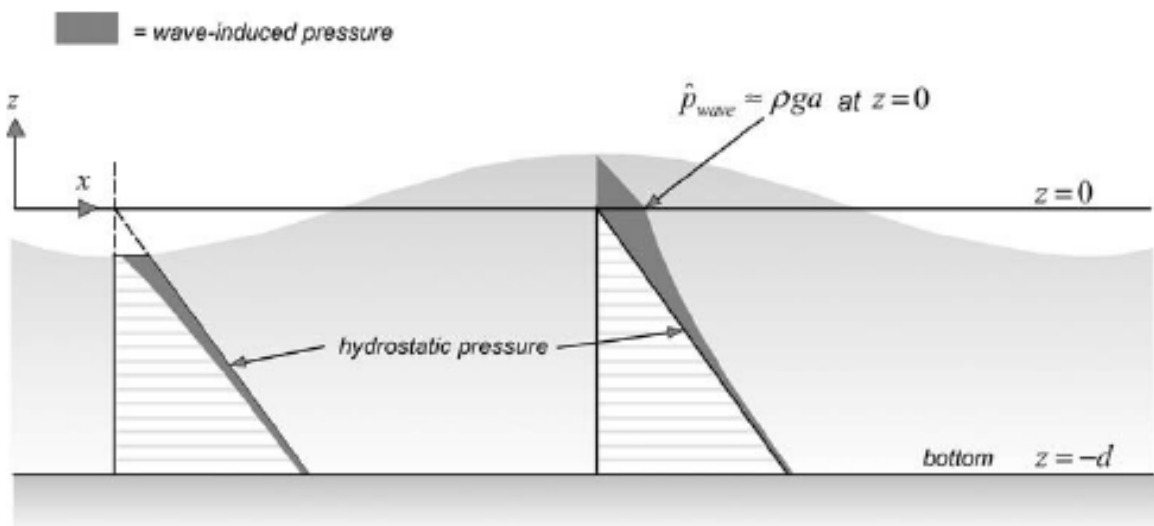
Figure 3.5: The dynamic pressure of the waves superimposed on the hydrostatic pressure of the water. The atmospheric pressure is ignored in this picture (Holthuijsen, 2009).

Other problems occur when using the linear wave theory in shallower waters. When

waves travel in shallow water, wavelength decreases and the wavenumber increases. When the wavenumber increases, the dynamic pressure increases, causing waves to become unrealistically high. (Bishop and Donelan, 1987) derived a method that prevents the dynamic pressure from becoming too large. When the elevation difference between the sensor and the bed level divided by the wavelength is smaller than a certain cut-off value, the $\frac{cosh[k(d+z)]}{cosh(kd)}$ is replaced by the cut-off value. A cut-off value of 0.33 is used based on the paper of Bishop and Donelan (1987).

$$P = P_{atmospheric} + P_{water} \tag{3.1}$$

$$P_{water} = -\rho_{sea}gz + \rho_{sea}ga\frac{cosh[k(d+z)]}{cosh(kd)}sin(\omega t - kx) \tag{3.2}$$

The water elevation during the week needs to be separated, as there was a tidal wave and a wavefield. Munk (1951) classification, as shown in figure 1.2 is used to separate the different waves. The figure shows that tides are happening at a frequency lower than 10^{-4} Hz. The water level that was observed can be separated into 'magnitude' and 'frequency' with a Fourier transformation. The Fourier transformation uses sinusoidal functions with different magnitudes and frequencies to imitate the original signal. In the measured water level, the tidal signal is separated based on the believe that the frequency below 10^{-4} Hz is the tidal signal. Waves with a frequency of less than 10^{-0} Hz are considered noise, and therefore removed from the signal. The pressure water elevation is now separated into a tidal signal, and a wavefield without noise.

The water level entails a summation of sinusoidal frequencies and amplitudes that can be separated into waves by using the downward zero-crossing method. The downward zero-crossing method classifies a wave period as the time the water takes to make a downward motion below the mean water level twice, with one elevation in between. The wave height is the difference between the lowest and highest point of the wave period. This is illustrated in figure 3.6. The wave field is separated into time intervals of 10 minutes, and all the individual waves are distinguished within these time intervals. The time intervals consist of different waves. However, the model predicts a significant wave. Out of the recorded waves, a significant wave is determined by averaging the highest one-third.
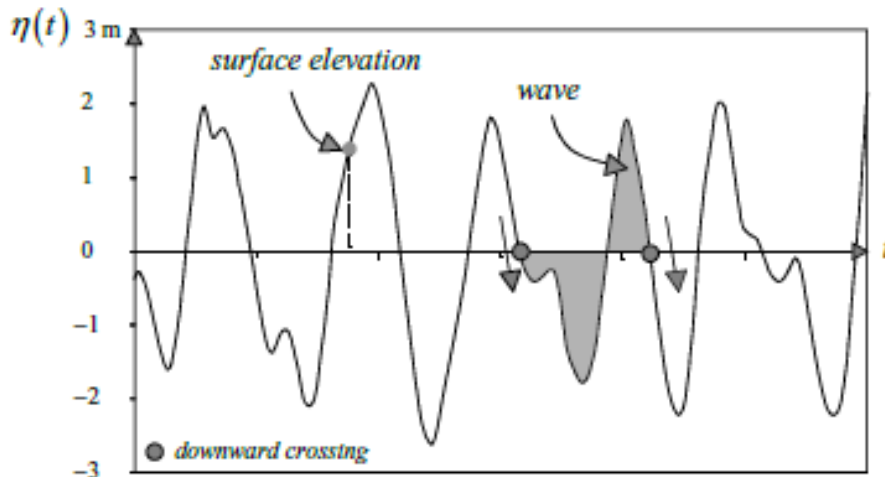
Figure 3.6: Showing water elevation over time on a single location. The darker part indicates a wave where two successful downward crossings of the wave where recorded (Holthuijsen, 2009).

3.3.2. Observation error of the pressure sensor
The sensor will have an error due to the device used and the conditions it is placed in. The device has an error of 0.05 % therefore the error of the device is considered neglectable. The

error of the conditions is determined using the expected signal and the standard deviation od this signal to derive the noise to signal ratio. This method was used on both location, at the offshore location a ratio of 18.5 and at the onshore location of 18.1. For both locations a ratio of 18 is used to be safe. The noise in the signal is $\frac{1}{18} = 0.05$. The pressure signal is changed with 5 % to see the effect of the error on the significant waves. The calculations are done in the same method as described above to estimate the significant wave this showed that the mean error of the noise is 0.08 meter at the offshore location and 0.09 meter at the onshore location.

3.3.3. Raw acoustic data transformation to bed level

The raw acoustic data has to be transformed into an average bed level every ten minutes. The raw acoustic data is a signal strength measured at different depths. It is assumed that the location where the signal increases the most is the location of the bed level. The acoustic sensors are placed in shallow water, and Jaarsma (2019) showed that the signal is influenced by sediment and air bubbles trapped in the water column. Therefore, different filters have to be applied to find the bed level. The filters used will be explained in the next paragraphs.

First, the data of unrealistic points are removed. The acoustic sensor is able to measure distances accurately from 0.15 meter. As a consequence, all signals received below 0.15 meters are removed. Distances greater than 0.6 meters are considered unrealistically large, and were therefore also removed. The second filter adds up all signals received every ten seconds, and then the maximum increase is used as bed level. This is done to filter out possible air bubbles and sediment as these are moving in the water. Over time, the signal strength will vary per distance, with the bed level as a consistent signal. The average signal is used to determine the location of the sharpest increase. The third filter that is applied ensures that the bed level is not moving towards outliners in the data. The third filter predicts the bed level based on the nearest 30 points, using the k-NN regression (Pedregosa et al., 2011). The system determines the nearest neighbour based on Euclidean distance. This method for distance increases the performance of the nearest neighbour algorithm, according to Wang et al. (2007). Because these 30 points are spread out, the 95% certainty spread is indicated. The results are presented in figure 3.7, where the original data is plotted in the red, to show the performance of the filters. Figure 3.8 shows the bed level over time and the spreading of the data.
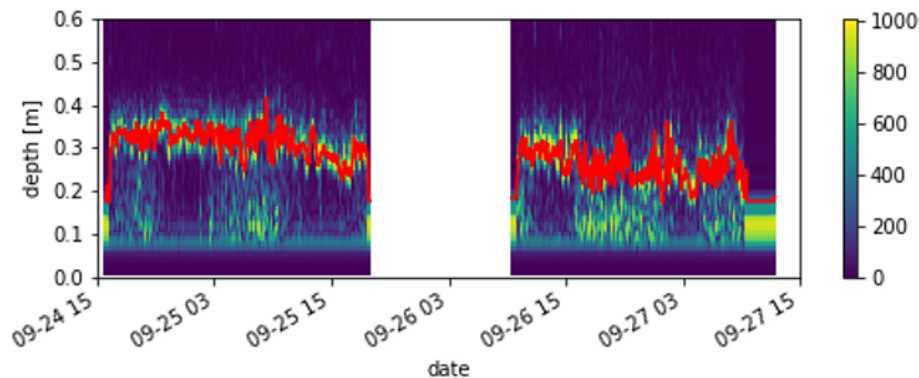
Figure 3.7: The offshore sensor. The x-axis is the time, the y-axis is the distance from the sensor. Showing the bed level as the red line, the colours are the raw acoustic signal strengths.
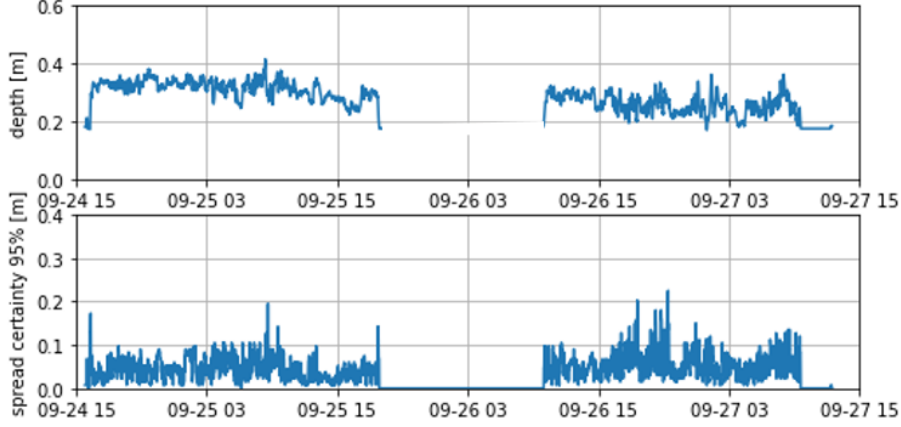
Figure 3.8: The offshore senor. The x-axis is the time, the y-axis is the distance from the sensor in the above panel. In the lower panel the y-axis is the spread of the signal.

The distance of the sensor to the bed level consists of three different parts: Noise from the sensor, oscillations from sand ripples and trend behavior of the bed. The research aims to see bed level erosion and aggregation. The noise and sand ripples are unwanted effects. Sand ripples are waves in the bed level that have an amplitude between 3 cm and 20 cm and move with speeds varying between 2 meters per day and 10 meters per day (Becker et al., 2007). Saulter et al. (2003) observed ripples at Egmond aan Zee between 0.5 cm and 1.5 cm, with periods of 10 to 30 minutes. A single spectrum analysis (SSA) is a method that can separate oscillations and noise from a signal over time (Claessen, 2002).

The SSA decomposes a signal by eigenvalues and vectors. The eigenvalues indicate the importance of the total signal. The vectors show the behavior. When all the eigenvalues and vectors are combined, it forms the original signal. The SSA used in this paper is based on the method explained in Claessen (2002). The data set after the filters is a value over time similar to $[x_0 x_1 ... x_n]$. First, the data is converted to a lagged matrix, this is done so a single time series is converted to a matrix so the empirical orthogonal functions can be determined (of 83 minutes to ensure all ripples are included), also called a Hankel matrix. An example is shown in equation 3.3 where the Hankel matrix is Y, that consist of the x values over time.

$$Y = \begin{bmatrix} x_0 & x_1 & x_2 \\ x_1 & x_2 & 0 \\ x_3 & 0 & 0 \end{bmatrix} \tag{3.3}$$

Secondly, the covariance matrix is drawn from the Hankel matrix. The covariance matrix is computed as follows.

$$C = \frac{YY'}{N} \tag{3.4}$$

Thirdly, the empirical orthogonal functions (EOF) and the vector-matrix are computed from the covariance matrix. The EOF are the eigenvalues of the covariance matrix and indicate the importance of the total signal. The data set can be rebuild using the vectors from the covariance matrix C. This is done by determining the principal components of the time series. The principal components are $P_c = Y \cdot vectors$. The principle components contain the different parts of the original signal. In order to transform the PC back to a time dependent series first, a new matrix needs to be constructed similar to Y, but the difference is that it is not based on the original data but on the PC, and the matrix is a step backwards in time. The new matrix is called Z and looks like:

$$Z = \begin{bmatrix} PC_0 & 0 & 0 \\ PC_1 & PC_0 & 0 \\ PC_2 & PC_1 & PC_0 \end{bmatrix} \tag{3.5}$$

Then the reconstructed components (RC) are derived from $RC_1 = \frac{Z \cdot vector_1}{M}$, where $vector_1$ is the first column of the eigenvectors computed from the covariance matrix, with m being the window length of the Hankel matrix. The result is a separation of oscillatory motion, trend and noise over the time series, as is shown in figure 3.9. The figure 3.10 shows the amount of variation associated with each EOF. The top figure is the offshore sensor, the EOF in the offshore sensor accounts for almost 80 percentage of the signal. The below figure is the onshore sensor, the EOF accounts for 50 percentage of the signal. This means that there are more oscillations, or noise in the onshore sensors signal. The end result shows the bed level over time. The bed level moves in the order of decimeters over days.
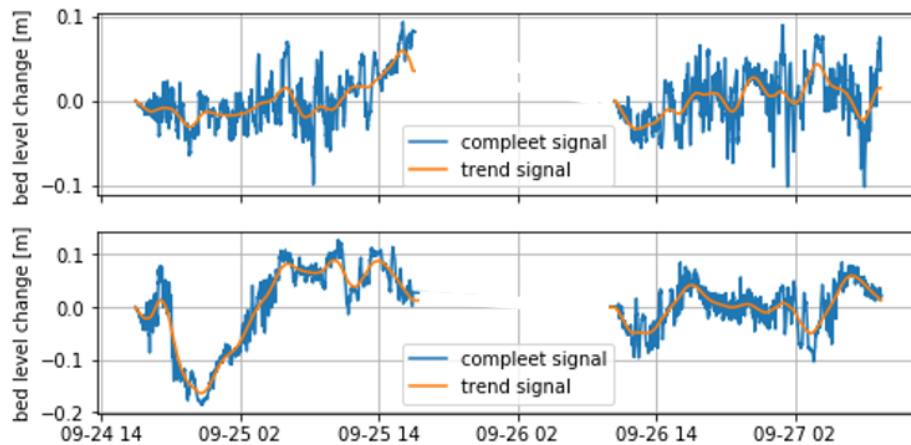
Figure 3.9: The above panel is the bed level change over time of the offshore sensor and the below panel is the onshore sensor. The x-axis is the time, the y-axis is the bed level change, with negative values indicating erosion and positive values indicating aggregation. The orange line is the filtered bed level
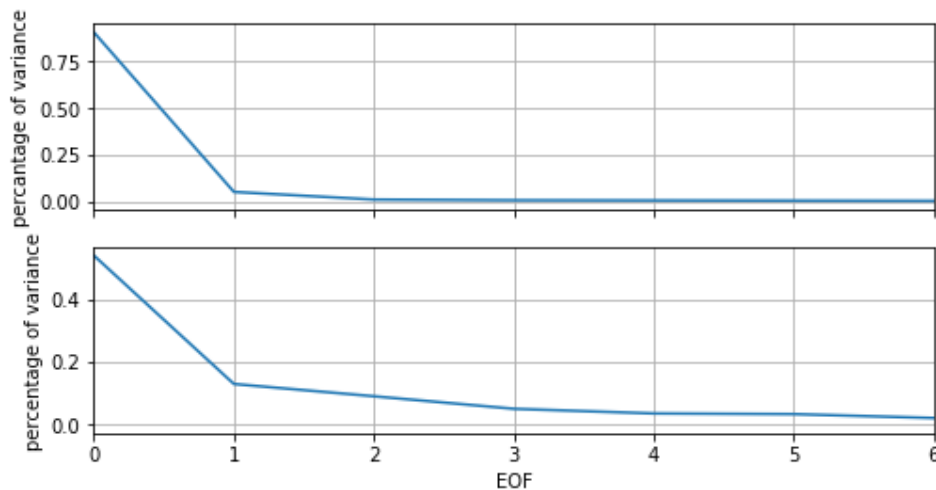
Figure 3.10: The above panel is the EOF of the offshore signal and the below panel is the EOF of the onshore sensor. The x-axis is the EOF, the y-axis is the percentage of variability of the complete signal.

Input model
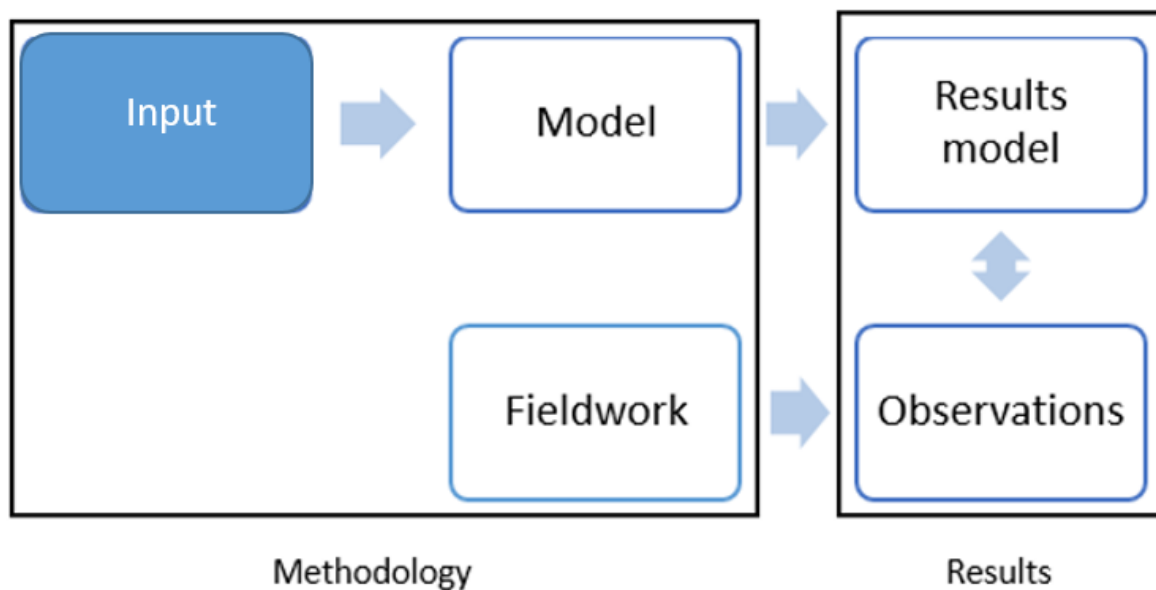
Figure 4.1: The chapter will cover the input conditions for the model

As was explained in section 2.1, the model needs several input conditions to predict bed level changes for different locations. The input conditions are the waves and the initial bed level. During the fieldwork, the deep water waves and bathymetry were not collected. Therefore these input conditions need to be derived. During the fieldwork waves were observed, and these observations are used to determine the wave breaker parameter. The method used will be explained in the following order: section 4.1 shows how the bed level is derived from jet-ski bathymetry measurements at the Sand Engine, section 4.2 describes how offshore waves observed at a measuring platform are transformed waves near the Sand Engine, and section 4.3 shows how the breaker parameter was derived from the water elevation of the fieldwork.

4.1. Bed profile

Between 3/8/2011 and 7/9/2016, the bathymetry of the Sand Engine was monitored regularly. During this time, 37 surveys were conducted. De Zeeuw et al. (2017) used LIDAR and jet-ski mounted with altimeters to make the surveys. The Sand Engine bathymetry was monitored with a 20-meter grid. The accuracy of the data set was not found.
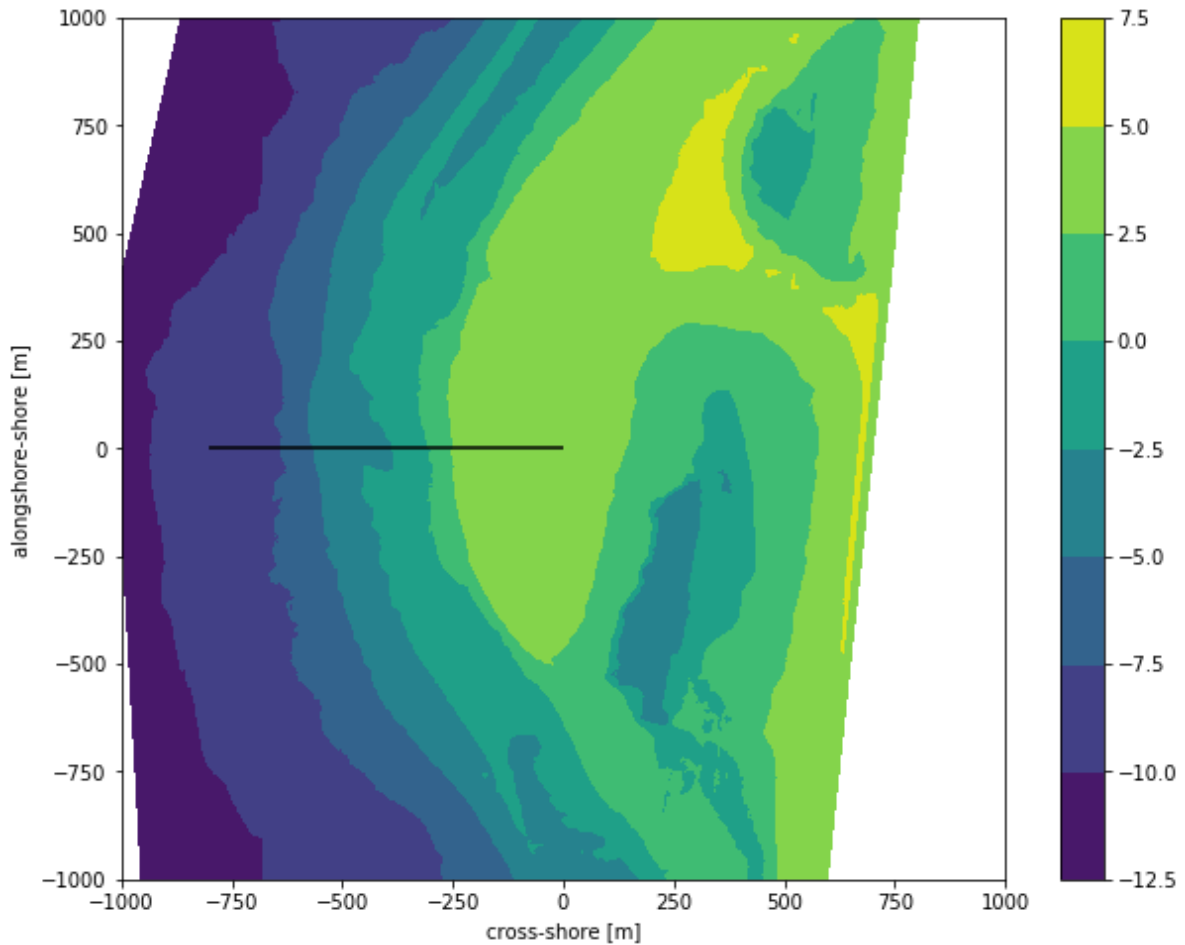
Figure 4.2: The jet-ski and LIDAR collected bed level at the sand engine at 1/4/2016. The coast was turned to align perfectly with the poles that were installed during the field experiment. The x-axis is the cross-shore distance. The y-axis is the alongshore distance. The black line is the profile of interest at the location of the poles. The bar on the side indicates the elevation from the Normaal Amsterdams Peil (NAP). (De Zeeuw et al., 2017)

The surveys bathymetry is used to extract the cross-shore profile at the location of interest. The location of interest is shown in the figure 4.2 as the black line. The coast-line of the Sand-Engine was changing over time, so in order to compare different cross-shore profiles they are all compared from an equal zero point. The location where the NAP is zero was used as a location to compare the profiles with each other. The Dean profile was used to estimate the sandbars overtime on the profiles. Dean profile was shortly mentioned in section 1.1 as a method to determine the average cross-shore bed profile for a long period. The method to derive the Dean profile is shown in the equation 4.1.

$$d = 2.25(\frac{w^2}{g})^{1/3}x^{2/3} \tag{4.1}$$
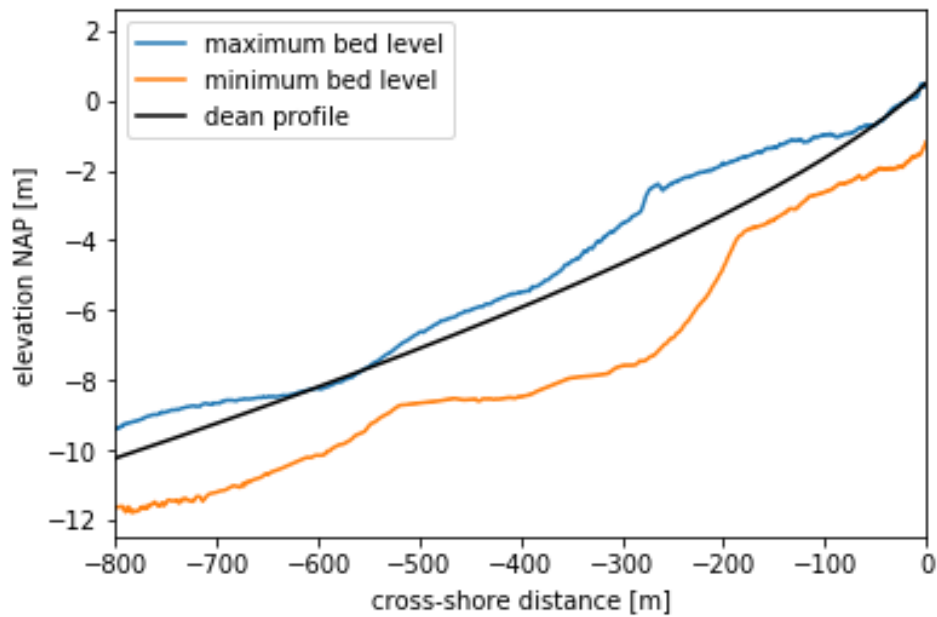
Figure 4.3: The maximum and the minimum elevations of the profiles are plotted, The blue line shows the maximum elevavation and the orange line shows the minimum elevation. The dean profile is the black line (De Zeeuw et al., 2017).

The coast of the Sand Engine is retreating. However, the profile of the Sand Engine is behaving 'reasonable' stable over the years with a permanently present sandbar between 100 and 200 meters offshore, for more elaboration appendix C. Therefore it is assumed that the best deep water profile that can be used for the field experiment is the average profile of the beach in the year 2016, as shown in figure 4.4.
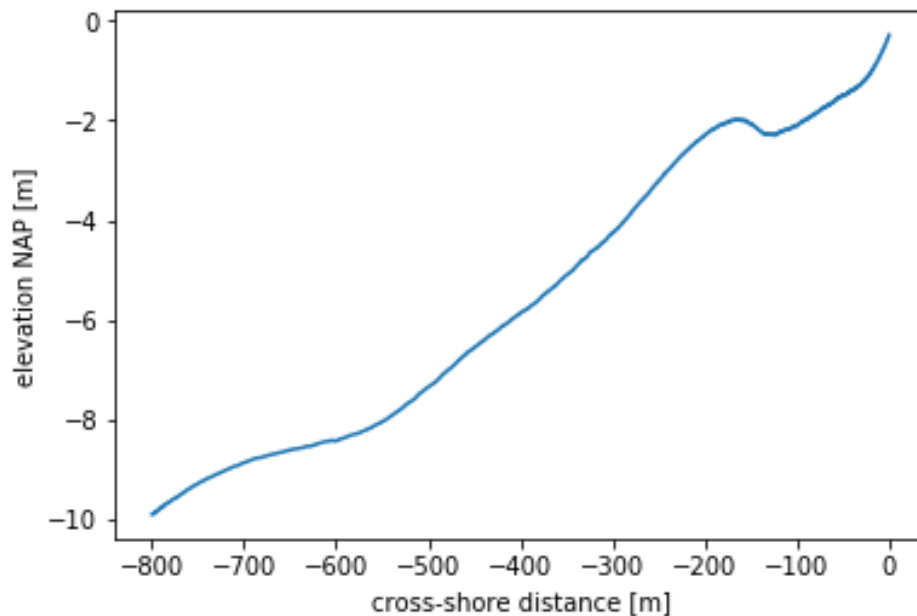
Figure 4.4: The average bed level profile from all observations done in 2016

During the field experiment bed level data was collected form the intertidal zone. This data is used to provide an accurate bed level where possible. The data is processed and combined with the deep water level to provide a total cross-shore profile
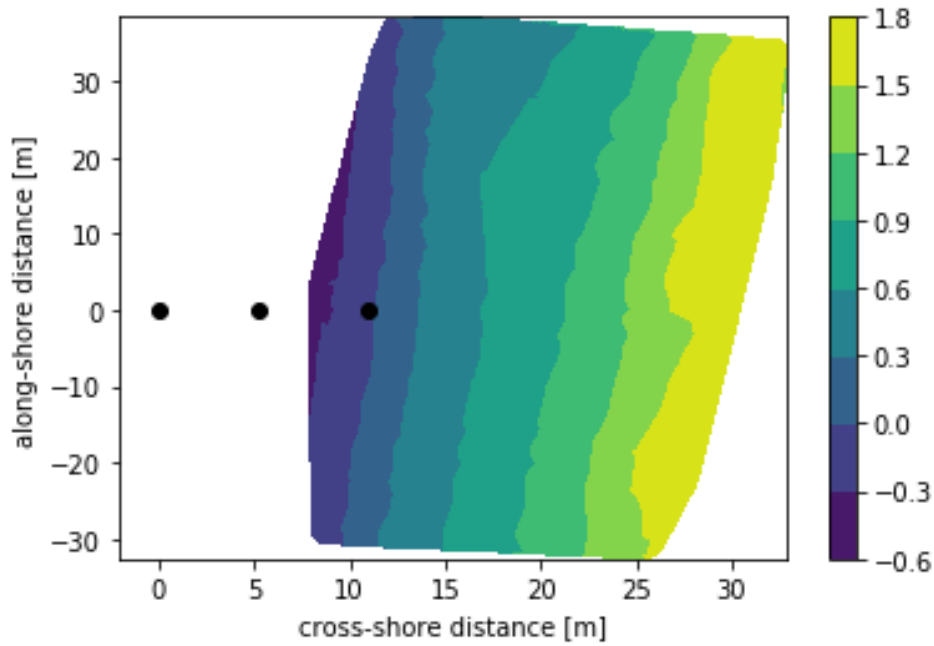
Figure 4.5: The intertidal zone measured at 24/9/2019. The x-axis is the cross-shore distance in meters. The y-axis is the alongshore distance in meters. The colour indicates the depth from the NAP. The black dots are the locations of the poles installed where pole A is at x = 0 and y = 0. Pole B is the second pole at x = 5 and y = 0.
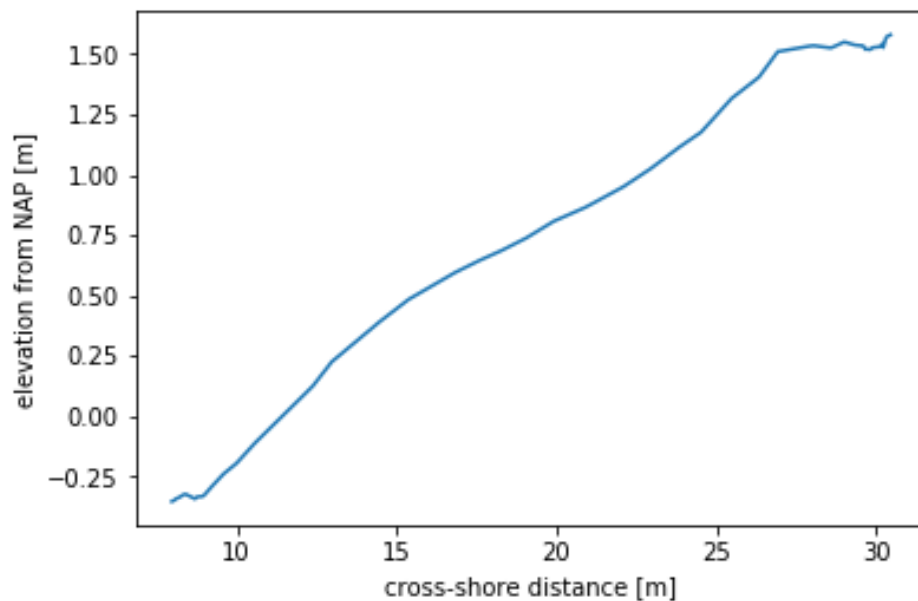
Figure 4.6: The cross-shore intertidal profile at 24/9/2019. The x-axis is the cross-shore distance in meters the y-axis is the elevations form the NAP.

The profile of the 24/9/2019 was made after installing the poles and captures the intertidal zone until a NAP of +1.5. However, this was not high enough as the tide reaches further during the fieldwork. Therefore the profile walked at the 22/9/2019 that reached further up the beach was used to compleet the cross-shore profile. The result is the initial bathymetry of the beach for the model shown in figure 4.7.
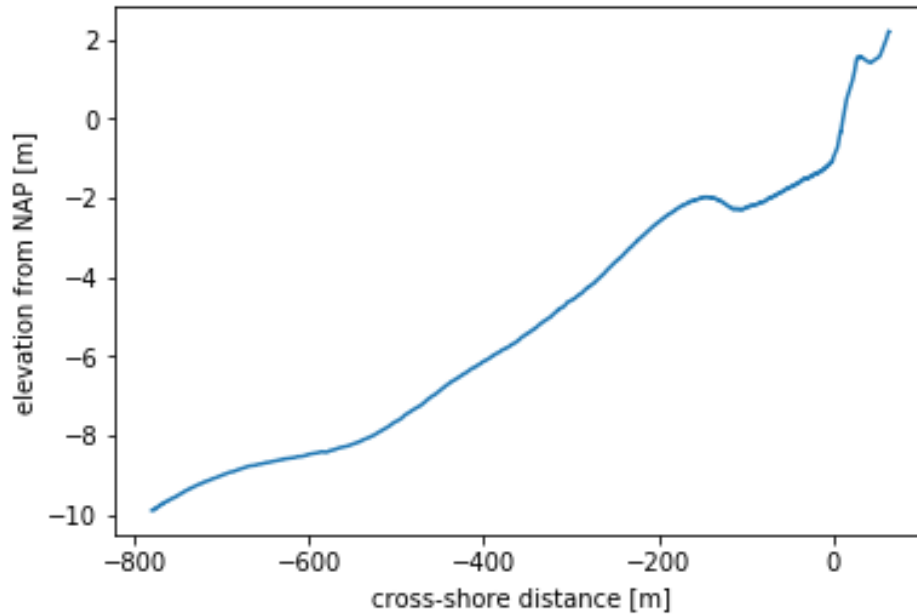
Figure 4.7: The initial bathymetry of the model. The x-axis is the cross-shore distance the y-axis is the elevation from the NAP.

4.2. Waves

The offshore waves were measured at platforms off the Dutch coast. These waves are deep water waves that need to be transformed into waves at the Sand Engine. Luijendijk and de Fockert (2011) designed a transformation matrix for waves that transforms waves from the offshore platform to an onshore location in the domain of the model, as shown in 4.8. The matrix was developed for PhD students on 'the working with nature' projects (Luijendijk and de Fockert, 2011). The transformation matrix shows that it can transform waves height from an offshore platform to an onshore location with a correlation factor 0.9 or higher. However, the period that the transformation matrix predicts for waves closer to shore has a correlation factor of 0.6 (Luijendijk and de Fockert, 2011). Depending on the direction of the waves, different offshore platforms are used to determine the onshore waves. For the Sand Engine waves reach the coast from two different platforms. When the wave direction is lower than 280° and higher than 200° degrees, waves come from the Europlatform. When the wave direction is higher than 280° and lower than 30°, waves are used from the offshore measuring station of IJmuiden.
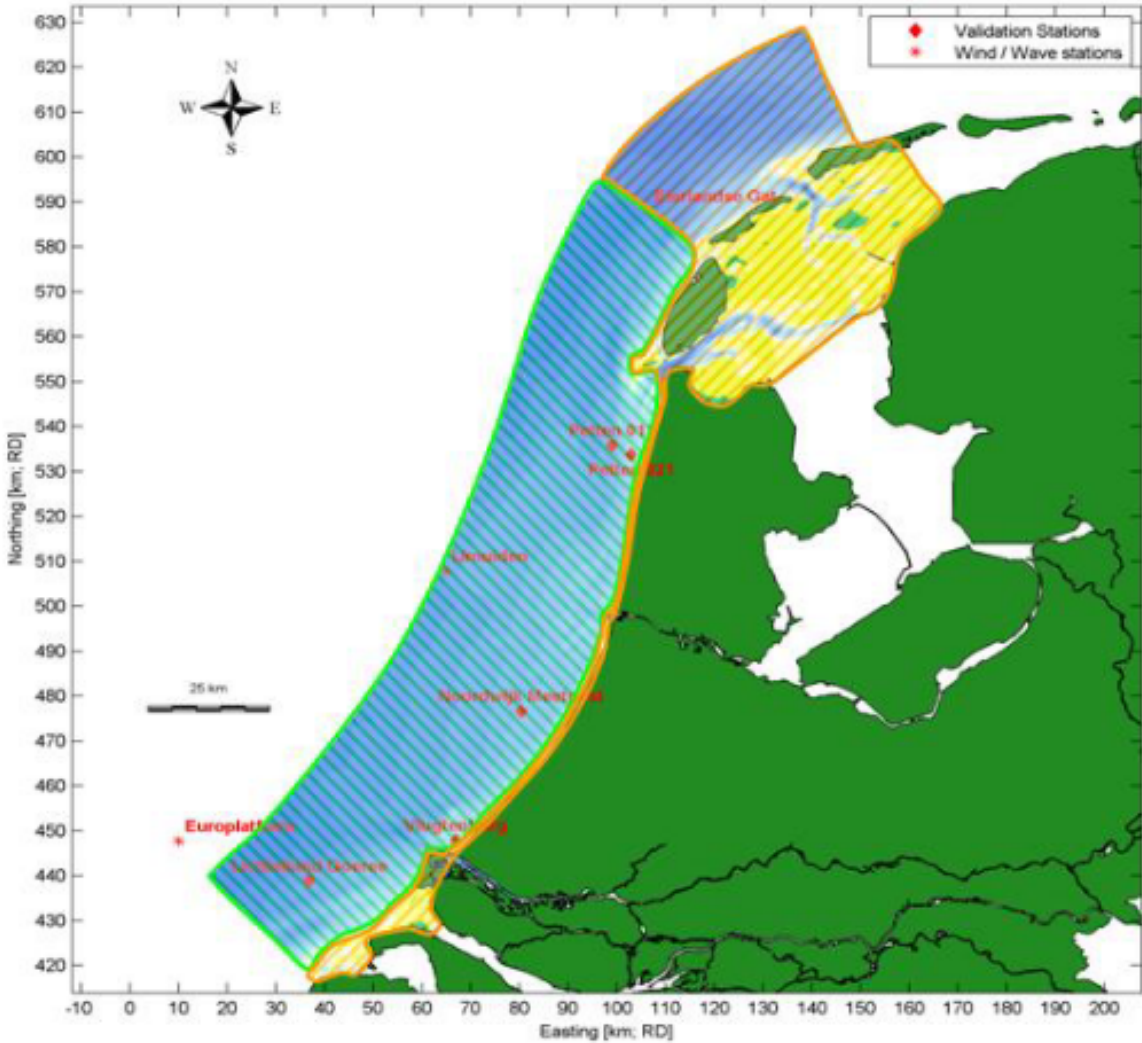
Figure 4.8: The domain of the wave transformation table. The red dots are points where the model was validated at and the red stars are locations where wave and wind data was gathered (Luijendijk and de Fockert, 2011) .
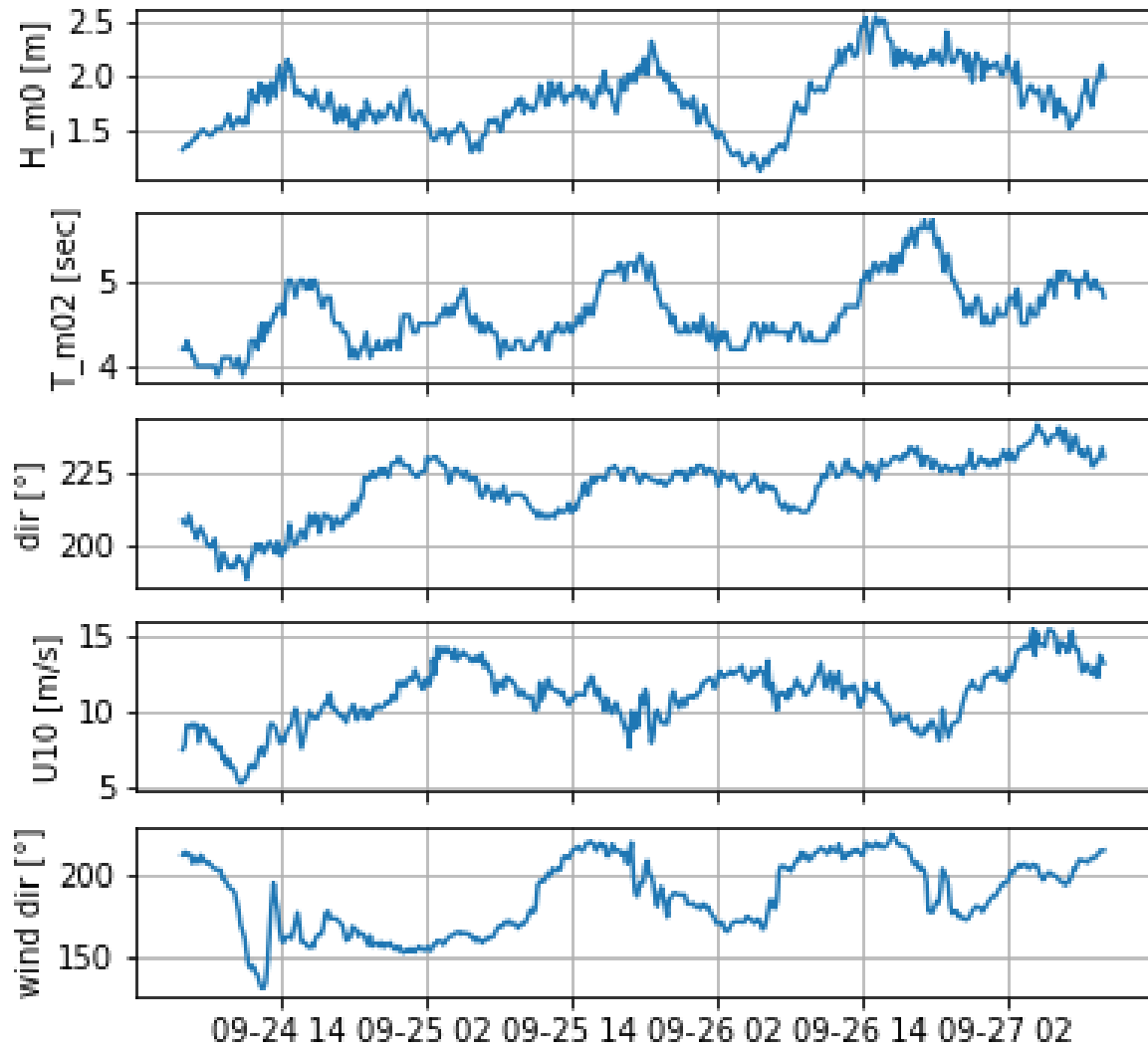
Figure 4.9: The offshore waves used in the model are the observations at the Europlatform. As waves where below 280 degrees north, this station was used to transfer the waves towards the Sand Engine. The top panel shows the significant wave height over time, the second panel shows the period over time, the third panel shows the direction of the waves from North normal, the panel figure shows the wind speed ten meters from the ground, the fifth figure shows the wind direction from North normal
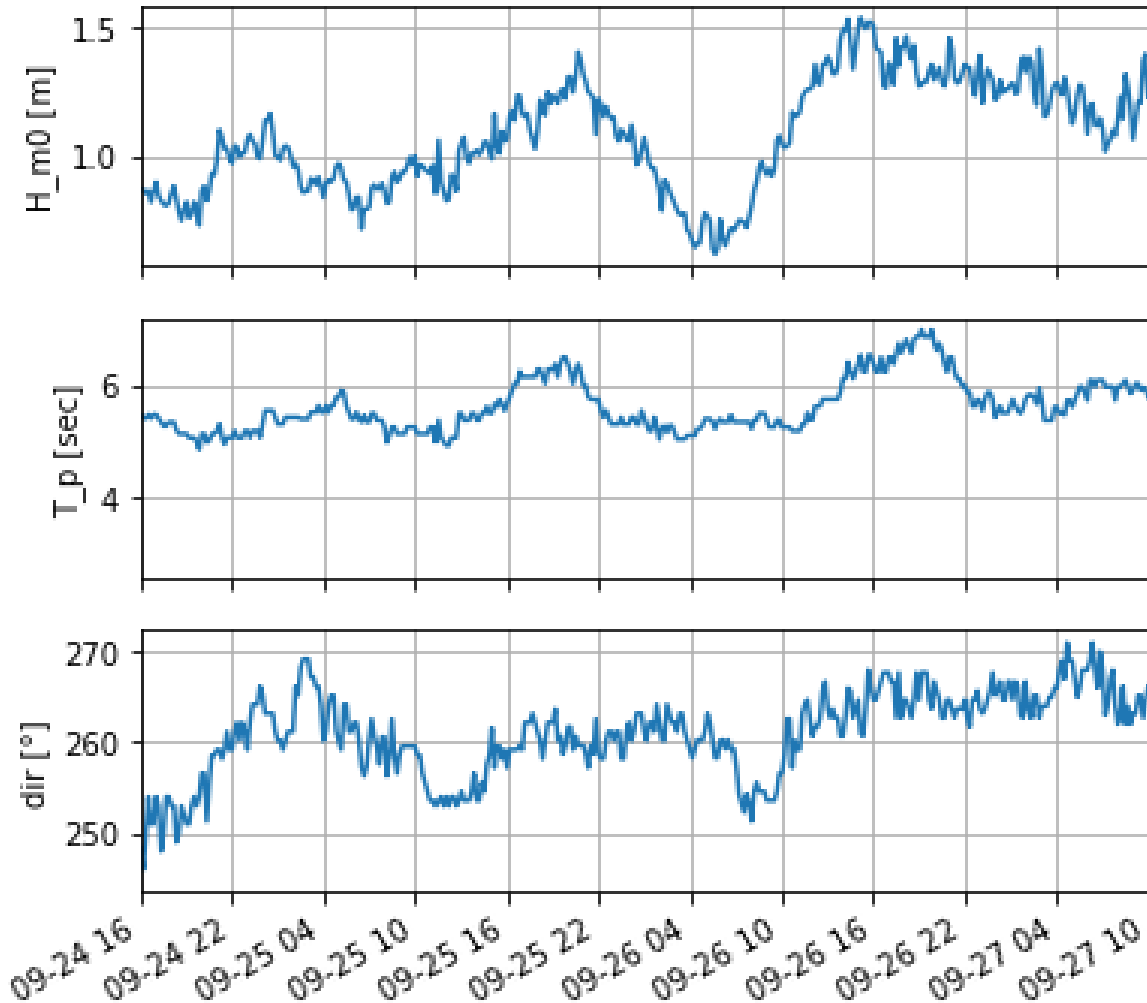
Figure 4.10: The deep water waves near the Sand engine is the result. the top panel is the significant wave height, the second panel is the peak period of the waves, the third panel is the wave direction from North normal. These are the waves used in the model

4.3. Wave breaker parameter

In section 1.3.2, wave shapes were explained. The skewness of the wave increases until the wave break, after which the skewness decreases again (Grasso et al., 2012; Svendsen, 2006). This means that when wave skewness is maximum, the waves are breaking. Wave skewness can be expressed by equation 4.2. The equation is derived from Svendsen (2006).

$$Sk = \frac{a_{crest}}{H} - 0.5 \tag{4.2}$$

The water elevation was recorded during the fieldwork. This will provide the waves needed to determine the breaker parameter. The water elevation of both sensors is divided into segments of ten minutes, after which the zero-down crossing method is applied to identify the waves. From every segment, the highest one-third of the waves is collected, the skewness of highest one-third of the waves is calculated and averaged. The wave height is averaged as well and divided by the water depth. The result is shown in figure 4.11.

The figure shows that the skewness of the wave increases as the relative wave height increases. However, while the relative wave height keeps increasing, the skewness drops. According to Svendsen (2006) the waves start breaking at the highest point of skewness. The location of the maximum skewness is determined using the rolling mean of every 100 points. The result is the red line in figure 4.11. From the red line it follows that the maximum

skewness is located at a relative wave height of 0.59. This value is in line with the literature. However, most studies show larger values for the breaker parameter. This might be possible because as the pressure was converted to waves using linear wave theory, decreasing the non-linear effects that would have increased the wave height. Using the error of the wave signal and the same method as described above, the wave breaker parameter was found to be 0.59 for the decreased pressure signal and 0.71 for the increased pressure signal.
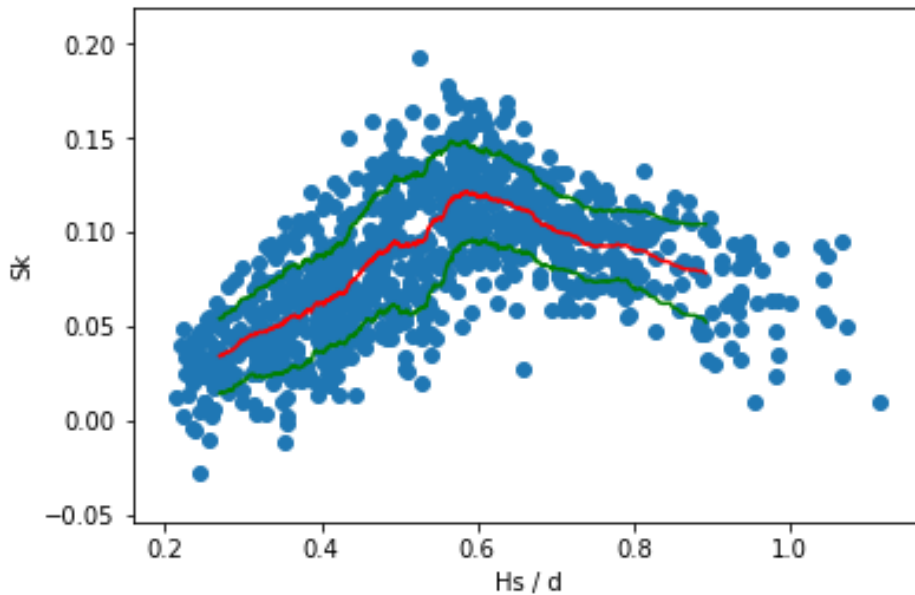
Figure 4.11: Where Sk is the average skewness of the significant waves over 5 minutes Hs/d is the relative significant wave height every 5 minutes. The blue dots are the mean of observed skewness at these relative significant wave heights every 5 minutes, The red line is the mean of every 100 points and the green lines are the mean +/- a standard deviation.

4.4. Settings model

There are two additional settings for the model: the time step between each cycle trough the modules, and the step in space between locations were the bed level change is estimated for. The time step is set at 10 minutes as the deep water waves are measured for every ten minutes. The step in space is set for 0.1 meters to ensure that small changes will be noticed.

5

Results

The main goal of this study is to gain knowledge about how the bed level is behaving on a small time scale and what effects are influencing this behavior. This chapter is divided into three different segments. First, the results of the field work, the observations, will be presented. A short elaboration is given on the results. The observations are used to see if short wave processes can be used to estimate bed level changes. Secondly, the model sensitivity is presented to see the effects of different waves on the model. Thirdly, the results of the model are presented and compared to the observations.

5.1. Observations
In this section, the observations from Chapter 3 were presented and explained. The observations made when the water depth is lower than 0.4 meters were ignored, as these observations were considered unreliable.
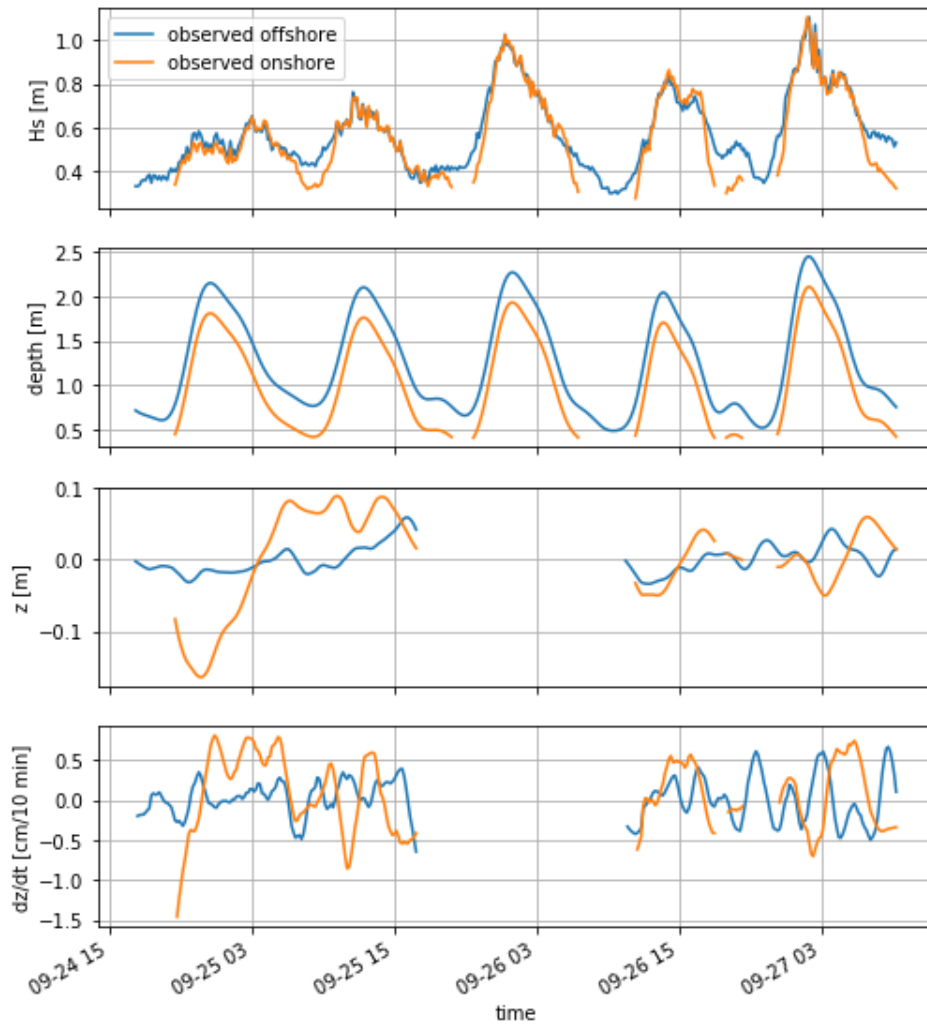
Figure 5.1: The observations at the offshore and onshore location of the sensors. The x-axis is the time. The top panel is the significant wave height. The y-axis is the wave height in meters. The second panel is the water depth. The y-axis is in meters. The third panel is the bed level compared to the initial bed level. The y-axis is in meters. The bottom panel is the bed level changes over time. The y-axis shows if there is erosion, a negative value, or aggregation, positive value, the axis is expressed in centimeters per 10 minutes.

The pressure sensors observed the water pressure and from the water pressure, the significant wave and tide were extracted. The significant waves observed during the week were almost similar for both locations during high tide, which can be seen in figure 5.1. When the water level dropped, the waves started to differ, as the waves at the onshore location decreased faster and became lower. During high tide, the maximum significant wave recorded at the offshore location was ≈ 1.1 meters, and the minimum recorded was ≈ 0.5 meters. The significant wave height increased throughout the days of the fieldwork. For the first tides, the maximum significant waves were lower than 0.8 meters. During the fourth and fifth high tide, the recorded waves were higher than 0.8 meters.

The third panel shows the bed level over time. At the offshore location, the bed level had a maximum rise of 6 centimeters and a maximum decrease of 3 centimeters. At the onshore location, the bed level had a maximum rise of 9 centimeters and a maximum decrease of 16 centimeters. The bed level on both locations was oscillating around the starting value. The onshore bed level increase and decrease were larger than the offshore bed level increase and decrease. Interestingly, the measurements of the first day showed large changes in the bed level at the onshore location.

The bed level rate of change for every ten minutes shows the direction and magnitude of

the change observed. The offshore location changes were observed and fluctuated between -0.5 and 0.5 centimeters, as is shown in the fourth panel. At the onshore location, bed level changes were more extensive. This indicates that closer to shore, the bed level is responding faster.

5.2. The measurements certainties

The waves were measured with pressure sensors that have an accuracy of 0.0005 % and a signal to noise ratio of 18. Reducing or increasing the pressure signal with the error effected the waves. The waves increased or decreased with 0.1 meters. Also, the pressure signal was converted to waves using the linear wave theory. This is known to cause errors in the nearshore. The error it causes is not known and will not be derived in this research, as this is considered out of the scope.

The bed level was observed with echo sounders. The echo sounders had a precision of millimetres in ideal circumstances. In chapter 3, the back scatter information was used to find the bed level. The back scatter gave possible locations of the bed level, and these locations were combined and averaged to determine the bed level. The spread of the locations was used to define the certainty of the bed level. The average spread of the bed level at the offshore location was 4.7 centimeters, and the average spread of the onshore location was 7.8 centimeters.

5.3. Relative wave height and bed level changes

To see if bed level changes could be predicted based on wave processes, the bed level changes were ranked depending on the relative wave height. The relative wave height was used to identify the wave process (Masselink et al., 2006). The observed data was used to see if bed level rise and fall could be predicted based on wave processes, as was derived from the sediment fluxes based on wave processes Masselink et al. (2006). The significant waves observed were divided by the local water depth to get the relative significant wave height. The bed level changes were normalised by dividing them by the maximum change observed, which is 0.811 centimeter in ten minutes at the onshore location. The observed bed level changes were categorised based on the relative wave height in bins with a size of 0.05 from the relative significant wave height to show the average bed level change.
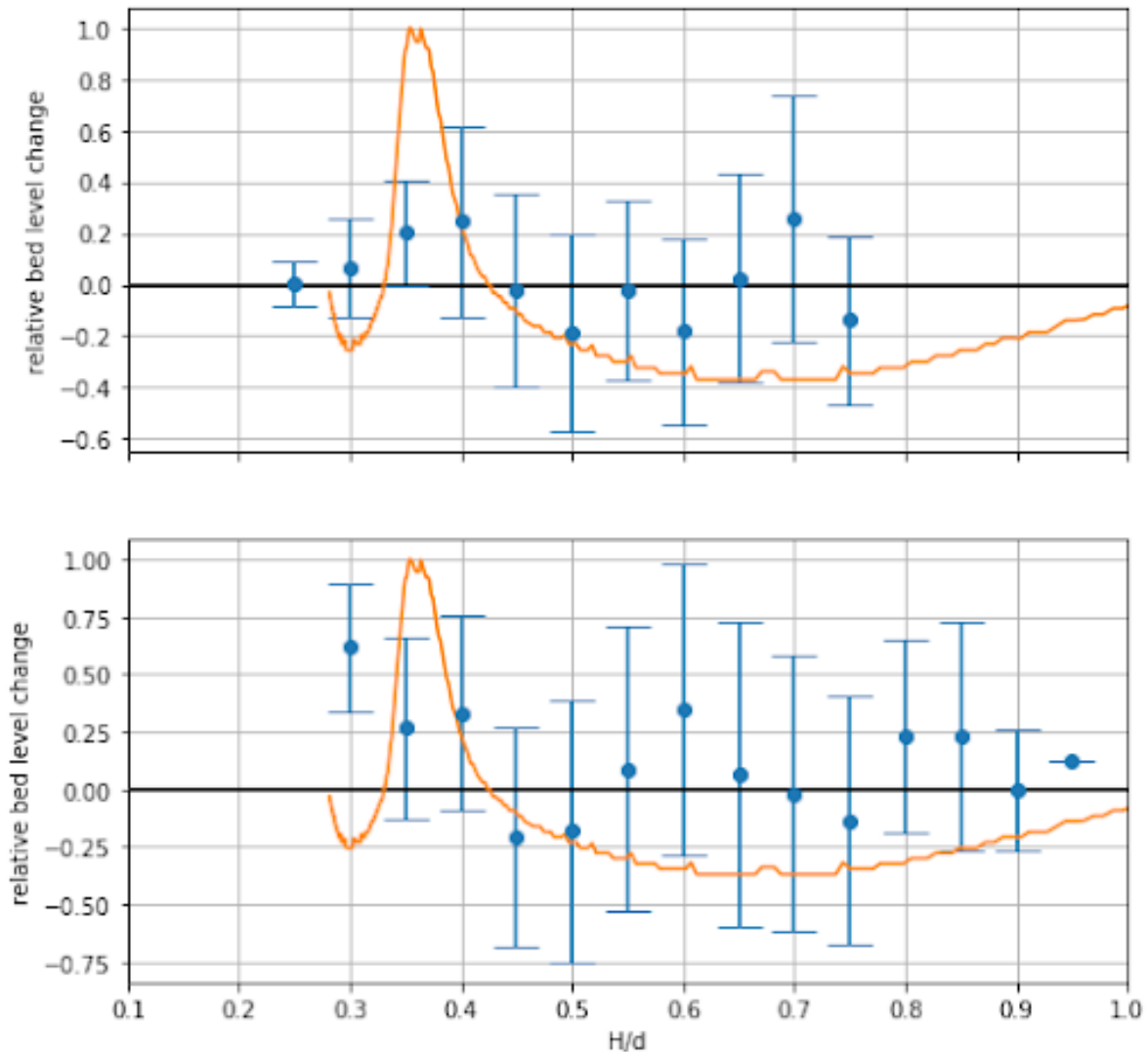
Figure 5.2: The bed level change pattern that was in the conceptual model compared to the observations in the field. The x-axis is the relative significant wave height. The y-axis is the relative bed level change. The top panel shows the offshore observations, while the panel below is the onshore observations. The orange line is the conceptual model suggested by Masselink et al. (2006) for a planar beach. The blue dots were the average values per relative wave height, and the blue lines show the standard deviation of the data used to determine the average.

At the offshore location, the average bed level change was mostly positive when the relative wave height was between 0.3 and 0.4. The average bed level change was negative between a relative wave height of 0.45 and 0.5. The average bed level change was shifting between positive and negative when the relative wave height is larger than 0.55, and deviated more as can be seen by the increase of the size of the standard deviation bar in the first panel. For the onshore location, the average bed level change was positive between a relative wave height of 0.3 and 0.4. The average bed level change was negative between a relative wave height of 0.45 and 0.5. The average bed level change from a relative wave height of 0.55 till 0.95 was shifting between positive and negative, as can be seen in the second panel.

In both locations, the average bed level change went in the same directions between a relative wave height of 0.3 till 0.5. When the relative wave height was higher than 0.5, the bed level changes deviated more, as can be seen by the blue bars (5.2). These blue bars reach from a negative bed level change to a positive bed level change indicating that the bed level does not change in an overall direction. The results indicate that there is a general bed level change when the relative significant wave height was between 0.3 and 0.5 and that there is

no general bed level change when the relative wave height was larger than 0.5.

5.4. Sensitivity of the model on different wave conditions

The second part discusses if water flows dominate bed level changes on a time scale of minutes. The bed level was predicted using a cross-shore model described in chapter 2. The cross-shore model only used velocity estimates to predict bed level changes. The model was tested to see how sensitive it reacted to different input conditions of the waves. The sensitivity was tested for three different input conditions: the significant wave height, the significant wave period, and the breaker parameter. The test was done with the input data collected in chapter 4. The different parameters were increased and decreased, to see the effects on the bed level change.
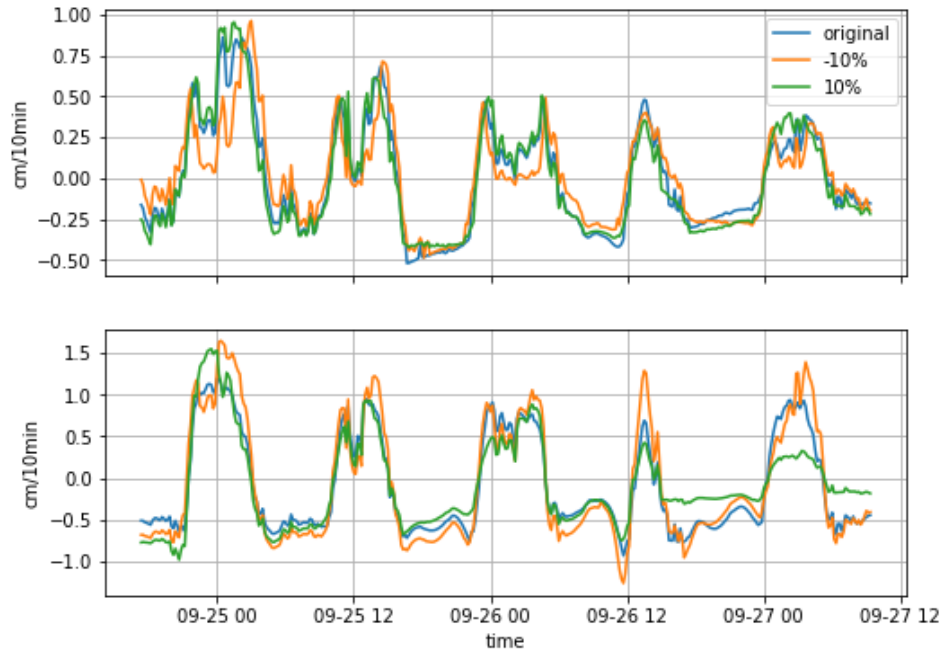
Figure 5.3: The effect of changes in the wave height for the bed level predictions. The top panel is the offshore location and the panel below is the onshore location. The y-axis is the bed level rate of change and direction of change every ten minutes, positive value means a rise of the bed level. The x-axis is the time. The blue line is the input found in chapter 4 for the significant wave height, the orange line is a decrease of 10 percent and the green line is an increase of 10 percent.
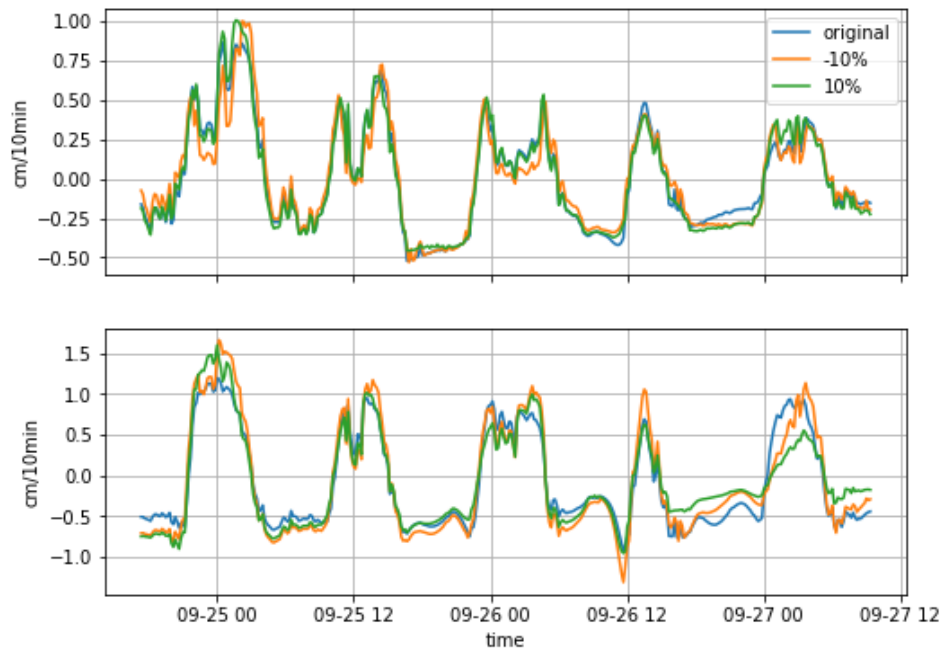
Figure 5.4: The effect of changes in the wave period for the bed level predictions. The top panel is the offshore location and the panel below is the onshore location. The y-axis is the bed level rate of change and direction of change every ten minutes, positive value means a rise of the bed level. The x-axis is the time. The blue line is the input found in chapter 4 for the significant wave period, the orange line is a decrease of 10 percent and the green line is an increase of 10 percent.
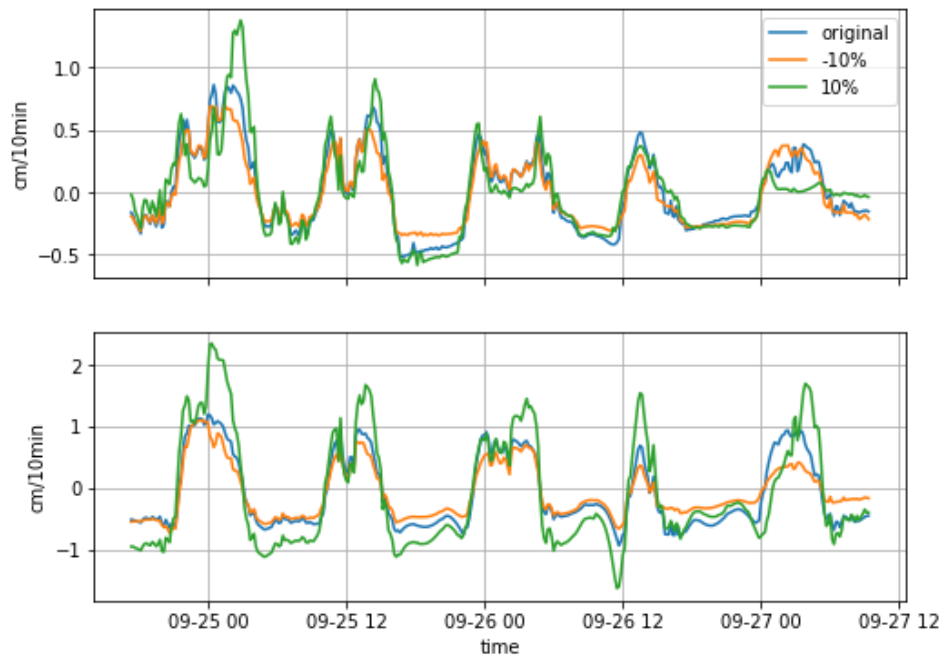
Figure 5.5: The effect of changes in the breaker parameter for the bed level predictions. The top panel is the offshore location and the panel below is the onshore location. The y-axis is the bed level rate of change and direction of change every ten minutes, positive value means a rise of the bed level. The x-axis is the time. The blue line is the input found in chapter 4 for the breaker parameter, the orange line is a decrease of 10 percent and the green line is an increase of 10 percent.

The 10 % change of the input conditions show that the direction of change was hardly effected. However, the rate of change was influenced by changes in the conditions. The model was effected the most by changes in the breaker parameter and the least effected by changes

in the period. The sensitivity test showed that the model is robust to minor differences in the input conditions, as the changes only influence the rate of change. The error of the waves observed was 0.1 meter from the signal to noise ratio. Therefore, the model was tested with this deviation added and subtracted from the wave height. Due to the error of the pressure sensor, the wave breaker parameter differed as well. The wave breaker parameter was spread between 0.59 and 0.71. Therefore the 0.71 value was tested to see the effect on the bed level predictions.
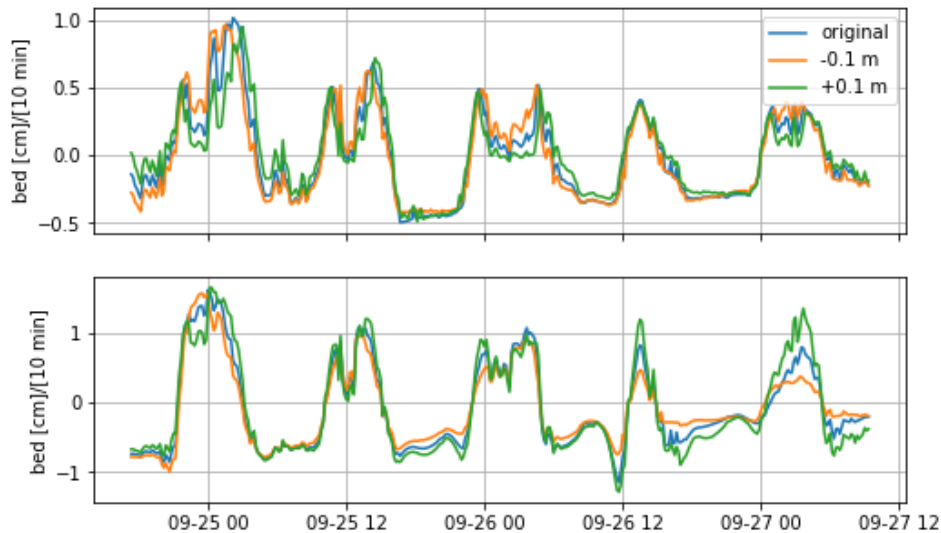
Figure 5.6: The effect of changes in the wave height for the bed level predictions. The top panel is the offshore location and the panel below is the onshore location. The y-axis is the bed level rate of change and direction of change every ten minutes, positive value means a rise of the bed level. The x-axis is the time. The blue line is the input found in chapter 4 for the significant wave height, the orange line is a decrease with 0.1 meter and the green line is an increase of 0.1 meter.
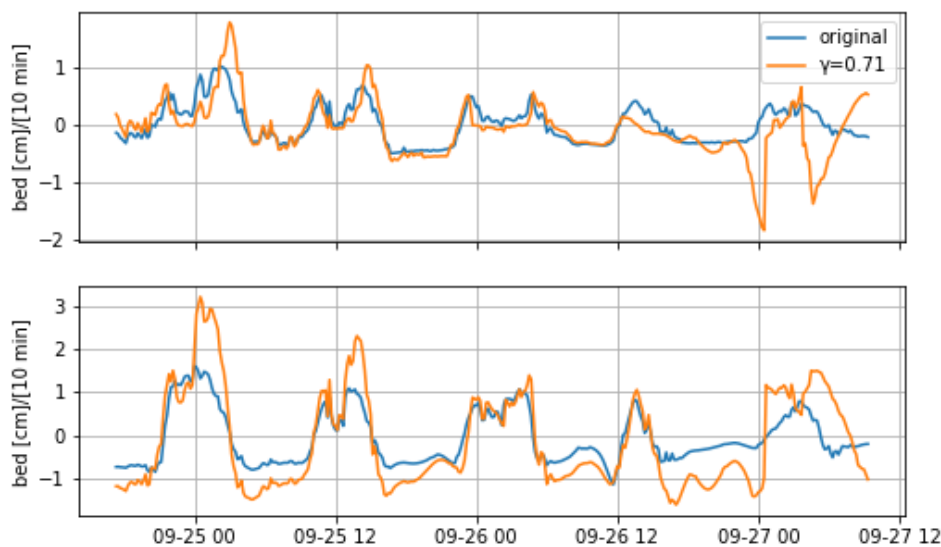
Figure 5.7: The effect of changes in the breaker parameter for the bed level predictions. The top panel is the offshore location and the panel below is the onshore location. The y-axis is the bed level rate of change and direction of change every ten minutes, positive value means a rise of the bed level. The x-axis is the time. The blue line is the input found in chapter 4 for the breaker parameter, the green line is the breaker parameter of 0.71.

Next to that, the input conditions were changed with 50 % to see the effects. The breaker parameter was only increased to 0.89, as values that were lower than 0.3 were considered not realistic (Holthuijsen, 2009).
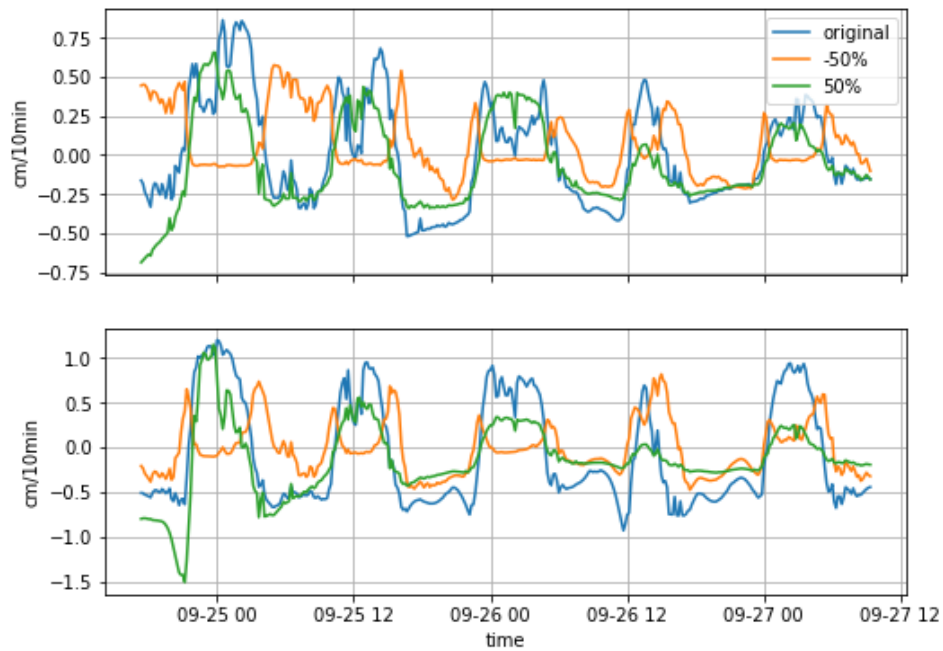
Figure 5.8: The effect of changes in the wave height for the bed level predictions. The top panel is the offshore location and the panel below is the onshore location. The y-axis is the bed level rate of change and direction of change every ten minutes, positive value means a rise of the bed level. The x-axis is the time. The blue line is the input found in chapter 4 for the significant wave height, the orange line is a decrease of 50 percent and the green line is an increase of 50 percent.
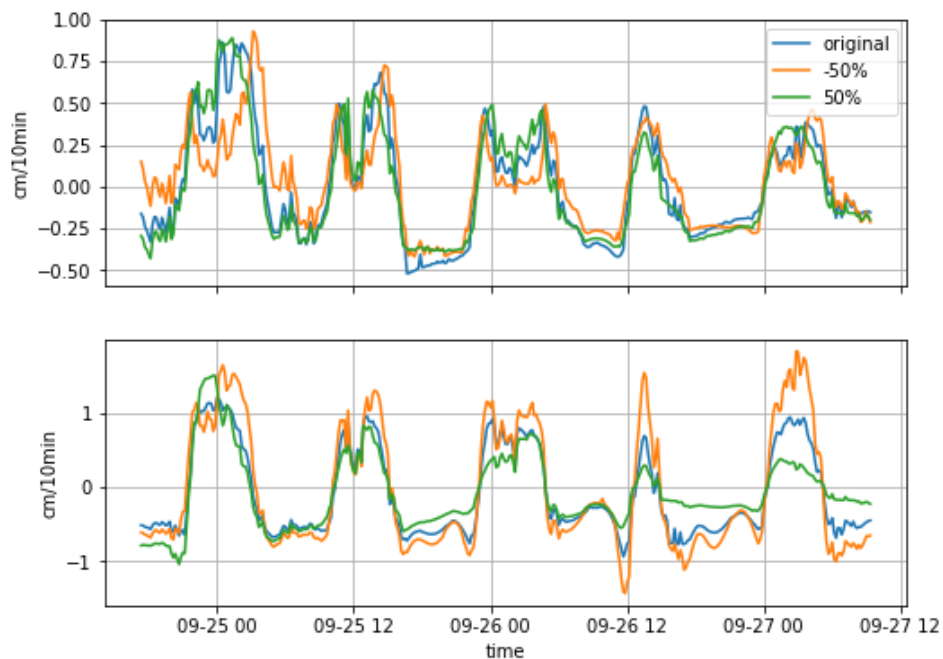
Figure 5.9: The effect of changes in the wave period for the bed level predictions. The top panel is the offshore location and the panel below is the onshore location. The y-axis is the bed level rate of change and direction of change every ten minutes, positive value means a rise of the bed level. The x-axis is the time. The blue line is the input found in chapter 4 for the significant wave period, the orange line is a decrease of 50 percent and the green line is an increase of 50 percent.
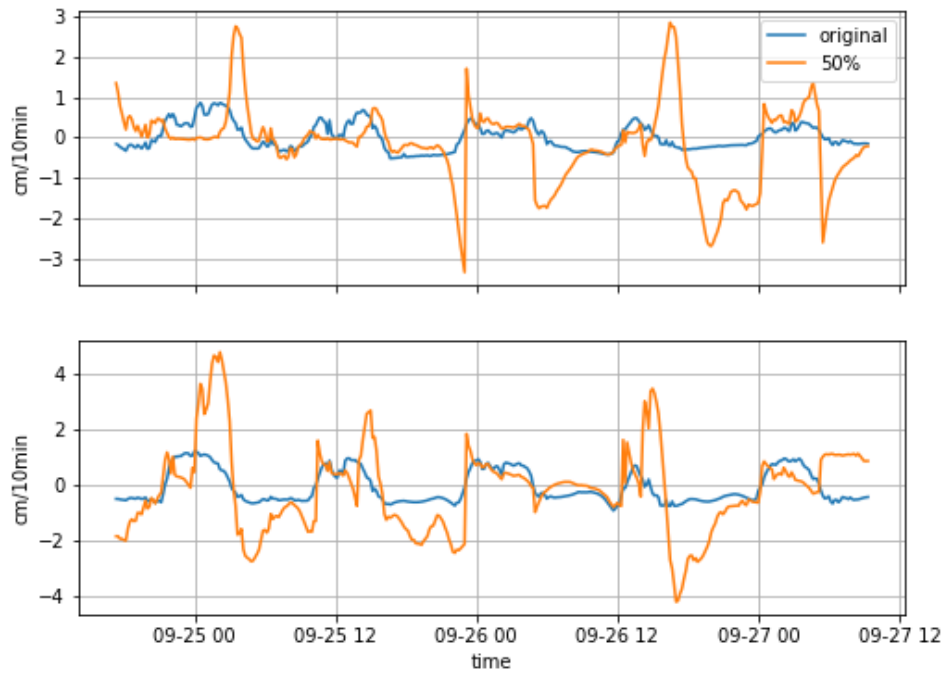
Figure 5.10: The effect of changes in the breaker parameter for the bed level predictions. The top panel is the offshore location and the panel below is the onshore location. The y-axis is the bed level rate of change and direction of change every ten minutes, positive value means a rise of the bed level. The x-axis is the time. The blue line is the input found in chapter 4 for the breaker parameter, the orange line is an increase of 50 percent.

With the 50 % change, the dominance of the breaker parameter became more pronounced. The breaker parameter had the most significant effect on the bed level change (figure 5.10). The wave height, when decreasing, influenced the direction of the bed level changes, as a decrease in the wave height was able to change the direction of the bed level predictions. The offshore location started to show an increasing bed level, where it first showed a decrease. The effect of the wave period remained limited.

parameter	deviation	offshore	onshore
wave height	−50%	0.41	0.57
	−10%	0.13	0.21
	-0.1 meter	0.09	-0.15
	+0.1 meter	0.14	0.17
	+10%	0.08	0.24
	+50%	0.21	0.37
wave period	−50%	0.17	0.28
	−10%	0.08	0.19
	+10%	0.05	0.21
	+50%	0.10	0.26
wave breaker parameter	γ=0.53	0.09	0.21
	γ=0.65	0.15	0.41
	γ=0.71	0.38	0.63
	γ=0.89	0.94	1.30

Table 5.1: overview of the root mean square errors from the original signal, in centimeter per 10 minutes for each deviation

The model was more sensitive to deviations at the onshore location than at the offshore location. A change in the breaker parameter effected the bed level predictions the most and the bed level predictions were the least influenced by an increase in the period of the waves.

5.5. Predictions of the model compared to the observations

In this section, the results of the model were compared to the observations. Firstly, the waves were compared. Secondly, the bed level was compared, and lastly the bed level changes were compared. A small conclusion will follow on the comparison of the results and the observations.

5.5.1. Waves
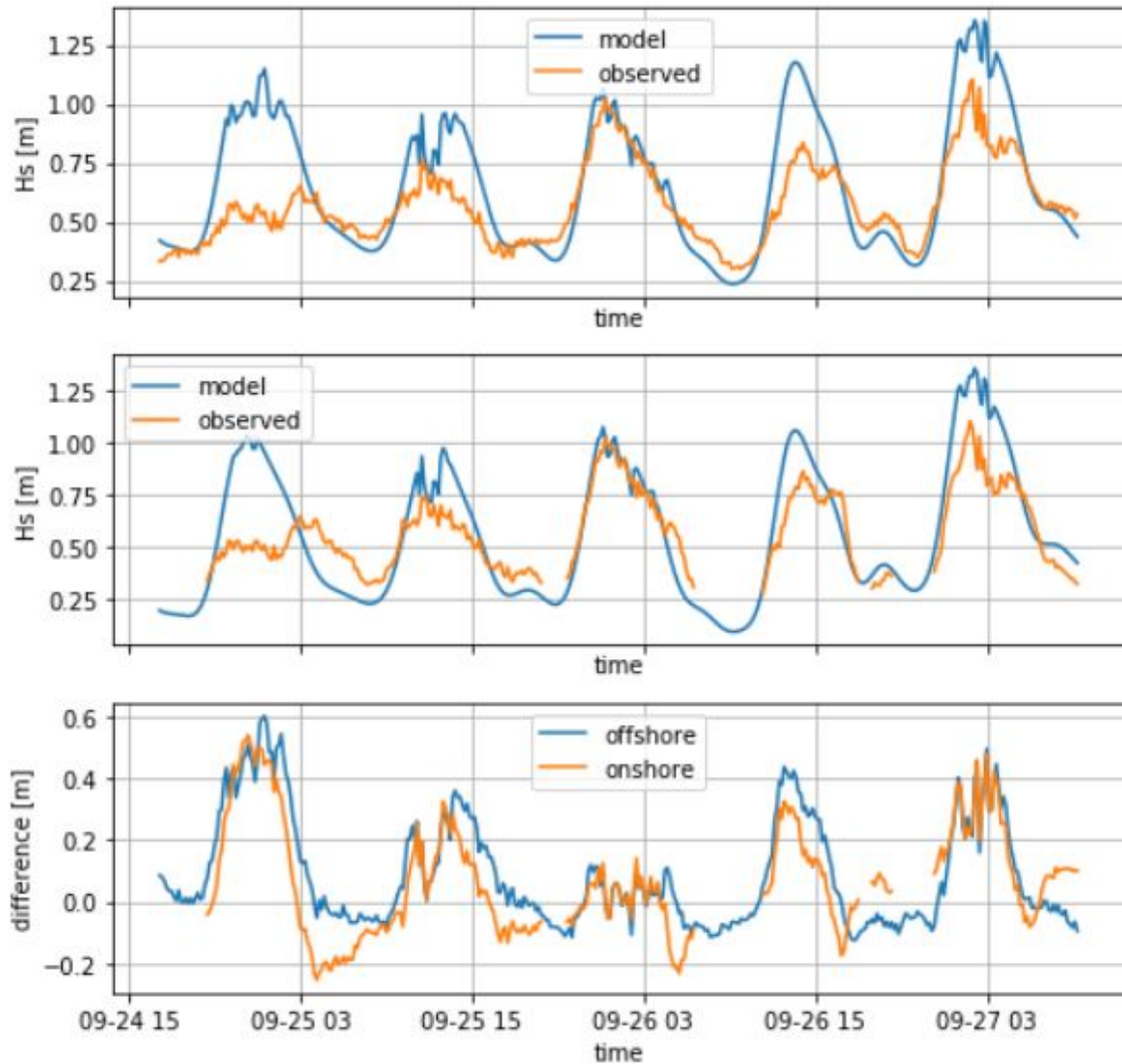
Figure 5.11: The waves predicted compared to the observed waves. The x-axis is the time the y-axis is the significant wave height in meters. The first panel shows the offshore location and the second panel shows the onshore location. The third panel shows the difference between the observations and the modelled waves at different locations.

There is a difference between the waves observed and the waves in the model. Apart from the third tide, the model overestimated the waves at both locations. When there was a low tide, the model underestimated the height of the waves. The most substantial difference between the waves observed and the waves in the model were seen in the first high tide, where differences of 0.6 meter were observed. The differences were the smallest for the third tide, where differences of 0.2 were observed.

5.5.2. Bed level
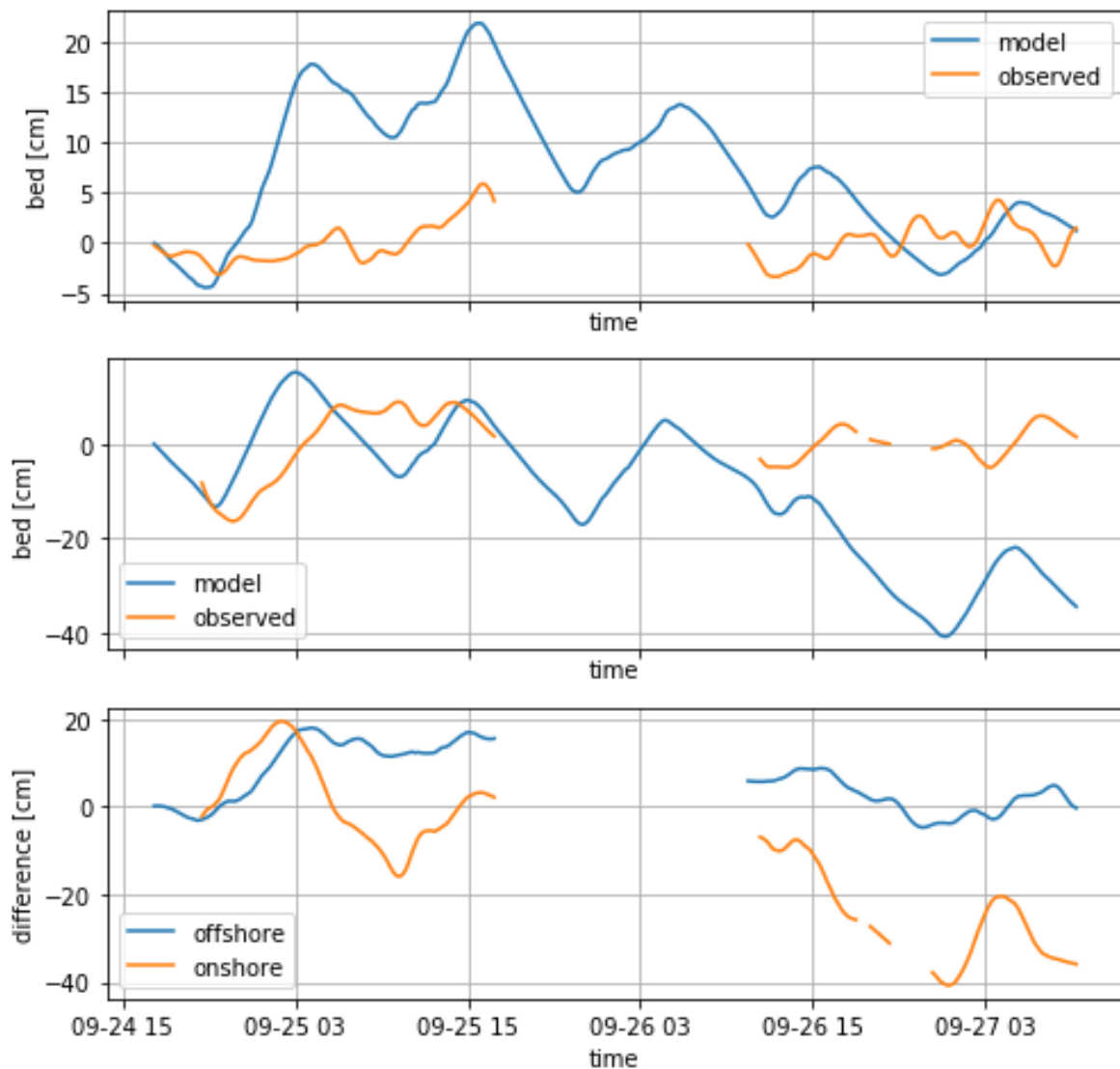
Figure 5.12: The bed level predicted over time. The first panel is the offshore location, and the second panel is the onshore location. The x-axis is the time. The y-axis shows the bed level; when the direction is negative, there is erosion. When the direction is positive, the bed level is aggregating. The third panel shows the difference between the bed level predicted by the model and the bed level observed.

The bed level was compared between the model and the observations for both locations. There was a difference between the bed level in the observations and the bed level derived from the model. The bed level at the offshore location showed that the model predicted a bed level rise of 20 centimeters, while in the observations there was a rise of only 5 centimeters. There was, however, a similar pattern of bed level change between the observations and the model. This was observed during the decrease of the second tide. The model predicted a fall after the rise of 20 centimeters, where the observations are missing. When the observations continued, the bed level had eroded back to the initial bed level. The second panel shows the onshore location. Here, the bed level changes were larger. The model predicted an erosion pattern that is not visible in the predictions made by the model. Over time, the differences between the observed onshore location and predicted onshore location grew.
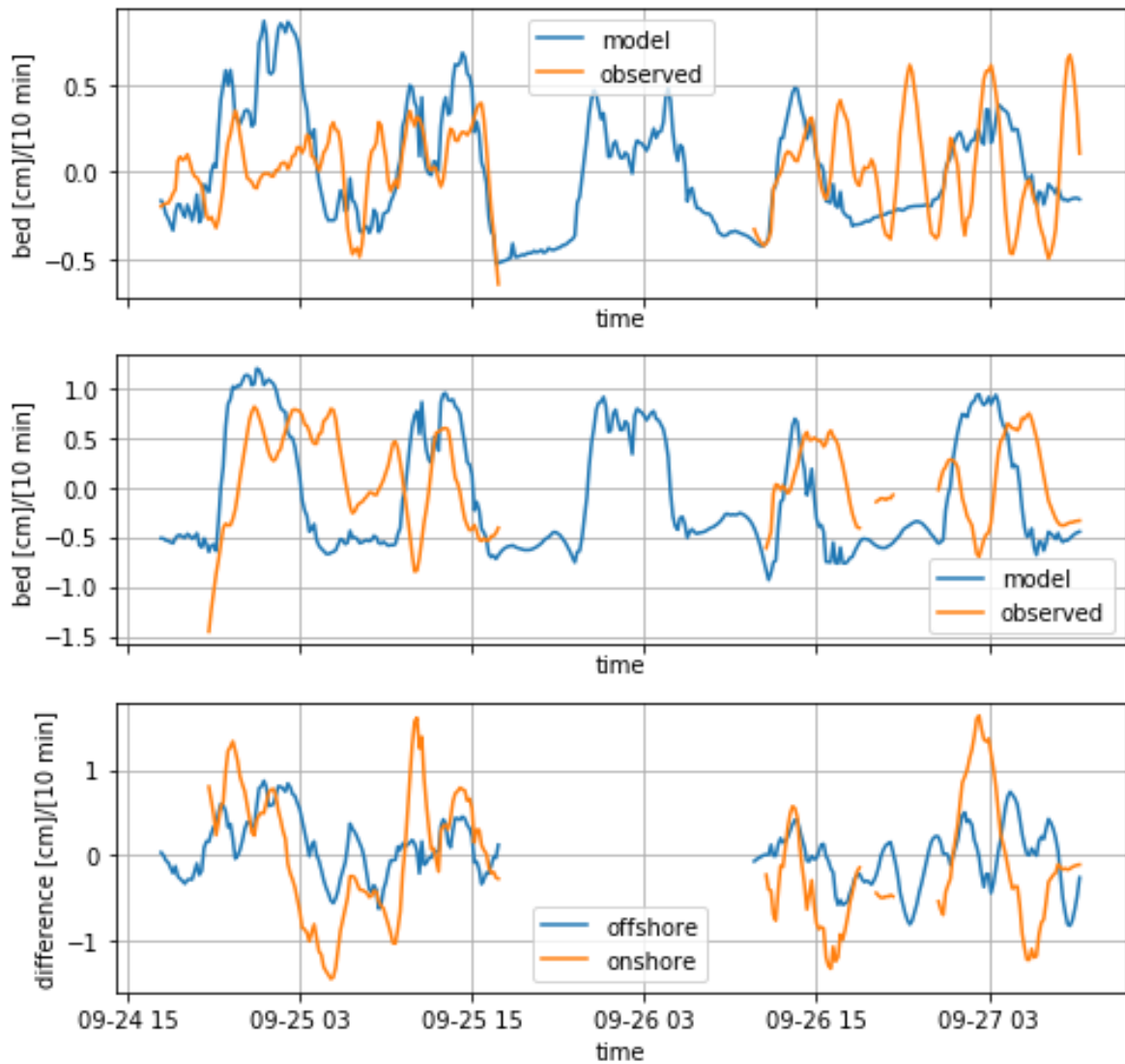
Figure 5.13: The predicted bed level changes and the observed bed level changes. The top panel is the bed level changes at the offshore sensor. The penal below is the onshore bed level changes. The x-axis is the time. The y-axis shows the change of the bed level in centimeters per 10 minutes. If the change is negative, the bed level is eroding.

(a)

(b)
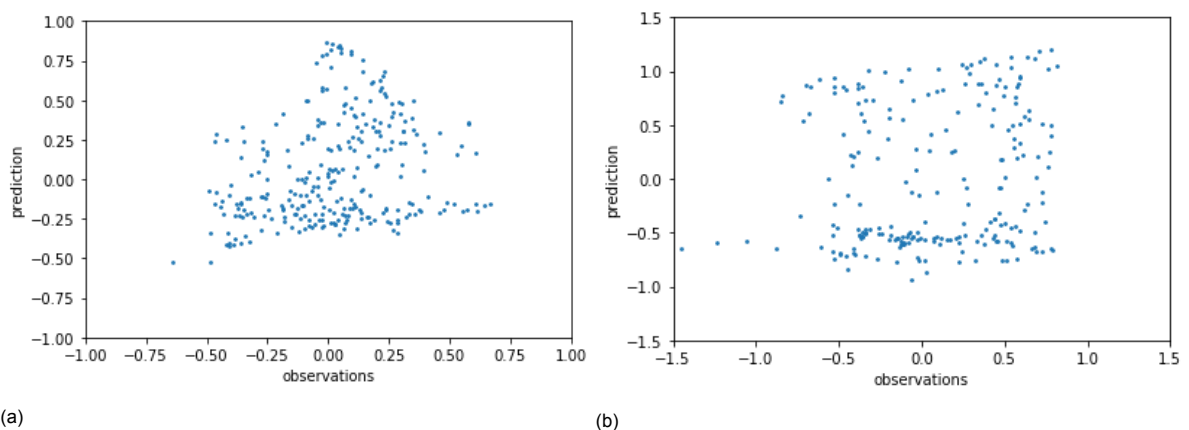
Figure 5.14: Correlation between the observations and the predictions at the offshore (a) and onshore (b) locations. The x-axis is the observed values and the y-axis is the model predictions. The offshore location had a $R^2 = 0.067$ and p-value = $1.3 \cdot 10^{-5}$, The onshore location had a $R^2 = 0.015$ and p-value = 0.09

5.5.3. Bed level changes

The bed level changes within ten minutes were compared between the model and the observations, as shown in figure 5.13. The model was predicting longer periods of bed level increase and decrease than the observations. The bed level changes predicted by the model ranged from ≈ -0.5 to 1 centimeters. The observations showed rates between -0.5 and 0.5 centimeters. Differences between the observations of the bed level change and model predicted bed level changes were between ≈ -1.5 and 1.5 centimeters.

The squared value of the correlation coefficient tells how much of the variances of the signals were related. The p-value shows how likely it is to receive the same amount of correlation with a random data set. The correlation between the observations and the prediction is shown in table 5.2. There is little to no correlation between the model and the bed level predicted.

Location	Correlation	Determinant of correlation	P-value
Offshore	0.26	0.067	$1.3 \cdot 10 - 5$
Onshore	0.11	0.015	0.090

Table 5.2: The results of the correlation

The model would ideally work on perfect matching wave conditions, but the waves in the model and the observation were different. During some high tide conditions, the waves matched better than other high tides. Therefore, the model was tested per tidal cycle to see if the correlation improved when the waves matched better during high tide.

5.6. Comparison per tide
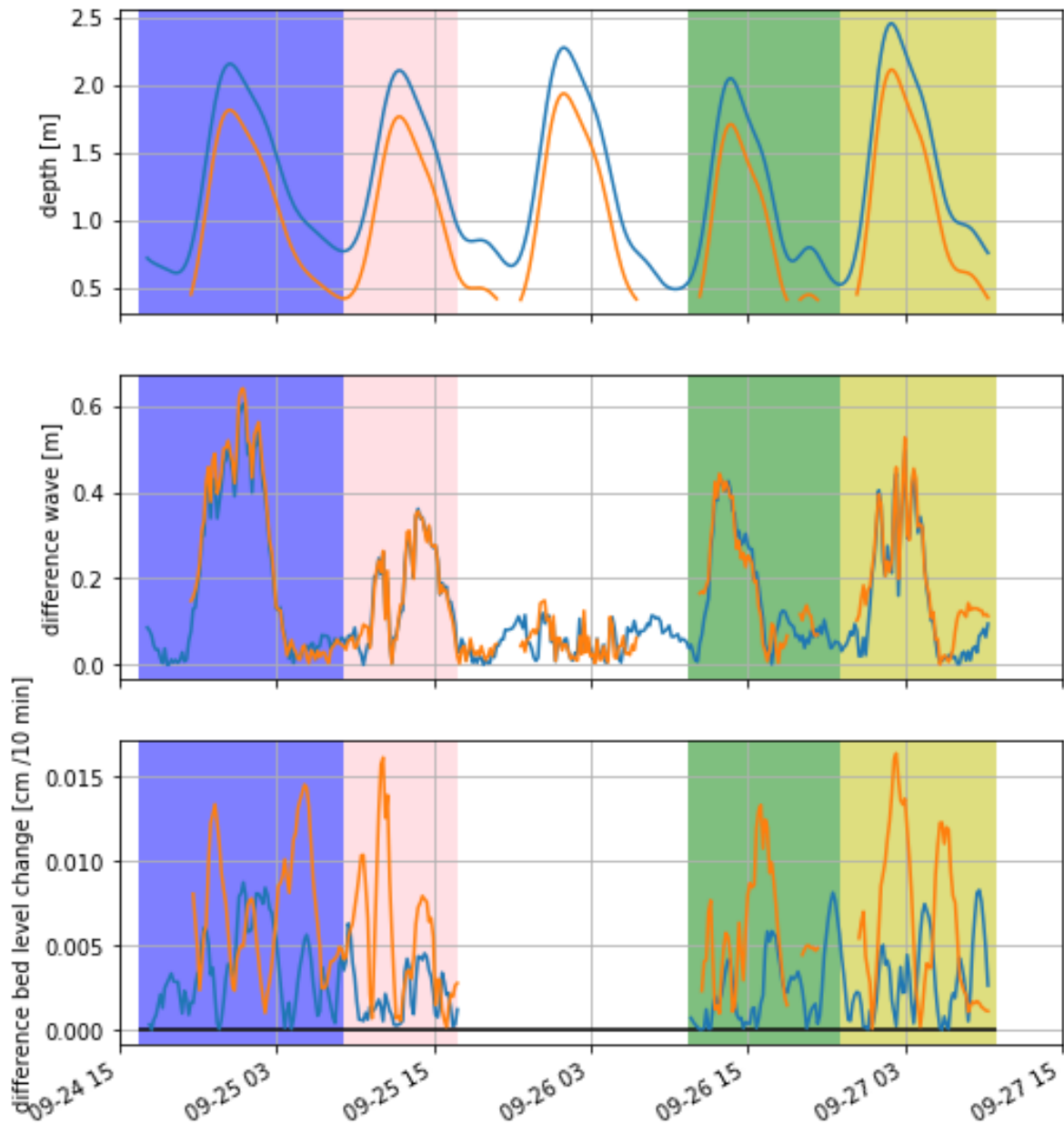
Figure 5.15: The data divided into four tides. The top panel shows the tidal signal observed. The middle panel shows the difference in the waves predicted, and the waves observed over time. The lowest panel shows the difference between the bed level change observed, and the bed level change predicted. The x-axis is the time, and the y-axis is the absolute value. The blue line is the offshore location, and the orange line is the onshore location. The transparent colours indicate the tide. The blue tide is the first tide, pink the seconds, green the third and yellow the fourth.

The data is divided into four different tides. The bed level predictions and the observations were compared to calculate the correlation coefficient for each tide. The aim is to see if the prediction of the bed level is improving when the waves match closer. The results for each tide is shown in table 5.3. The wave error is the maximum difference between the observed wave and the predicted wave for a whole tidal cycle.

Location	Tide	Wave error [m]	Correlation	Determinant of correlation	P-value
Offshore	1st	0.6	0.28	0.08	0.0074
	2nd	0.36	0.61	0.38	$1.3 \cdot 10^{-6}$
	3rd	0.44	0.31	0.10	0.0090
	4th	0.50	0.12	0.014	0.33
Onshore	1st	0.54	0.25	0.061	0.039
	2nd	0.33	0.15	0.023	0.29
	3rd	0.32	0.29	0.090	0.040
	4th	0.48	-0.19	0.038	0.14

Table 5.3: Results per tide per location

The correlations show that for the offshore location, the best performance of the model is achieved when the wave error is the lowest. However, during this tide, the same improvement was not observed for the onshore location. This indicates that the model is not able to predict the bed level at the onshore location. The results of the model over the whole week show that the model is incapable of predicting the bed level changes with precision during the week with the given input. The sensitivity analysis shows that this can occur due to large differences between the waves as input for the model and the waves observed. The wave breaker parameter can also be the reason.

Discussion

6.1. Observations

During the fieldwork, two echo sounders were used to make observations of the bed level. These observations are interesting on their own. It was observed that the bed level at the onshore location was able to move 20 centimeters within a single tide. The bed level of the offshore location, however, showed less fluctuations. These large changes could have happened because of different reasons.

One of these reasons can be sand ripples. When ripples move over the bed level, movement is observed by the echo sounder. Becker et al. (2007) used video images and echo sounders to observe ripple behavior in the nearshore, and showed in an overview that 1 meter long ripples with an amplitude of 0.15 s were observed on a beach in New Jersey. However, the sand ripples can have different migration rates. Becker et al. (2007) found that sand ripples move between 2 to 10 meters a day and have a length ranging between 2 centimeters and one meter. So, the observed bed level change can be the result of sand ripple only if the amplitude is 0.1 meters and the ripple length and migration rate are at such a length and speed that it passes over in 5 hours.

Next to sand ripples, there is another reason which can result in large bed level changes. This might happen when the coast moves between states. Due to changing wave conditions, the shape of the beach changes. The change of the shape can cause erosion and aggregations on different locations (Coco et al., 2014). This can be the case, as the wave conditions may have been different a day before the measurements started. During the fieldwork, when the wave conditions changed, no large changes in the bed level were observed. Therefore, this reason was not likely to be the case during the fieldwork.

Furthermore, a migrating sandbar at the location of measurement can be another explanation . Nielsen and Shimamoto (2015) observed that a sandbar under a single wave could cause a bed level shift of 0.5 meters during a single tide. However, in the field, more waves are present. This can result from the sandbars having a smaller crest. This is because different sized waves cause different sediment transport along a cross-shore profile, damping the effect of a sandbar (Mariño-Tapia et al., 2007b). This can be the case as there was a sandbar forming in the intertidal zone during the fieldwork, which can be seen in appendix A. The significant bed level change is most likely caused by a large slowly migrating ripple or a sandbar.

The bed level observations showed that the rate of change was below a centimeter per ten minutes, with a single exception at the beginning of the fieldwork. Changes of the bed level observed at the onshore location were larger than the onshore location. The average change during the flume experiment described by Nielsen and Shimamoto (2015) was around 1.67 centimeters every ten minutes. This is larger than was observed in the field. The difference results from the fact that the flume experiment was conducted with a single wave, while during the field work there were multiple waves influencing the bed level changes. The multiple waves spread the sediment fluxes and decreased the bed level response rate.

Bed level change have been observed in the field in the surf zone with a depth less than 1 meter at the beach of Egmond aan Zee. At this location, similar maximum bed level change rates were found. These were between 0.2 and 2.2 centimeters per ten minutes (Saulter et al., 2003). This shows that the observations are realistic and in line with previous research.

The differences in the depth could have been the reason for the differences in responses at both locations. Depending on the depth, the flow velocity was influenced by a passing wave (Holthuijsen, 2009). Sediment transport depends on the dissipation of energy on the bed level and bed friction depends on the flow velocity of the water in a higher-order (Bailard and Inman, 1981). Therefore, the sediment fluxes are larger closer to shore, and bed level changes due to sediment fluxes happen faster in shallower water. This can be a reason for the faster bed level changes closer to shore.

There are limitations to these observations. The bed level was observed using the backscatter information from two echo sounders. The certainty spread of the bed level observations were in the order of centimeters while the observed changes every ten minutes were in the order of millimeters. Therefore, it was impossible to distinguish between measurement errors and bed level changes. The observations of the pressure sensor had errors in the magnitude of decimeters of the wave height and the direct influence of the significant wave height did not significantly impact the model. However, the wave parameter changes due to this error had a significant impact on the root mean square error. The root mean square error of the breaker parameter difference was 0.38 centimeters at the offshore location and 0.63 centimeters at the onshore location. The accuracy of these observations is a major limitation to the research, as the errors are larger than the observations.

6.2. Wave process and bed level changes

The bed level changes are linked to wave processes using the relative wave height. When a beach is planar, cross-shore sediment fluxes are expected based on wave processes (Masselink et al., 2006). These fluxes can be used to predict bed level changes. Relative wave height is used to identify wave processes. Masselink et al. (2006) stated that

- Waves are shoaling when the relative wave height of the significant wave is lower than 0.3.

- The waves are breaking when the relative waves are between 0.3 till 0.5.

- When the relative waves are between 0.5 and 1, the waves are in the inner surf zone travelling as bores towards the coast.

The results showed that the bed level was rising when the relative wave height was between 0.3 and 0.4 and the bed level was falling between 0.4 and 0.5. After 0.5, the bed level movement went in both directions. When linking these results back to wave processes, it showed that there was aggregation as a result of waves breaking. This was predicted by the planar beach model (Mariño-Tapia et al., 2007a; Masselink et al., 2006). When waves are shoaling, they are non-linear, and this effect causes onshore sediment transport. However, when waves start breaking, undertow becomes more dominant. The undertow counters the effect of the shoaling waves causing the sediment to aggregate at that location. The undertow depends on the dissipation of energy of the waves. When more waves are breaking, the undertow becomes stronger. This causes more sediment to move offshore, and thus explains the erosion observed. This is again in line with the expected behavior (Mariño-Tapia et al., 2007a; Masselink et al., 2006). The results show that after 0.5 the bed level is not moving in a single direction. However, according to Mariño-Tapia et al. (2007a); Masselink et al. (2006) there should be erosion. This shows that the short wave predictions are not valid for the inner surf zone observations. From the mentioned studies and the results, it follows that the bed level behavior in the outer surf regions is understood and short waves can be used to describe the direction of change. However, this is not applicable to the inner surf zone.

There are two limitations to this method. The waves were observed using pressure sensors. The pressure was used to estimate the waves using the linear wave theory. However, this theory is known to cause errors in coastal regions where the waves are not linear (Holthuijsen, 2009). The pressure sensors installed in these conditions also have errors; these errors change the wave height. This can have large consequences as was seen for the breaker parameter, where the relative wave height changed with 0.2 due to this difference. The beach was assumed to be planar, but this was not certain as no deep bathymetry measurements

were taken that week. Therefore, the response of the bed level may have been different as a beach that is not planar would react differently.

6.3. Applications of the cross-shore model

The model was tested to see the sensitivity of the wave parameters. The model predicted sediment transport similar to Mariño-Tapia et al. (2007b). The predicted sediment transport in case of a planar beach caused a bed level response that had erosion along the entire cross-shore profile, and solely aggregation where the waves were breaking. This bed level reaction is in line with the break point hypothesis, which is used to describe sandbar movement and predict sandbar generation (Mariño-Tapia et al., 2007b). However, if this hypothesis is true for sediment transport, it can also be a method to predict bed level behavior where no sandbar is present. When the tide changes the water level, the location where the waves break changes as well. So does the sediment fluxes along the beach and the bed level response for each location Mariño-Tapia et al. (2007b). The model was tested to see the response to changing input conditions. The model was tested on deviations of 10 % and 50 %, and the noise found in the pressure signal. The input conditions that changed were the wave height, the wave period, and the wave breaker parameter. The bed level predictions were compared based on the rate and direction of change to the model predictions in line with the found parameters in chapter 4.

When the input conditions were changed with 10%, the rate of change responded. However, the direction of change remained similar to the original predictions. The effect did not change the shape of the bed level response. The maximum root mean square error was found for the breaker parameter and was 0.41 centimeters, which is large. The model did not respond significantly to the change of 10% for the direct waves. However, when the wave breaker parameter changed, the effect was considerable.

When the input conditions were changed with 50%, the bed level response changed significantly. The bed level response direction was especially vulnerable for a decrease in wave height for both locations. The vulnerability showed when the wave height influenced the location of the break point. The decrease in the waves caused the breaking waves to move closer to shore. In the original situation, the waves were breaking at the offshore location, which caused sedimentation. In the reduced wave height situation, there was erosion due to wave shoaling at the same location. When the tide decreased in the original situation, the breaker point moved deeper into the surf zone, which caused erosion. However, with the reduced waves, this was where the breaking started. When the wave height was increased, this was not the case, as the breaking point never passed the location similar to the original signal. When the breaker parameter was increased with 50 %, the bed level respond changed completely. The rate of change predicted by the model exceeded 4 centimeters per ten minutes. The direction of change matched for most of the time. However, the root mean square error was the largest observed with the onshore location having an error of 1.3 centimeters. This, in turn, showed the dependence of the cross-shore model on the location of wave breaking and the wave breaker parameter. In short, the model was affected heavily by the large changes in the input conditions and showed to be vulnerable to errors in the breaker parameter.

The noise of the pressure sensor was used to see the effect on the bed level prediction. The significant waves were increased and decreased by 0.1 meters. The effect of this increase in wave height was limited. The largest root mean square error of 0.17 centimeters was found at the onshore location after an increase of 0.1 meters. The pressure noise had an effect on the wave breaker parameter. The wave breaker parameter was found between 0.59 and 0.71. The increase of 0.71 had a large impact on the bed level prediction, the root mean square error was found to be 0.63 centimeters.

The model depended heavily on an accurate wave breaker parameter. When the model is used, care should be taken to find the right breaker parameter. The breaker parameter found in this research contained a large spread and therefore, a large error in the end results. This turned out to be a large limitation to this research.

6.4. The model predictions of the bed level

The cross-shore model was unable to predict the bed level changes with a correlation of at least 0.3. The reasons could be the large difference between the waves observed and the waves from the model. Testing the model showed that when the difference between the waves is 50%, the root mean square error of the prediction is 0.37 centimeter. A difference of 50% was observed during the first tide. However, the waves in the model and the observation do match closely at some occasions. If the difference in waves causes the low correlation between the model and the observations, then the bed level predictions should match better when the waves match better.

The observations and the model predictions were split into four tidal responses with a duration of one tidal cycle per response. The waves were compared when the water depth was more than 1.5 meters. The second tide had the best match with an maximum difference of 0.36 meters. The correlation improved to 0.61 for the offshore location. The improvement was not observed at the onshore location. This indicates that the model is not able to predict the bed level with correlation closer to shore.

The model performed differently for the two locations. A possible explanation can be the exclusion of processes that influence sediment transport. Fernández-Mora et al. (2015) used two different cross-shore models to predict sandbar evolution over a cross-shore profile. The first model was a velocity based model that only includes the effect of water flow estimates similar to the model used in this research. The second model used velocity and accelerations of the water to predict the cross-shore profile. Fernández-Mora et al. (2015) found that the model that included acceleration performed better closer to shore. The findings from Fernández-Mora et al. (2015) and the results from this research indicate that closer to shore, the bed level changes are influenced by water flow and acceleration.

Another reason is that closer to shore, the contribution of long waves is larger and should be included in the normalization of the shape function. In this research, the shape function was normalized using only short waves and mean currents. This may have underestimated the flow of water near the bed in the shallower regions in the inner surf zone and close to the swash zone. In section 1.3, it was explained that the near-bed flow velocity consists of short waves oscillations, mean currents, and long waves oscillations. Mariño-Tapia et al. (2007a) showed that the effect of long waves is important closer to the shore. This might explain the reason for the difference.

Another reason can be the alongshore effects. It was assumed that the alongshore effects were negligible. However, the waves observed during the fieldwork were not perpendicular to the beach. The angle of the waves would have created alongshore effects that can be dominant over the cross-shore effects (Mariño-Tapia et al., 2007b). At the onshore location, it can be that these effects are larger as more energy dissipation happens as more waves are breaking at that location. This, in turn, causes a stronger alongshore current (Grasmeijer, 2002). During the fieldwork, the shape of the intertidal beach was not reacting uniform along the shore, as shown in the appendix C. This shows that the alongshore effects should not have been ignored and can be the reason the weak correlation between the model and the observations.

In the model, there were several parameters taken from other studies at different locations. However, these parameters still need calibration for this beach and research. This lack of calibration will cause errors in the predictions. These are reasons within the model that explain why the model may not have predicted the bed level with more correlation. However, this would influence the bed level prediction on both locations and does not explain the different performance at the locations.

The cross-shore profile used as initial starting bathymetry was based on GPS measurements taken that week of the intertidal zone, and deepwater bathymetry measurements taken in 2016 De Zeeuw et al. (2017). The bed level observations were the most recent deepwater observation found of the location. However, the deepwater profile is not stable and looks different after three years. This can result in different wave propagation towards the shore and influences the bed level predictions.

The waves used as input in the model were transformed from the offshore Euro platform, 60 kilometers from the location. Luijendijk and de Fockert (2011) showed that the transfor-

mation table is able to predict the waves hitting the Dutch coast with a correlation of 0.91. However, based on the observations made and the waves transformed, it does not seem the case for the location of this research. Two reasons can explain this. First, the Sand Engine is sheltered by the Maasvlakte 2, which influences wave predictions. Next to that, Luijendijk and de Fockert (2011) assumed that the wind came from the same direction as the waves for the transformation. However, this was not the case during the fieldwork. Therefore, the waves from the transformation can be larger. The transformation table, as used in this research, proved to be unable to provide the model with accurate waves.

7

Conclusion and recommendations

7.1. Conclusion

This research aimed to increase the understanding of the bed level behavior at a time scale of minutes, and see if this behavior is well understood. In this chapter, the research questions that were presented in section 1.2 will be answered, and the hypotheses that were presented in section 1.4 are tested.

How does the bed level behave on a time scale of minutes in the surf zone and the shoaling zone?

   The hypothesis stated: it is expected that the bed level moves with the tide, and there is an erosion and aggregation pattern visible of at least 10 centimeters when the tide passes over. The tidal signal was not observed at both locations. The hypothesis is rejected.

   The bed level did not respond to the changing tide. The bed level moved in the order of decimeters and was fluctuating at the starting value. The bed level showed changes that are smaller than a centimeter per ten minutes. The bed level observed at the onshore location moved more than the offshore location. The error in the measurement was larger than the observed changes. Therefore the results can be a possible measurement error.

How well suited are short wave processes to predict bed level changes?

   The hypothesis stated: There is a clear distinction between erosion and aggregation visible for different relative wave heights, and the mean of the bed level change is within 0.05 to the bed level change predicted by figure 1.11. The model did match the hypothesis between 0.4 and 0.5. However, it did not match the full figure. Therefore, the hypothesis is rejected.

   The results show that the short wave processes can be used to predict bed level changes at the beginning of the breaker zone. However, it does not hold for the inner surf zone. The pressure sensor and the linear wave theory prove to be a limitation to the certainty of this research, as the wave breaker parameter changed with 0.2 due to noise in the pressure sensor.

How accurate is a velocity based model in predicting the bed level changes in the shoaling and surf zone?

   The hypothesis stated that the cross-shore model only uses flow velocity can predict bed level changes with a correlation of at least 0.3. The results show that this was not the case for both locations. Therefore, this hypothesis is also rejected.

   The waves in the model differed significantly from the waves observed. The sensitivity analysis for the model showed that the model, when the waves are more than 50 % off, the bed level predictions are subdued to large errors. The model correlated 0.61 at the offshore location when the wave difference was 0.36 meters. Furthermore, the model was unable to predict the bed level changes accurately for the onshore location. The model only used near bed flow velocity estimates of short waves and mean currents to predict the sediment transport. But studies showed that different processes become important closer to shore (Fernández-Mora et al., 2015; Mariño-Tapia et al., 2007a). This shows that the model was unable to predict the bed level changes accurately for the complete profile.

61

7.2. Recommendations

This study attempted to study the bed level behavior on a timescale of minutes. Therefore, highly accurate results were necessary. The nearshore is a place were multiple processes happen. For instance, sediment moves into the water or turbulent flow causes air bubbles in the water. These can all interrupt the echo sounder signals. Getting an accurate bed level reading in these conditions proved to be difficult. As a result, it is recommended that measurement certainty is improved for any feather research on small scale changes in the nearshore. As for this research, it is regretful that no second bed level measurements with the precision of millimeters were made to see the performance of the echo sounder.

A better method for the wave observations is recommended for future research. This is due to the sensitivity of the model to the wave breaker parameter. Large errors were found in the model where there were deviations in the wave breaker parameter. The method used in this research, with a spreading of 20%, did not provide an accurate enough wave breaker parameter. The sensitivity analysis showed that the root mean square error is 0.41 centimeters, and errors need to be less than millimeters to accurately observed bed level changes.

The cross-shore model has the potential to work, despite the limitations of the input conditions in this study and the poor performance. The model should be tested with more accurate input conditions to study the effect of the near bed flow velocity, as well as the sediment transport resulting from this water flow estimates. The model is reasonably robust when the wave breaker parameter and it does not require many equations. As a result, the model is computationally inexpensive.

The results of the study showed that there is more movement of bed at the onshore location. This implies that the bed level changes quicker closer to shore. So, there might be a location near shore where the bed level does have a tidal signal, or whether the bed level responds to the tidal signal when there are larger waves. These are potentially interesting question for future research on bed level changes on a smaller time scale.

Bibliography

George Biddell Airy. *Tides and waves*. B. Fellowes, 1845.

Laurent O. Amoudry and Alejandro J. Souza. Deterministic coastal morphological and sediment transport modeling: A review and discussion. *Reviews of Geophysics*, 49(2), 6 2011. ISSN 87551209. doi: 10.1029/2010RG000341.

R A Bagnold. Mechanics of marine sedimentation. *The sea*, 3:507–528, 1963.

J. A. Bailard and D. L. Inman. An energetics bedload model for a plane sloping beach: local transport. *Journal of Geophysical Research*, 86(C3):2035–2043, 3 1981. ISSN 01480227. doi: 10.1029/JC086iC03p02035.

James A. Bailard. Modeling On-Offshore Sediment Transport in the Surfzone. In *Coastal Engineering 1982*, pages 1419–1438, New York, NY, 11 1982. American Society of Civil Engineers. ISBN 9780872623736. doi: 10.1061/9780872623736.087. URL http://ascelibrary.org/doi/10.1061/9780872623736.087.

V. Barthel and E. R. Funke. ESTIMATES OF LONG WAVES IN THE WESER ESTAURY. In *Proceedings of the Coastal Engineering Conference*, volume 1, pages 782–797. ASCE, 1 1985. ISBN 0872624382. doi: 10.9753/icce.v19.53.

Willard N. Bascom. Characteristics of natural beaches. *Coastal Engineering Proceedings*, 1 (4):10, 1 1953. ISSN 0589-087X. doi: 10.9753/icce.v4.10.

J. A. Battjes and J. P. F. M. Janssen. Energy Loss and Set-Up Due to Breaking of Random Waves. In *Coastal Engineering 1978*, pages 569–587, New York, NY, 8 1978. American Society of Civil Engineers. ISBN 9780872621909. doi: 10.1061/9780872621909.034. URL http://ascelibrary.org/doi/10.1061/9780872621909.034.

J.A. Battjes. Surf Similarity. In *Coastal Engineering 1974*, pages 466–480, New York, NY, 6 1974. American Society of Civil Engineers. ISBN 9780872621138. doi: 10.1061/9780872621138.029. URL http://ascelibrary.org/doi/10.1061/9780872621138.029.

J. M. Becker, Y. L. Firing, J. Aucan, R. Holman, M. Merrifield, and G. Pawlak. Video-based observations of nearshore sand ripples and ripple migration. *Journal of Geophysical Research*, 112(C1):C01007, 1 2007. ISSN 0148-0227. doi: 10.1029/2005JC003451. URL http://doi.wiley.com/10.1029/2005JC003451.

William A Birkemeier. The effects of the 19 december 1977 coastal storm on beaches in North Carolina and New Jersey. *THE EFFECTS OF THE 19 DECEMBER 1977 COASTAL STORM ON BEACHES IN NORTH CAROLINA AND NEW JERSEY*, 1979.

Craig T. Bishop and Mark A. Donelan. Measuring waves with pressure transducers. *Coastal Engineering*, 11(4):309–328, 11 1987. ISSN 03783839. doi: 10.1016/0378-3839(87)90031-7.

A J Bowen. Simple models of nearshore sedimentation. In *Beach profiles and longshore bars*, pages N8–10. 1981.

J A Brinkkemper. Modeling the cross-shore evolution of asymmetry and skewness of surface gravity waves propagating over a natural intertidal sandbar, 2013.

Per Bruun. Forms of equilibrium of coast with littoral drift - SERIES 3, ISSUE 347. Technical report, CALIFORNIA UNIV BERKELEY WAVE RESEARCHLAB, 1953.

Nicholas C. Kraus and Magnus Larson. Beach Profile Change Measured in the Tank for Large Waves 1956-1957 and 1962. page 167, 1988.

CERC. Shore protection manual. Technical report, USACE, 1984.

David Claessen. A beginner's guide to SSA. 2002.

Giovanni Coco, N. Senechal, A. Rejas, K. R. Bryan, S. Capo, J. P. Parisot, J. A. Brown, and J. H.M. MacMahan. Beach response to a sequence of extreme storms. *Geomorphology*, 204:493–501, 1 2014. ISSN 0169555X. doi: 10.1016/j.geomorph.2013.08.028.

R De Zeeuw, De Schipper, M.A. (Matthieu), and De Vries, S. (Sierd). Sand Motor gridded bathymetric and topographic survey, 2017. URL https://data.4tu.nl/repository/uuid:c40da555-3eff-4c3c-89d6-136994a07120.

Robert George Dean. *Equilibrium beach profiles: US Atlantic and Gulf coasts.* Department of Civil Engineering and College of Marine Studies, University of~..., 1977.

John C. Doering and Anthony J. Bowen. Skewness in the nearshore zone: A comparison of estimates from Marsh-McBirney current meters and colocated pressure sensors. *Journal of Geophysical Research*, 92(C12):13173, 11 1987. ISSN 0148-0227. doi: 10.1029/jc092ic12p13173.

Thomas G. Drake and Joseph Calantoni. Discrete particle model for sheet flow sediment transport in the nearshore. *Journal of Geophysical Research: Oceans*, 106(C9):19859–19868, 9 2001. ISSN 2169-9291. doi: 10.1029/2000jc000611.

R.I. Ferguson and M. Church. A Simple Universal Equation for Grain Settling Velocity. *Journal of Sedimentary Research*, 74(6):933–937, 11 2004. ISSN 1527-1404. doi: 10.1306/051204740933.

A. Fernández-Mora, D. Calvete, A. Falqués, and H. E. de Swart. Onshore sandbar migration in the surf zone: New insights into the wave-induced sediment transport mechanisms. *Geophysical Research Letters*, 42(8):2869–2877, 4 2015. ISSN 00948276. doi: 10.1002/2014GL063004. URL http://doi.wiley.com/10.1002/2014GL063004.

Edith L. Gallagher, Steve Elgar, and R. T. Guza. Observations of sand bar evolution on a natural beach. *Journal of Geophysical Research: Oceans*, 103(C2):3203–3215, 2 1998. ISSN 21699291. doi: 10.1029/97jc02765.

Berend Tamme Grasmeijer. Process-based cross-shore modelling of barred beaches. Technical report, 11 2002.

F. Grasso, B. Castelle, and B. G. Ruessink. Turbulence dissipation under breaking waves and bores in a natural surf zone. *Continental Shelf Research*, 43:133–141, 7 2012. ISSN 02784343. doi: 10.1016/j.csr.2012.05.014.

R. T. Guza and Edward B. Thornton. Velocity Moments in Nearshore. *Journal of Waterway, Port, Coastal, and Ocean Engineering*, 111(2):235–256, 3 1985. ISSN 0733-950X. doi: 10.1061/(ASCE)0733-950X(1985)111:2(235). URL http://ascelibrary.org/doi/10.1061/%28ASCE%290733-950X%281985%29111%3A2%28235%29.

Stephen M. Henderson and J. S. Allen. Nearshore sandbar migration predicted by an eddy-diffusive boundary layer model. *Journal of Geophysical Research C: Oceans*, 109(6), 6 2004. ISSN 01480227. doi: 10.1029/2003JC002137.

Dennis E Hinkle, William Wiersma, and Stephen G Jurs. *Applied statistics for the behavioral sciences*, volume 663. Houghton Mifflin College Division, 2003.

Fernanda Hoefel and Steve Elgar. Wave-induced sediment transport and sandbar migration. *Science*, 299(5614):1885–1887, 3 2003. ISSN 00368075. doi: 10.1126/science.1081448.

Leo H Holthuijsen. *Waves in Oceanic and Coastal Waters*. Cambridge University Press, Cambridge, 2009. ISBN 978-0-521-12995-4.

Tian Jian Hsu, Steve Elgar, and R. T. Guza. Wave-induced sediment transport and onshore sandbar migration. *Coastal Engineering*, 53(10):817–824, 9 2006. ISSN 03783839. doi: 10.1016/j.coastaleng.2006.04.003.

Ruurd Jaarsma. Performance of New in-site Altimeters in Dutch Coastal Environments, 2019.

IG Jonsson. Proceedings of the 10th International Conference on Coastal Engineering 1966. 1967.

Magnus Larson and Nicholas Kraus. SBEACH: Numerical model for simulating strom-induced beach change. Technical report, US Army Corps of Engineers, Washington, 1989.

Arjen P. Luijendijk and Anton de Fockert. Wave look-up table: Building with Nature. page 8, 2011.

Arjen P. Luijendijk, Roshanka Ranasinghe, Matthieu A. de Schipper, Bas A. Huisman, Cilia M. Swinkels, Dirk J.R. Walstra, and Marcel J.F. Stive. The initial morphological response of the Sand Engine: A process-based modelling study. *Coastal Engineering*, 119: 1–14, 1 2017. ISSN 03783839. doi: 10.1016/j.coastaleng.2016.09.005.

E. P.D. Mansard and V. Barthel. SHOALING PROPERTIES OF BOUNDED LONG WAVES. In *Proceedings of the Coastal Engineering Conference*, volume 1, pages 798–814. ASCE, 1 1985. ISBN 0872624382. doi: 10.9753/icce.v19.54.

I. J. Mariño-Tapia, T. J. O'Hare, P. E. Russell, M. A. Davidson, and D. A. Huntley. Cross-shore sediment transport on natural beaches and its relation to sandbar migration patterns: 2. Application of the field transport parameterization. *Journal of Geophysical Research*, 112 (C3), 3 2007a. ISSN 0148-0227. doi: 10.1029/2005jc002894.

I. J. Mariño-Tapia, P. E. Russell, T. J. O'Hare, M. A. Davidson, and D. A. Huntley. Cross-shore sediment transport on natural beaches and its relation to sandbar migration patterns: 1. Field observations and derivation of a transport parameterization. *Journal of Geophysical Research*, 112(C3):C03001, 3 2007b. ISSN 0148-0227. doi: 10.1029/2005JC002893. URL http://doi.wiley.com/10.1029/2005JC002893.

G. Masselink, A. Kroon, and R. G.D. Davidson-Arnott. Morphodynamics of intertidal bars in wave-dominated coastal settings - A review. *Geomorphology*, 73(1-2):33–49, 2006. ISSN 0169555X. doi: 10.1016/j.geomorph.2005.06.007.

Gerhard Masselink and Kerry P. Black. Magnitude and cross-shore distribution of bed return flow measured on natural beaches. *Coastal Engineering*, 25(3-4):165–190, 7 1995. ISSN 03783839. doi: 10.1016/0378-3839(95)00002-S.

Gerhard Masselink and Paul Russell. Flow velocities, sediment transport and morphological change in the swash zone of two contrasting beaches. *Marine Geology*, 227(3-4):227–240, 2006.

Walter H Munk. Origin and generation of waves. Technical report, Scripps Institution of Oceanography La Jolla Calif, 1951.

Peter Nielsen and Tomoko Shimamoto. Bar response to tides under regular waves. *Coastal Engineering*, 106:1–3, 12 2015. ISSN 03783839. doi: 10.1016/j.coastaleng.2015.09.001.

F Pedregosa, G Varoquaux, A Gramfort, V Michel, B Thirion, O Grisel, M Blondel, P Prettenhofer, R Weiss, V Dubourg, J Vanderplas, A Passos, D Cournapeau, M Brucher, M Perrot, and E Duchesnay. Scikit-learn: Machine Learning in {P}ython. *Journal of Machine Learning Research*, 12:2825–2830, 2011.

Iris R. Pit, Martin J. Wassen, Annemieke M. Kooijman, Stefan C. Dekker, Jasper Griffioen, Sebastiaan M. Arens, and Jerry van Dijk. Can sand nourishment material affect dune vegetation through nutrient addition? *Science of the Total Environment*, 725:138233, 7 2020. ISSN 18791026. doi: 10.1016/j.scitotenv.2020.138233.

N. G. Plant, B. G. Ruessink, and K. M. Wijnberg. Morphologic properties derived from a simple cross-shore sediment transport model. *Journal of Geophysical Research: Oceans*, 106(C1):945–958, 1 2001. ISSN 01480227. doi: 10.1029/2000JC900143. URL `http://doi.wiley.com/10.1029/2000JC900143`.

J. A. Puleo, T. Lanckriet, and C. Blenkinsopp. Bed level fluctuations in the inner surf and swash zone of a dissipative beach. *Marine Geology*, 349:99–112, 3 2014. ISSN 00253227. doi: 10.1016/j.margeo.2014.01.006.

LC van Rijn. Basic Hydrodynamic Processes in the Coastal Zone. Technical report, 2003. URL `www.leovanrijn-sediment.com,`.

Dano Roelvink, Ad Reniers, Ap van Dongeren, Jaap van Thiel de Vries, Robert McCall, and Jamie Lescinski. Modelling storm impacts on beaches, dunes and barrier islands. *Coastal Engineering*, 56(11-12):1133–1152, 11 2009. ISSN 03783839. doi: 10.1016/j.coastaleng.2009.08.006.

J. A. Roelvink and I. Brøker. Cross-shore profile models. *Coastal Engineering*, 21(1-3):163–191, 12 1993. ISSN 03783839. doi: 10.1016/0378-3839(93)90049-E.

P E Russell and D A Huntley. A cross-shore transport" shape function" for high energy beaches. *Journal of Coastal Research*, pages 198–205, 1999.

A. N. Saulter, P. E. Russell, E. L. Gallagher, and E. L. Miles. Observations of bed level change in a saturated surf zone. *Journal of Geophysical Research C: Oceans*, 108(4):9–1, 4 2003. ISSN 01480227. doi: 10.1029/2000jc000684.

J. S. Schoonees and A. K. Theron. Evaluation of 10 cross-shore sediment transport/ morphological models. *Coastal Engineering*, 25(1-2):1–41, 5 1995. ISSN 03783839. doi: 10.1016/0378-3839(94)00040-5.

Francis Shepard. Beach cycles in southern California. Technical report, 1950. URL `http://hdl.handle.net/11681/3369`.

AD Short. *Handbook of beach and shoreface morphodynamics*. 1999. URL `http://www.sidalc.net/cgi-bin/wxis.exe/?IsisScript=FCL.xis&method=post&formato=2&cantidad=1&expresion=mfn=007204`.

Lennard Spaans. Cross-shore morphodynamics of intertidal bars: A conceptual model, empirical evidence and numerical modelling, 2019. URL `https://repository.tudelft.nl/islandora/object/uuid%3A7f0fe44f-4f8a-44b7-9bbd-23043e1a8e68`.

I. A. Svendsen. Mass flux and undertow in a surf zone. *Coastal Engineering*, 8(4):347–365, 11 1984. ISSN 03783839. doi: 10.1016/0378-3839(84)90030-9.

Ib A Svendsen. *Introduction to nearshore hydrodynamics*, volume 24. World Scientific, 2006.

B. G. Thom and W. Hall. Behaviour of beach profiles during accretion and erosion dominated periods. *Earth Surface Processes and Landforms*, 16(2):113–127, 3 1991. ISSN 10969837. doi: 10.1002/esp.3290160203.

E. B. Thornton, R. T. Humiston, and W. Birkemeier. Bar/trough generation on a natural beach. *Journal of Geophysical Research C: Oceans*, 101(C5):12097–12110, 5 1996. ISSN 01480227. doi: 10.1029/96JC00209.

J. Tinker, P. Russell, G. Masselink, T. O'Hare, T. Butt, M. Austin, P. Ganderton, and E. Gallagher. Field measurements of velocity moment shape function (the x-shore project). In *Coastal Engineering 2006*, pages 3987–3999. World Scientific Publishing Company, 4 2007. ISBN 978-981-270-636-2. doi: 10.1142/9789812709554{_}0335. URL `http://www.worldscientific.com/doi/abs/10.1142/9789812709554_0335`.

Inge Van Den Ende. Onshore sandbar migration Processing PIV measurements to analyse wave driven sediment transport in the nearshore. Technical report, 2017. URL `http://repository.tudelft.nl/`.

Arnold van Rooijen. *Modelling Sediment Transport in the Swash Zone*. PhD thesis, 2011.

Jigang Wang, Predrag Neskovic, and Leon N. Cooper. Improving nearest neighbor rule with a simple adaptive distance measure. *Pattern Recognition Letters*, 28(2):207–213, 1 2007. ISSN 01678655. doi: 10.1016/j.patrec.2006.07.002.

Ping Wang, James H. Kirby, Joseph D. Haber, Mark H. Horwitz, Paul O. Knorr, and Jennifer R. Krock. Morphological and Sedimentological Impacts of Hurricane Ivan and Immediate Poststorm Beach Recovery along the Northwestern Florida Barrier-Island Coasts. *Journal of Coastal Research*, 226(226):1382–1402, 11 2006. ISSN 0749-0208. doi: 10.2112/05-0440.1. URL `http://www.bioone.org/doi/abs/10.2112/05-0440.1`.

A
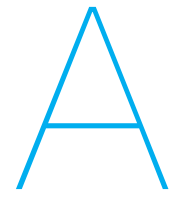
GPS

The GPS intertidal beach measurements made during the fieldwork.
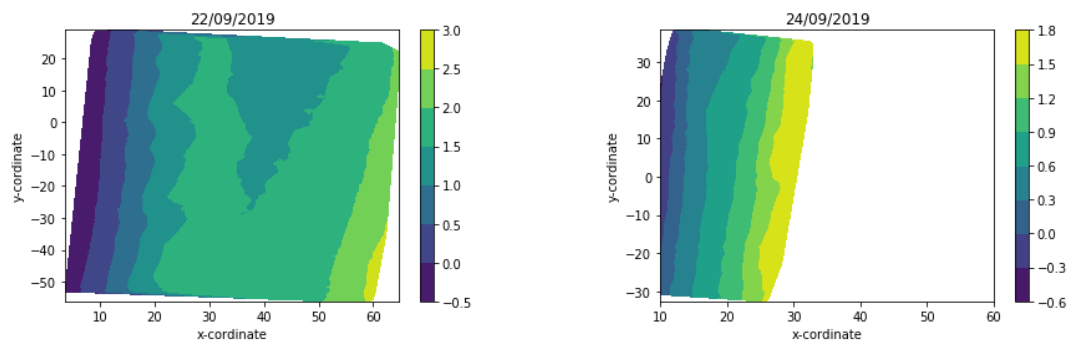
a) The intertidal beach at 22/09/2019, the colorbar on the side shows the depth related with with different colours

b) The intertidal beach at 24/09/2019, the colorbar on the side shows the depth related with with different colours
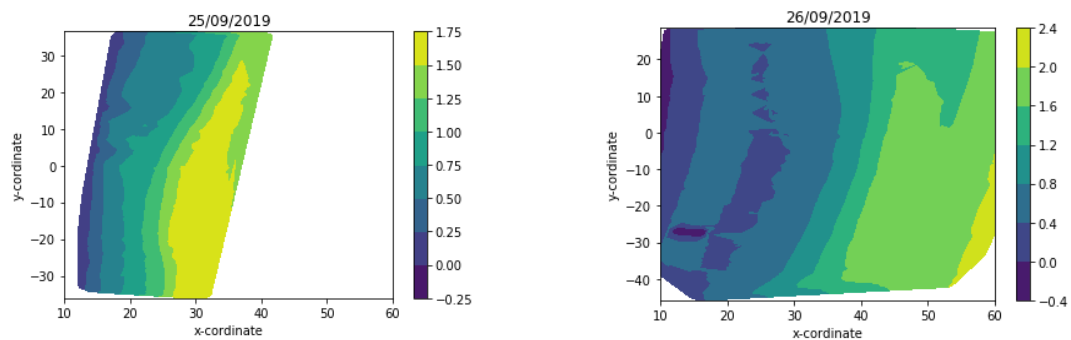
c) The intertidal beach at 25/09/2019, the colorbar on the side shows the depth related with with different colours

d) The intertidal beach at 26/09/2019, the colorbar on the side shows the depth related with with different colours
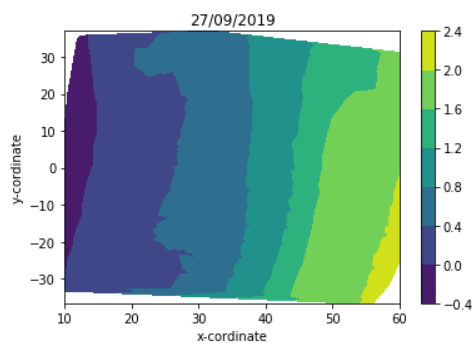
Figure A.3: f) The intertidal beach at 27/09/2019, the colorbar on the side shows the depth related with with different colours

68

B

Testing of the model

In this part the model from chapter 2 is tested, using different conditions. The effects are shown in the figures below. The standard conditions unless changes are a wave of 0.8 meters. The dean profile based on the dean profile in 4. The gamma is set at 0.59.
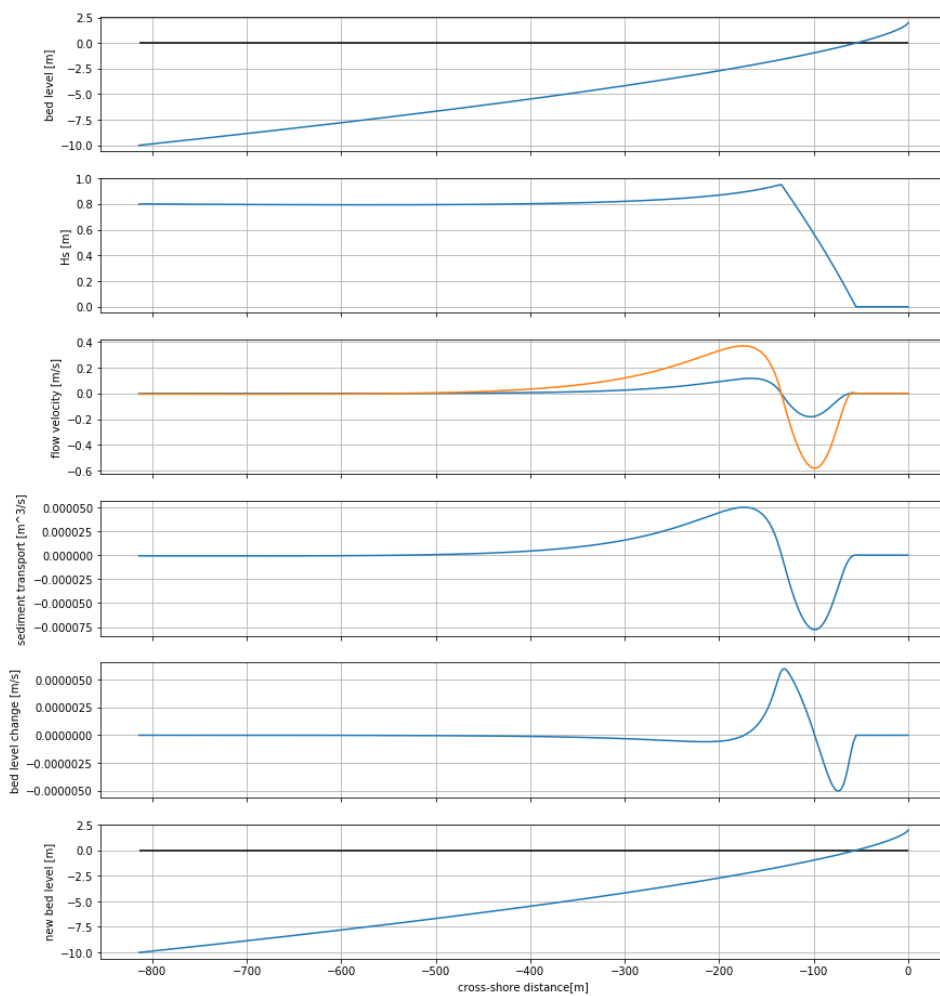
Figure B.1: A single run of the model on a dean profile, the top figure is the bed level, second figure is the significant wave height,third figure the velocity moments, the fourth figure sediment transport, fifth figure bed level change, the new bed level
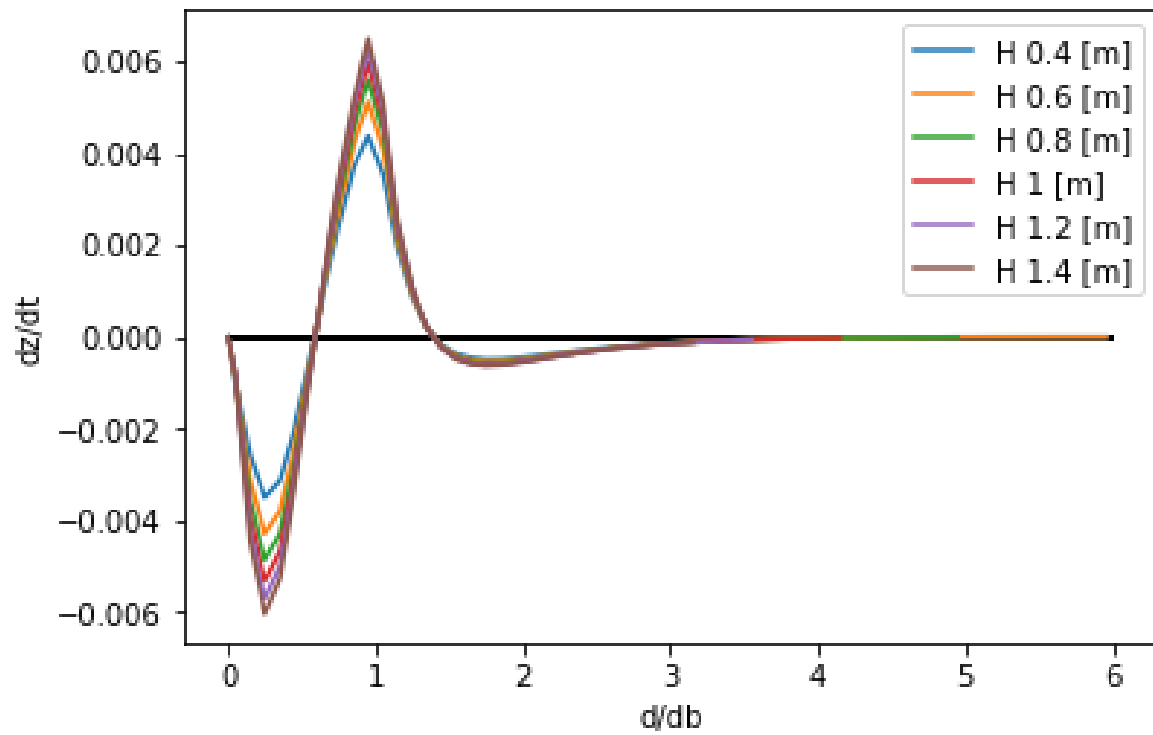
Figure B.2: Different waves and the effect on the amount of bed level changes
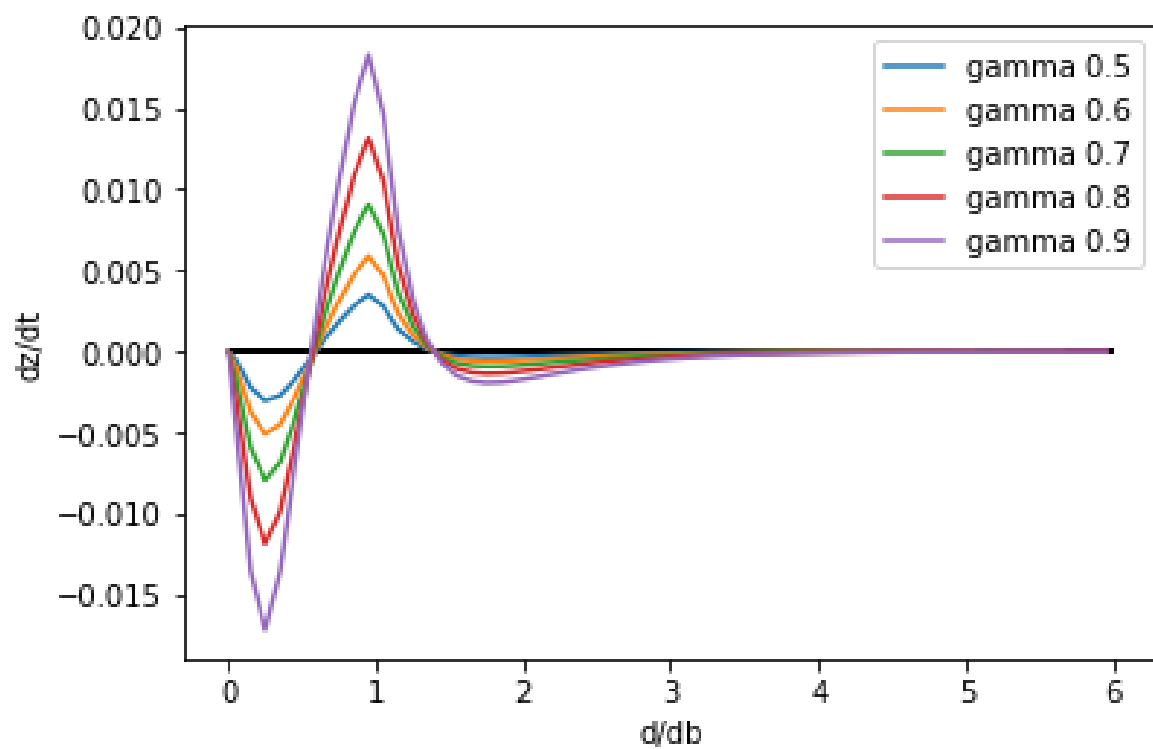
Figure B.3: Different gamma values and the effect on bed level changes
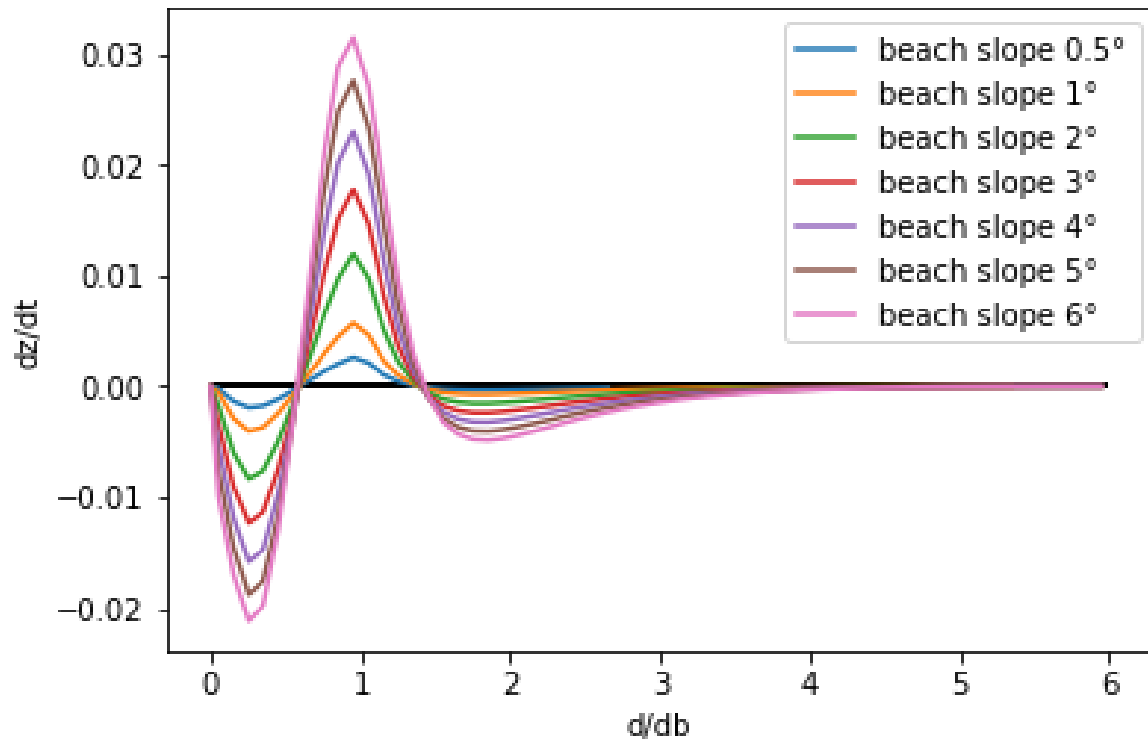
Figure B.4: Different slopes and the effect on bed level transport
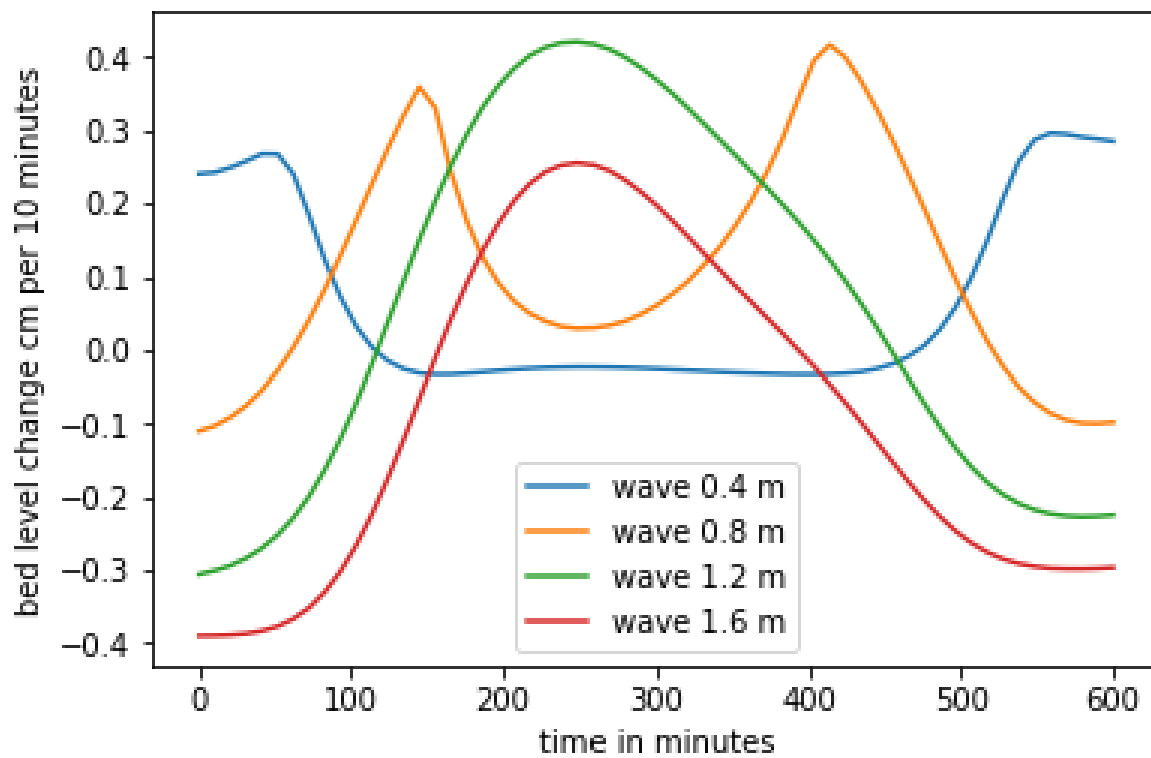
Figure B.5: The bed level behavior of a location at a depth of 0.5 meters during the passing of a single tide, with different waves.

C
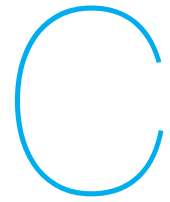
Deep water profile

the deep water bed level based on jet-ski altimeter data collected by De Zeeuw et al. (2017).
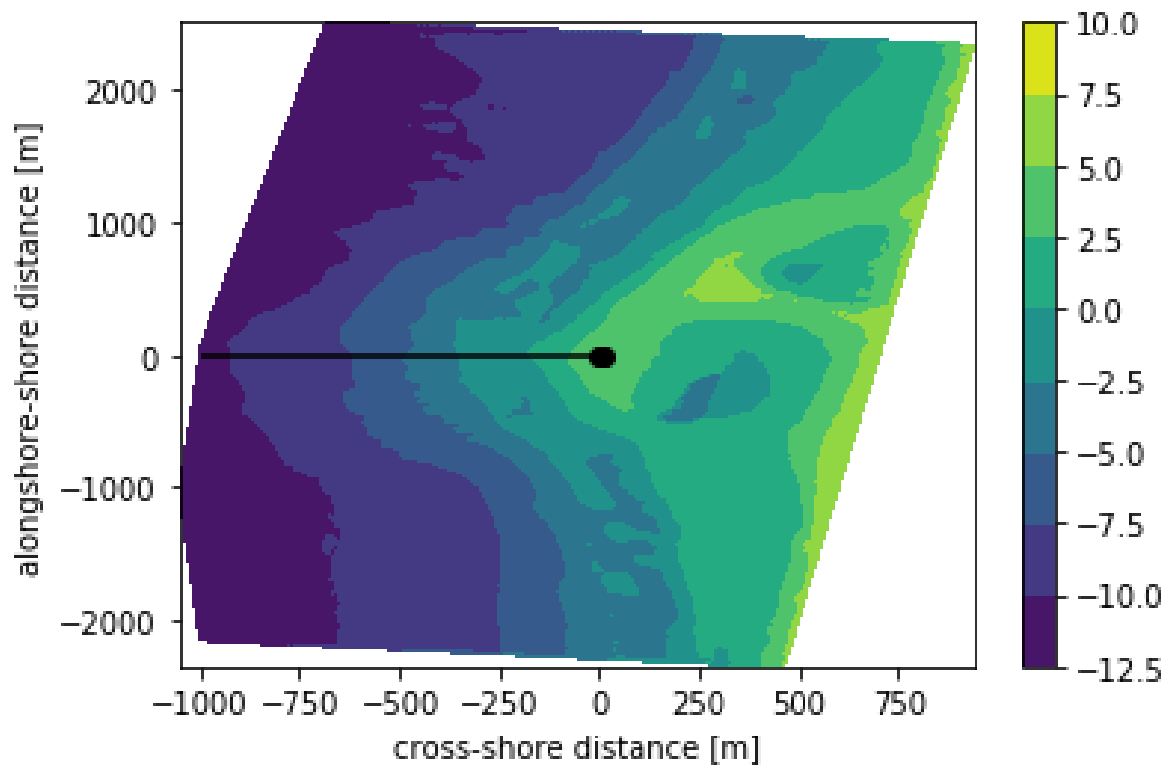
Figure C.1: The jet-ski and LIDAR collected bed level at the sand engine at 1/4/2016. The coast was turned to align perfectly with the poles that where installed during the field experiment. The x-axis is the cross-shore distance, the y-axis is the alongshore distance. The black line is the profile of interest at the location of the poles. The bar on the side indicates the elevation of the location where 0 is the NAP.

There are 37 bathymtery measurements ranging from 3/8/2011 till 7/9/2016 (De Zeeuw et al., 2017). The profiles are normalized over distance from the shore. The cross-shore distance is set to be 0 where the elevation of the profile is equal to the zero NAP value. Since there is no average beach over multiple years a Deans profile is used to show the deviations of the profile from the dean profile 4.1. The first year the profile slope was changing and the profile was not matching the dean profile, therefore these profiles are ignored for the sandbar location analysis and the deep water profile.
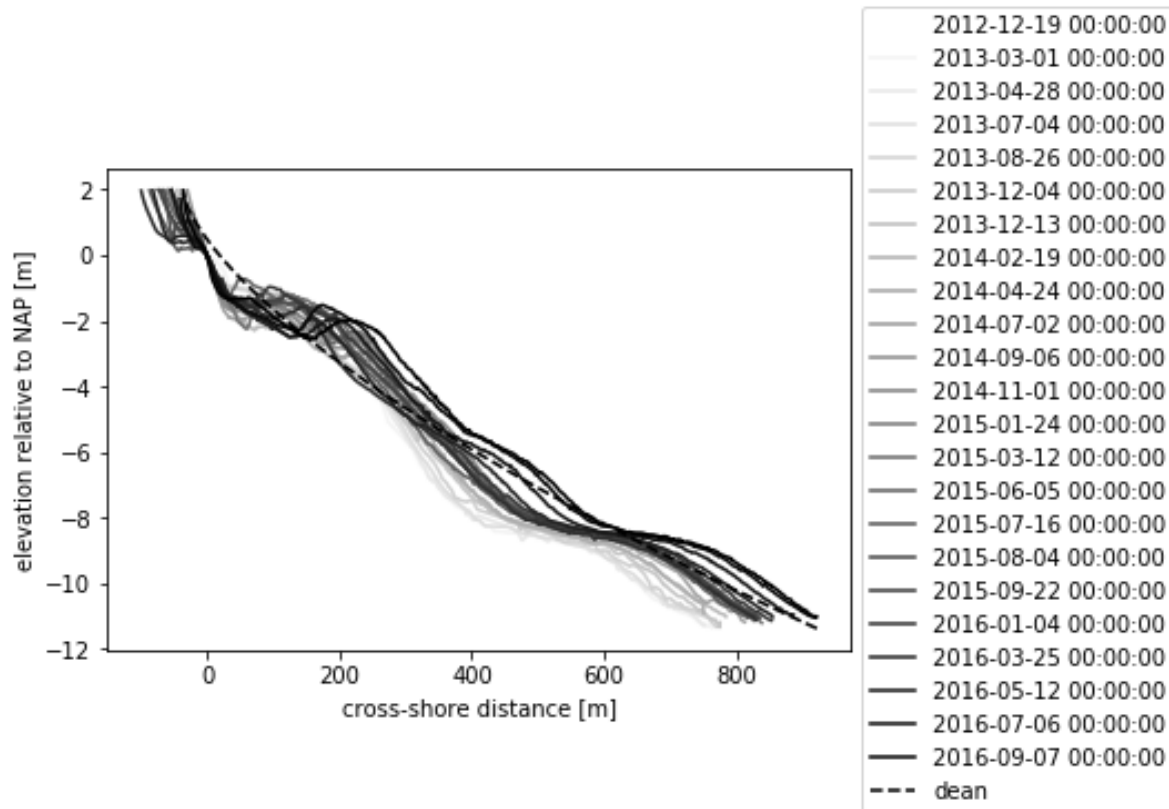
Figure C.2: The profiles normalized. The x-axis is the cross-shore distance from shore. The y-axis is the elevation level compared to the NAP. The lines represent different beach profiles over time the darker the line the more recent the profile measurement. The dotted line is the Dean profile.

In figure C.2 it can be seen that the slope is still decreasing over time. The beach profile has sandbars between 0 and 400 meter offshore. Sandbars location will be identified in this analysis by the crest of the sandbar, the crest of the sand bar will be the maximum deviation from the Dean profile.
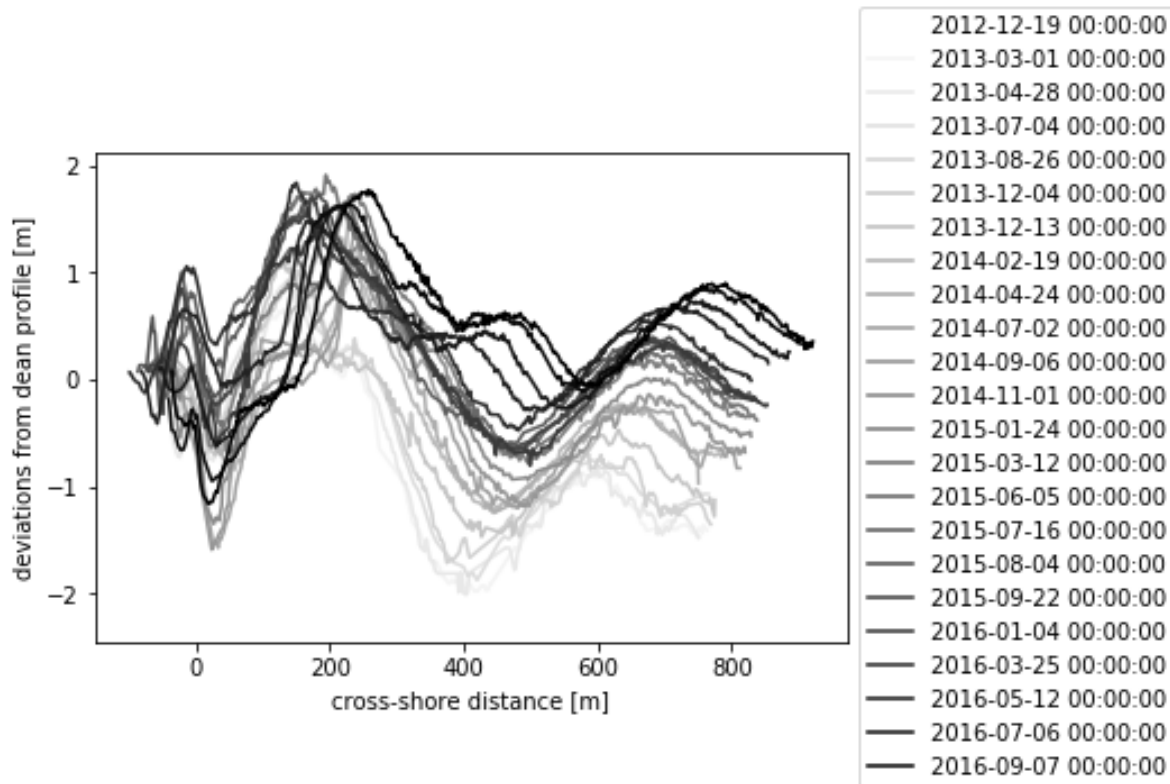
Figure C.3: The deviations of the profiles from the Dean profile. The x-axis is the cross-shore distance. The y-axis the zero represents the dean profile and the positive values indicate that the profile is more shallow than the Dean profile and the negative values indicate the profile is deeper than the Dean profile.

In figure C.3 the sandbars crest was present between 140 and 260 meters offshore. The profiles deviations from the Dean profile indicate that the slope of the is changing over time. When the location of the crest of the sandbar is plotted over time the migration of the sandbar becomes valuable. The crest depth of the sandbar is plotted as well over time.
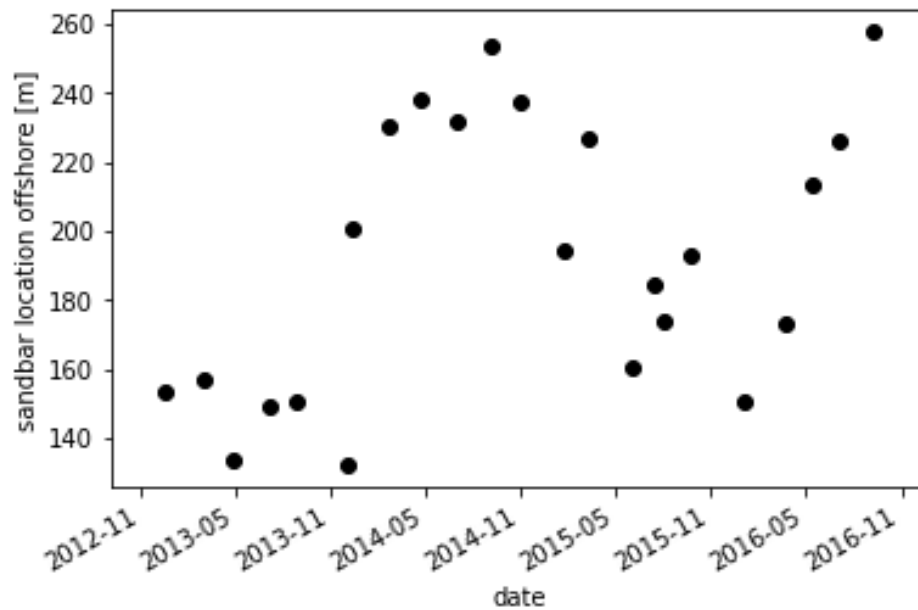
Figure C.4: The dots are the offshore location of the sandbars crest. The x-axis is the time. The y-axis is the distance from the shore.
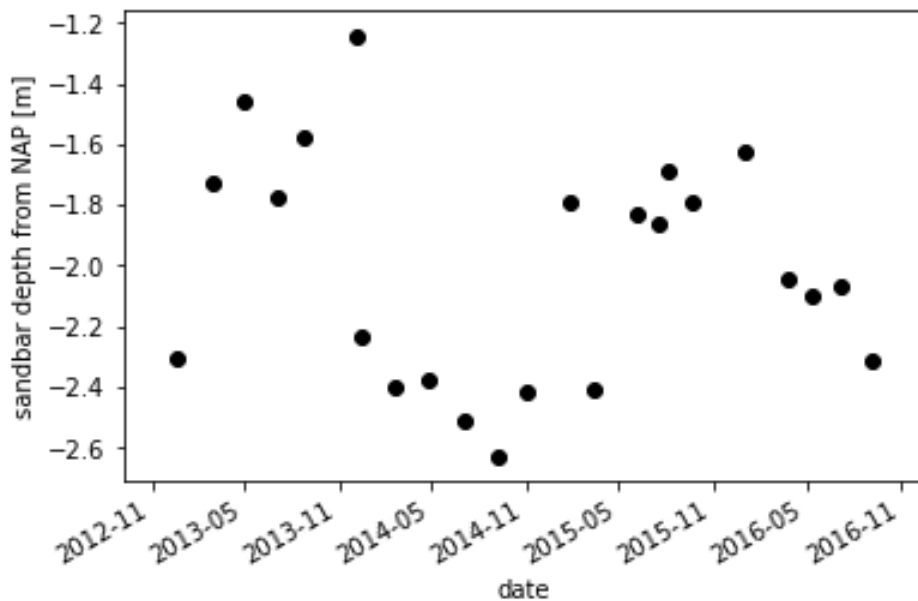
Figure C.5: The dots are the sandbars crest height below the NAP. The x-axis is the time. The y-axis is the depth of the crest of the sandbar.

Form figure C.4 it can be seen that the sandbar is moving over time near the 200 meters offshore from where the NAP reaches the beach. Figure C.5 the height of the crest shows, the depth of the sandbar is moving around -2 meters from the NAP. From the height and the location of the sandbar, an average location and an average depth can be determined. Table C.1 the statistics of the sandbars are presented.

Sandbar	Mean	Standard deviation
Location	192.24 meters	38.98 meters
Depth	-2.01 meters	0.37 meters

Table C.1: The location of the sandbars and the depth of the crest of the sandbars

The coast of the Sand Engine is retreating, however the profile of the Sand Engine is behaving reasonable stable over years with a sandbar on a stable location and a close match to a deans profile. Therefore it is assumed that the best deep water profile that can be used for the field experiment is the average profile of the beach in the year 2016.